



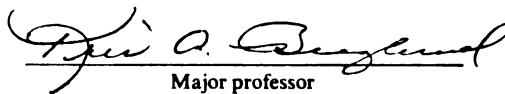


This is to certify that the  
dissertation entitled  
MONITORING PROTEIN CRYSTALLIZATION USING  
VIBRATIONAL SPECTROSCOPIES

presented by  
Albert Martin Schwartz

has been accepted towards fulfillment  
of the requirements for

Ph.D. degree in Chemistry and Chemical  
Engineering

  
Major professor

Date Aug 19, 1999



**PLACE IN RETURN BOX** to remove this checkout from your record.  
**TO AVOID FINES** return on or before date due.  
**MAY BE RECALLED** with earlier due date if requested.

DATE DUE	DATE DUE	DATE DUE
<hr/>	<hr/>	<hr/>
<hr/>	<hr/>	<hr/>
<hr/>	<hr/>	<hr/>
<hr/>	<hr/>	<hr/>
<hr/>	<hr/>	<hr/>

MONITORING PROTEIN CRYSTALLIZATION USING VIBRATIONAL  
SPECTROSCOPIES

By

Albert Martin Schwartz

A DISSERTATION

Submitted to  
Michigan State University  
in partial fulfillment of the requirements  
for the degree of

DOCTOR OF PHILOSOPHY

Department of Chemistry  
&  
Department of Chemical Engineering

1999



## ABSTRACT

### MONITORING PROTEIN CRYSTALLIZATION USING VIBRATIONAL SPECTROSCOPIES

By

Albert Martin Schwartz

The key process in structure-based rational drug design relies on mapping the three-dimensional structure of a specific protein. X-ray and neutron diffraction techniques can supply the required structural information at atomic resolution. However, the success rate in growing single crystals of proteins of suitable size and quality for structural determination is low. Experiments to determine the necessary for protein crystal growth rely on screening methods, which are trial and error methods. These methods are labor intensive and unpredictable. Therefore, protein crystallization experiments must be monitored. Both attenuated total reflectance infrared spectroscopy and Raman spectroscopy were examined as possible means of monitoring protein crystallization.

Due to the success of previous crystallization experiments monitored via ATR-FTIR spectroscopy, ATR-FTIR was employed to monitor lysozyme crystallization. The use of infrared spectroscopy will allow the detection of a change in concentration of the protein solution and a change in structure due to the interaction between protein molecules. Unfortunately, proteins will adhere to the inorganic surface of the internal reflection element of the ATR probe. Therefore, the ATR-IR method was found to be invasive to the hanging drop systems under study, and was eliminated as a possible method of monitoring protein crystallization in the hanging drop experiment.

We have demonstrated that fiber optic Raman spectroscopy combined with a partial least-squares regression model can be utilized to monitor lysozyme concentration. This method allows the lysozyme concentration to be measured in real time during crystallization in a hanging drop. Raman spectral features of the buffer and protein were employed to build the regression model. The use of fiber optic technology coupled with Raman spectroscopy, which is ideal for use with aqueous solutions, results in a powerful noninvasive probe of the changing environment within the solution. Monitoring the concentration changes of the lysozyme within the hanging drop permits a measurement of the level of supersaturation of the system and enhances dynamic control of the crystallization process. Extension of this model to other protein systems has also proven to be an effective means of monitoring and controlling crystallization in a hanging drop without *a priori* solubility data. Finally, results from these experiments indicate that the current method of performing the hanging drop experiment is not reliable. An element of control must be introduced to increase the effectiveness of the hanging drop experiment.

**Dedicated to Mom**

**&**

**In Memory of Dad**

## ACKNOWLEDGEMENTS

I would first of all like to thank my research advisor, Dr. Kris A. Berglund, for the many opportunities he has given me. Joining the Berglund group has allowed me to pursue my interests as both a chemist and chemical engineer. I would like to thank Kris for both the guidance and freedom he has given me while I was here at Michigan State. Thanks Kris, for being both a mentor and a friend. I would also like to thank the other members of my committee Dr. Stanley Crouch, Dr. Alec Scranton, Dr. Patrick Oriel, and Dr. Gary Blanchard for their time, effort, and helpful criticisms. I would like to thank those at Kaiser Optical Inc. and ASI Applied Systems for their support through partial instrument donation.

I would like to acknowledge the Berglund group members who have helped to make graduate school easier in many ways. I would especially like to thank Dr. Marketta Uusi-Penttilla, Dr. Dilum Dunuwila, Dr. Trisha Wang, and Dr. Sanjay Yedur for helping me through those first few engineering courses. Finally, to the Berglund group members who are currently pursuing a dual degree, it is definitely worth it! However, the paperwork may make you think otherwise. I would also like to thank Lamont Terrell, Gabe Wing, John Asara, and the basketball crew from Tuesday mornings for their support and friendship.

I am grateful to my mother for all of the sacrifices she has made over the years. Without you this would not have been possible. I would also like to thank my sisters Rosemarie and Ramona for all of their encouragement. I would like to acknowledge my friends from Chicago: Aaron, James, Andy, Lee, Doug, John, and the rest of the alpha

delts for making Michigan feel a little less far away. Finally, I would like to thank my fiancée, Jen Horne. Thanks for all of your love, patience, support, and for being my best friend. Jen, thanks for asking me to play softball!

## TABLE OF CONTENTS

	Page
List of Tables.....	ix
List of Figures.....	x
Chapter 1: Introduction and Background on Protein Crystallization.....	1
Introduction.....	1
Protein Crystallization.....	2
The Hanging Drop Crystallization Technique.....	3
Control of Protein Crystallization Experiments.....	10
Vibrational Spectroscopy.....	12
Partial Least Squares Regression.....	18
Literature Cited.....	21
Chapter 2: Using ATR-FTIR Spectroscopy to Monitor Lysozyme Crystallization in a Hanging Drop.....	23
Introduction.....	23
Materials and Methods.....	25
Results and Discussion.....	27
Literature Cited.....	34
Chapter 3: The Use of Raman Spectroscopy for <i>In Situ</i> Monitoring of Lysozyme Concentration during Crystallization in a Hanging Drop.....	35
Summary.....	35
Introduction.....	35
Materials and Methods.....	36
Results and Discussion.....	38
Conclusion.....	43
Literature Cited.....	45
Chapter 4: <i>In Situ</i> Monitoring and Control of Lysozyme Concentration during Crystallization in a Hanging Drop.....	46
Summary.....	46
Introduction.....	46
Experimental Procedure.....	48
Protein Sample Preparation.....	48
Supersaturation Measurements.....	50
Data Analysis.....	51
Results and Discussion.....	52
Conclusions.....	64

Literature Cited.....	66
<b>Chapter 5: Extension of the Raman Control Scheme for the Hanging Drop</b>	
Experiment to Proteins other than Lysozyme.....	68
Summary.....	68
Introduction.....	69
Experimental Procedure.....	72
Protein Sample Preparation.....	72
Raman Spectra of the Proteins.....	73
Data Analysis.....	74
Results and Discussion.....	76
Discussion and Conclusions.....	96
Literature Cited.....	99
<b>Chapter 6: A Comparison of Control Mechanisms Employed on Lysozyme</b>	
Crystallization Experiments in a Hanging Drop.....	101
Summary.....	101
Introduction.....	102
Experimental Procedure.....	103
Protein Sample Preparation.....	103
Experimental Design.....	104
Data Analysis.....	104
Results and Discussion.....	107
Conclusions.....	115
Literature Cited.....	118
<b>Chapter 7: Conclusions.....</b>	<b>119</b>
Methods Used to Monitor Protein Crystallization.....	119
The Hanging Drop Experiment.....	122
<b>Chapter 8: Future Directions.....</b>	<b>124</b>
The Raman Method.....	124
The Hanging Drop Experiment.....	125

## LIST OF TABLES

Table 4.1	A summary of the results of uncontrolled crystallization experiments in terms of rates of supersaturation and numbers of crystals produced. The abbreviation ppt indicates that the outcome of the experiment was the formation of amorphous precipitate. As the rate of supersaturation increased the number of crystals produced also increased.....	59
Table 5.1	A comparison of the quality of Raman spectrum acquired with respect to the molecular weight of the protein. As the molecular weight of the protein increases the Raman spectrum is more susceptible to interference due to background fluorescence.....	79
Table 5.2	A summary of the results of uncontrolled and controlled crystallization experiments for $\alpha$ -amylase in terms of rates of supersaturation, times of nucleation, and numbers of crystals produced. The abbreviation "ppt" indicates that the outcome of the experiment was the formation of amorphous precipitate and the abbreviation "xtal" indicates the formation of crystal. As the rate of supersaturation increased the time of nucleation decreased and the onset of precipitate formation increased.....	87
Table 5.3	A summary of the results of uncontrolled and controlled crystallization experiments for subtilisin in terms of rates of supersaturation, times of nucleation, and numbers of crystals produced. The abbreviation "ppt" indicates that the outcome of the experiment was the formation of amorphous precipitate and the abbreviation "xtal" indicates the formation of crystal. As the rate of supersaturation increased the time of nucleation decreased and the onset of precipitate formation increased.....	88
Table 6.1	A summary of the results of the controlled crystallization experiments in terms of nucleation times, numbers of crystals produced, and size of crystals produced. The application of control by either feedback control (step change) or programmed control (differential change) increases the size of the resultant crystal. The data indicate that the method most often used in the hanging drop experiment (constant reservoir) does not give the best results.....	114



## LIST OF FIGURES

Figure 1.1	The supersaturation feedback loop modified from [20]. This loop describes how both the nucleation and growth rates depend on the level of supersaturation of the protein solution.....	4
Figure 1.2	This illustration depicts the hanging drop experiment. A protein drop is inverted over a reservoir of higher ionic strength. $[Pr]_{res}$ and $[Pr]_{drop}$ indicate the precipitant ionic strength in the reservoir and the drop, respectively. Typically, the reservoir contains twice the number of ions as the hanging drop. The net result is that water is drawn from the drop to the reservoir.....	7
Figure 1.3	A diagram of the hanging drop experiment in terms of protein concentration and solubility. The smooth curve describes the protein solubility with respect to increasing amounts of precipitant. Initially, the hanging drop of protein is below solubility at a low concentration of both protein and precipitant (A). As water is drawn from the hanging drop, the drop concentrates. Eventually, the drop becomes supersaturated and nucleation occurs (B). The protein continues to nucleate and grow crystals, resulting in a decrease in concentration (C).....	8
Figure 1.4	A schematic of the operation of attenuated total internal reflection infrared spectroscopy. The optically denser medium, $n_1$ , is in contact with the optically rarer medium, $n_2$ . The long vertical line, symbolized by dots and dashes, represents a line normal to the internal reflection element and the rarer medium. The evanescent field is generated by the infrared radiation and penetrates into the rarer medium (sample). The evanescent wave decays exponentially. As a result the sample and internal reflection element must be in intimate contact.....	15
Figure 1.5	Energy-level diagram illustrating Raman scattering: dark solid lines = electronic states, solid lines = vibrationally excited states, dashed lines = virtual states.....	17
Figure 1.6	A flow chart of the partial least squares regression techniques as a “black box” [37]. The method requires three inputs and produces one output. Two inputs, comprising the calibration set, are needed to build the regression model. The third input is the spectrum of unknown concentration. The PLS algorithm empirically models the variation in the calibration set and builds a regression model. The output is the estimated concentration matrix of the species responsible for the unknown spectrum.....	20

Figure 2.1	A schematic of the ATR-IR experimental set-up for monitoring protein crystallization in the hanging drop.....	26
Figure 2.2	A graph representing the relationship between the Amide I peak position in wavenumbers ( $\text{cm}^{-1}$ ) and concentration of lysozyme. As expected the peak shifts toward lower wavenumbers as the concentration of lysozyme approaches that of a crystal.....	29
Figure 2.3	A comparison of the concentration profiles of a control experiment (circles) and a crystallization experiment (triangles). Both profiles increase in concentration eventually reaching a steady state value. The process that these profiles describe is the adsorption of lysozyme onto the diamond tip of the ATR-IR probe.....	31
Figure 3.1	Solubilities of lysozyme in buffer solutions of varying ionic strength were determined using Raman spectroscopy. All measurements used 5 $\mu\text{l}$ hanging drops of lysozyme solutions.....	40
Figure 3.2	Real time concentration change of a hanging drop of lysozyme at 0.2 M ionic strength suspended above a reservoir of 0.33 M ionic strength. The lines represent the following: line A [slope = $0.008 \text{ g}/(\text{ml}\cdot\text{hr})$ ] shows the change in concentration as the hanging drop becomes more concentrated, line B follows the decrease in supersaturation of the drop after nucleation has occurred, and line C follows the growth of lysozyme crystals.....	41
Figure 3.3	Real time concentration change of a hanging drop of lysozyme at 0.2 M ionic strength suspended above a reservoir of 0.84 M ionic strength. The lines represent the following: line A [slope = $0.015 \text{ g}/(\text{ml}\cdot\text{hr})$ ] shows the change in concentration as the hanging drop becomes more concentrated, line B follows the decrease in supersaturation of the drop after nucleation has occurred, and line C follows the growth of lysozyme crystals.....	42
Figure 4.1	A schematic of the experimental set-up used throughout the lysozyme vapor diffusion experiments, consisting of a 6 ml vial with input and output channels. These channels were attached to a set of syringes, which allow the composition of the reservoir to be altered. The fiber optic probe assembly is positioned directly above the hanging drop of lysozyme solution and focused into the drop utilizing a 10X microscope objective.....	49
Figure 4.2	A real time concentration change of a hanging drop of lysozyme obtained with the fiber optic Raman method. The ionic strengths of the reservoir and the drop are 1.02 M and 0.34 M, respectively. The rate of supersaturation, the time of nucleation, and the eventual decrease in supersaturation of the protein within the solution of the hanging drop can be measured in real time.....	53

Figure 4.3	A comparison of the relative crystallization kinetics between hanging drop experiments with an initial lysozyme concentration of about 0.16 g/ml and varying reservoir ionic strengths. As the reservoir ionic strength decreases the concentration trajectories of the lysozyme begin to flatten out.....	56
Figure 4.4	A comparison of the relative crystallization kinetics between hanging drop experiments with an initial lysozyme concentration of about 0.23 g/ml and varying reservoir ionic strengths. As the reservoir ionic strength decreases the concentration trajectories of the lysozyme begin to flatten out.....	57
Figure 4.5	A direct comparison of the lysozyme concentration trajectories for hanging drop crystallization experiments which were controlled and uncontrolled. By applying control of the ionic strength of the reservoir, the induction time in the controlled experiment is increased by a factor of 4.....	61
Figure 4.6	These lysozyme crystals correspond to the trajectories of the controlled and uncontrolled experiments in Figure 5. These photographs are at the same magnification, and encompass identical viewing areas. The top picture represents the uncontrolled experiment, and the bottom picture represents the controlled experiment. Through the application of control of the crystallization process the size of the resultant crystals is increased and the number of crystals is decreased.....	63
Figure 5.1	A typical Raman spectrum of a 5 $\mu$ l hanging drop of lysozyme obtained with the Kaiser Optical, Inc. Hololab Series 1000® instrument. The Raman spectrum depicts a 0.22 g/ml sample of lysozyme over the Raman shift range of 200 $\text{cm}^{-1}$ to 3900 $\text{cm}^{-1}$ . The vibrational regions corresponding to the Amide I stretch, the Amide III stretch, the CH stretches, and the OH stretches are labeled. The fluorescence background is also clearly visible. The fluorescence distorts the baseline yielding a Raman baseline with convex curvature.....	77
Figure 5.2	A comparison of the fluorescence corrected Raman spectra of lysozyme, $\alpha$ -amylase from barley malt, and Carlsberg subtilisin. The CH stretches in all three spectra contain shoulders near 2900 $\text{cm}^{-1}$ and peak maxima near 2950 $\text{cm}^{-1}$ . The OH stretching region in all the spectra is comprised of a single broad peak ranging from 3100 $\text{cm}^{-1}$ to 3700 $\text{cm}^{-1}$ .....	81
Figure 5.3	A comparison of the relative crystallization kinetics between hanging drop experiments with an initial $\alpha$ -amylase concentration of about 0.11 g/ml and varying reservoir ionic strengths. The profile plotted as triangles corresponds to a reservoir ionic strength of 1.90 M and the profile plotted as circles corresponds to a reservoir ionic strength of 1.32 M.....	84
Figure 5.4	A comparison of the relative crystallization kinetics between	

hanging drop experiments with an initial subtilisin concentration of about 0.05 g/ml and varying reservoir ionic strengths. The profile plotted as triangles corresponds to a reservoir ionic strength of 3.17 M and the profile plotted as circles corresponds to a reservoir ionic strength of 2.47 M.....85

Figure 5.5 A direct comparison of the  $\alpha$ -amylase relative concentration profiles for hanging drop crystallization experiments which were controlled and uncontrolled. By applying control of the ionic strength of the reservoir, the induction time in the controlled experiment is increased by approximately 1 hour.....90

Figure 5.6 These  $\alpha$ -amylase crystals correspond to the relative concentration profiles of the controlled and uncontrolled experiments in Figure 5. These photographs are at the same magnification, and encompass identical viewing areas. The top picture represents the uncontrolled experiment, and the bottom picture represents the controlled experiment. Through the application of control of the crystallization process both the size of the resultant crystal and the quality of the crystal was increased.....92

Figure 5.7 A direct comparison of the subtilisin relative concentration profiles for hanging drop crystallization experiments which were controlled and uncontrolled. By applying control of the ionic strength of the reservoir, the induction time in the controlled experiment is increased by approximately 1 hour.....94

Figure 5.8 These subtilisin crystals correspond to the relative concentration profiles of the controlled and uncontrolled experiments in Figure 7. These photographs are at the same magnification, and encompass identical viewing areas. The top pictures labeled A<sub>1</sub> and A<sub>2</sub> represent the uncontrolled experiment, and the bottom picture represents the controlled experiment. Through the application of control to the crystallization process the onset of precipitate formation was avoided and the nucleation and growth of subtilisin crystals was favored, picture B.....95

Figure 6.1 A schematic of the experimental set-up used throughout the lysozyme vapor diffusion experiments, consisting of a 6 ml vial with input and output channels. These channels were attached to syringes or peristaltic pumps, which allow the composition of the reservoir to be altered. The fiber optic probe assembly is positioned directly above the hanging drop of lysozyme solution and focused into the drop utilizing a 10X microscope objective. ....105

Figure 6.2 A real time ionic strength profile of the reservoir conditions. The three profiles depict a constant reservoir ionic strength (diamonds), a step change in reservoir ionic strength (line), and a differential change in ionic strength (circles). These profiles are associated with the three control schemes

applied to the lysozyme hanging drop. The three control mechanisms are uncontrolled, feedback control, and programmed control of the ionic strength of the reservoir.....109

Figure 6.3 A comparison of the relative crystallization kinetics between hanging drop experiments with an initial lysozyme concentration of about 0.23 g/ml. The lysozyme concentration profiles correspond to the control schemes depicted in Figure2. The difference in trajectory of the lysozyme concentration indicates that the path taken by the lysozyme concentration is dependent on the control scheme implemented.....111

Figure 6.4 These lysozyme crystals correspond to the trajectories of the experiments in Figure 3. These photographs are at the same magnification, and encompass identical viewing areas. The pictures represent the uncontrolled experiment at a constant reservoir ionic strength (A), the feedback control experiment obtained through a step change in reservoir ionic strength (B), and the programmed control obtained through a differential change in reservoir ionic strength (C). The application of control of the crystallization process of lysozyme increases the size of the resultant crystals and decreases the number of crystals produced.....113

## **Chapter 1: Introduction and Background on Protein Crystallization**

### **Introduction**

The key process in structure based rational drug design relies on mapping the three-dimensional structure of a specific protein. X-ray and neutron diffraction techniques can supply the required structural information at atomic resolution [1,2]. Once the structure of a particular protein has been identified, specific compounds can be synthesized with the correct steric or charge requirements to bind to the active site of the protein [2,3]. Once bound to the active site of a protein, these compounds can disrupt propagation of a disease related to the particular protein. Unfortunately, the success rate in growing single crystals of proteins of suitable size and quality for structural determination is low and poses a barrier to the drug development process.

Determinations of the conditions for protein crystal growth are most often adventitious and are found by trial and error screening methods [1,4]. In an attempt to decrease the amount of time and the number of experiments needed to find the necessary conditions for crystal growth, statistical methods have been employed [5,6]. Striving to better understand the crystal growth process has lead various workers to monitor small batch crystallizers containing protein solutions. These studies have included fluorescence based anisotropy measurements [7], static light scattering [3,8,9], dynamic light scattering (DLS) [3,10,11], and calorimetric techniques [9,12]. Though these findings revealed a wealth of information about protein crystal growth, they were incomplete predictors of whether a solution would nucleate to form crystals. The experiments previously mentioned have all employed batch or microbatch crystallization techniques.

However, the most used crystallization techniques by crystallographers are the vapor-diffusion techniques. Though there are similarities between microbatch and vapor-diffusion techniques [13], their driving forces are vastly different. Most recently, some workers have shifted their goal from predicting crystal growth in a batch setting to monitoring and controlling crystal growth.

Dynamic light scattering (DLS) combined with humidity sensors [14], a gravimetric technique [15], a thermal gradient [16], and Raman spectroscopy [17] have all been employed in monitoring and controlling protein crystallization. The first of these techniques combines the ability of DLS to detect trends in particle size with humidity sensors to observe the evaporation rate of water in a hanging drop experiment. The second technique measures the evaporation rate of water from the hanging drop directly. The third technique, based on thermal gradients, alters the solubility of the protein *in situ* in a batch experiment. The fourth technique, based on Raman spectroscopy [17], allows simultaneous measurement of the concentration of protein and the amount of water within the hanging drop and is the subject of this dissertation.

## **Protein Crystallization**

Protein crystallization is a complex process depending on both thermodynamic factors controlling solubility and kinetic factors controlling nucleation and growth [18]. For the crystallization of a protein to occur the solution must first be supersaturated. Supersaturation is a thermodynamically metastable state, in which nucleation and crystal growth occur [18,19]. The level of supersaturation of a solution dictates whether protein crystals will nucleate to form crystals or will precipitate to form an amorphous solid.

Higher levels of supersaturation lead to the formation of small crystals or precipitate and lower levels of supersaturation lead to the formation of larger crystals.

Supersaturation (S) can be described as the ratio of the activity of the solute divided by the activity at solubility of the solution under identical conditions [19,20]. Since the activity coefficients are difficult to measure in a changing environment, the ratio of activity coefficients is assumed to be unity. Therefore, supersaturation is typically approximated as the ratio of the concentration of the solute divided by the concentration of the solution at solubility. Infrared spectroscopic measurements of the concentration of a supersaturated solution *in situ* has proven to be an effective means of monitoring and controlling the crystallization process [21,22,23,24]. Therefore, vibrational spectroscopy was applied to monitor and control the protein crystallization process in the current work.

Supersaturation describes the degree to which a solution's concentration is above solubility. Figure 1.1 depicts a crystallization feedback loop [20]. The nucleation and growth rates are dependent upon the level of supersaturation of the protein in solution. The rate of nucleation is proportional to the level of supersaturation to the  $k^{\text{th}}$  power, and the rate of growth is proportional to the level of supersaturation to the  $i^{\text{th}}$  power. The  $i^{\text{th}}$  power is always less than the  $k^{\text{th}}$  power [19,20]. This presents a dilemma in protein crystallization. In order to promote nucleation, higher degrees of supersaturation are desired; however, a higher degree of supersaturation tends to favor small crystal or amorphous precipitate formation. A lower degree of supersaturation will favor crystal growth; however, low degrees of supersaturation will either drastically increase



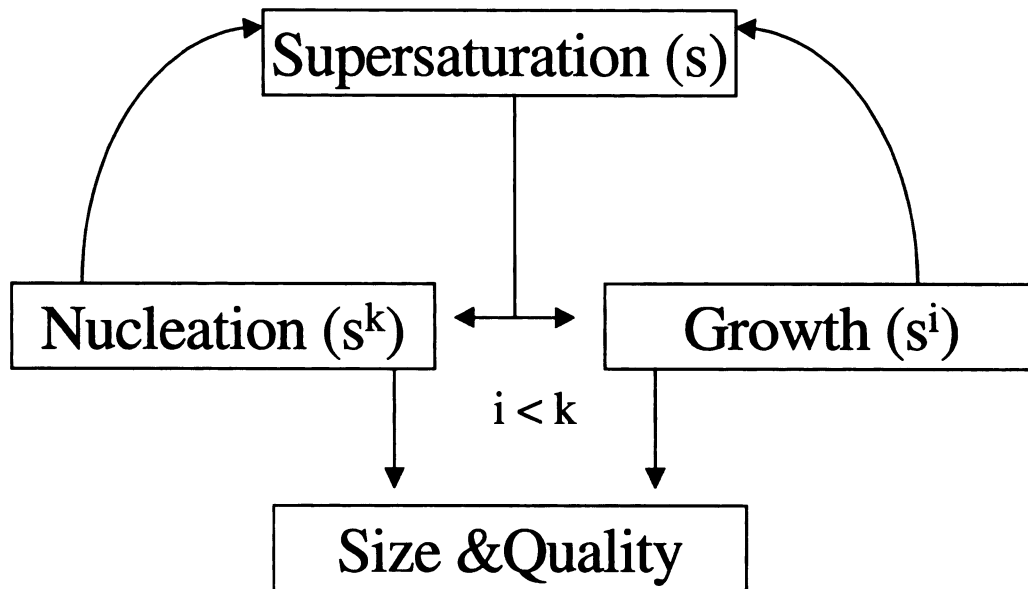


Figure 1.1 The supersaturation feedback loop modified from [20]. This loop describes how both the nucleation and growth rates depend on the level of supersaturation of the protein solution.

nucleation times or will not promote the nucleation of protein crystals. Therefore, it is imperative that a method be discovered that will enable researchers to both monitor and control protein crystallization.

There are a number of methods that are commonly employed to reduce the solubility, or increase the level of supersaturation, of protein solutions. These methods include thermal gradients, addition of a precipitant, the evaporation of solvent, and a change in pH [2,3,4,18]. Though the use of thermal gradients and changes in pH are practiced techniques, the methods that are most commonly applied to protein crystallization are the addition of a precipitant and the evaporation of a solvent. The addition of a precipitant can include the addition of soluble organic and inorganic salts, the addition of volatile organic solvents, or the addition of polymers such as polyethyleneglycol (PEG). These additives alter the composition of the protein solution and decrease the solubility of the protein. As a result the level of supersaturation of the protein solution is increased. The evaporation of a solvent results in an increase in the protein concentration. As the concentration of the protein solution increases, the solution becomes supersaturated.

The schools of thought, concerning protein crystallization mechanisms can be divided into two categories: electronic and entropic. The electronic interactions include electrostatic effects, dispersion forces, hydrogen bonding, and hydrophobic interactions [2,3,18], while the entropic view encompasses volume exclusion and hydration sphere competition arguments [1,2,3,4]. Though this point is still very much in debate, the true mechanism is probably a combination of these effects. For the remainder of this discussion the electrostatic interactions will be used to describe the typical protein crystallization experiments.

## **The Hanging Drop Crystallization Technique**

The addition of a precipitant and the evaporation of solvent are considered batch and vapor diffusion techniques, respectively [1,4,18]. The batch technique mixes equal volumes of twice the desired concentration of precipitate and protein solution. The addition of the inorganic salts decreases the solubility of the protein solution. This has been termed “salting out” [1,4]. It has been suggested that an increase in ionic strength of a protein solution aids in shielding the surface charges of the protein, thereby allowing the protein monomers to approach one another. The vapor diffusion technique concentrates the protein solution beyond solubility by evaporating the solvent. The combination of these techniques is termed the hanging drop experiment.

Figure 1.2 depicts the hanging drop experiment. The hanging drop experiment draws likeness to both the batch and vapor diffusion experiments. A protein drop, which contains a small amount of precipitant, is placed above a reservoir with a higher ionic strength. The top of the vessel is greased to insure an airtight seal. Typically the reservoir buffer contains twice the concentration of precipitant than the hanging drop of protein solution. The drop and reservoir attempt to reach equilibrium, which results in water being drawn from the drop into the reservoir.

Figure 1.3 is a protein solubility diagram. The smooth curve represents the protein solubility as a function of increasing ionic strength. The points labeled A, B, and C and the arrows illustrate a hypothetical hanging drop experiment. Initially, the hanging drop contains low concentrations of both protein and precipitant at point (A). The reservoir and hanging drop begin to equilibrate, and water is drawn from the drop to the reservoir. As the water is withdrawn the concentrations of both the protein and precipitant in the

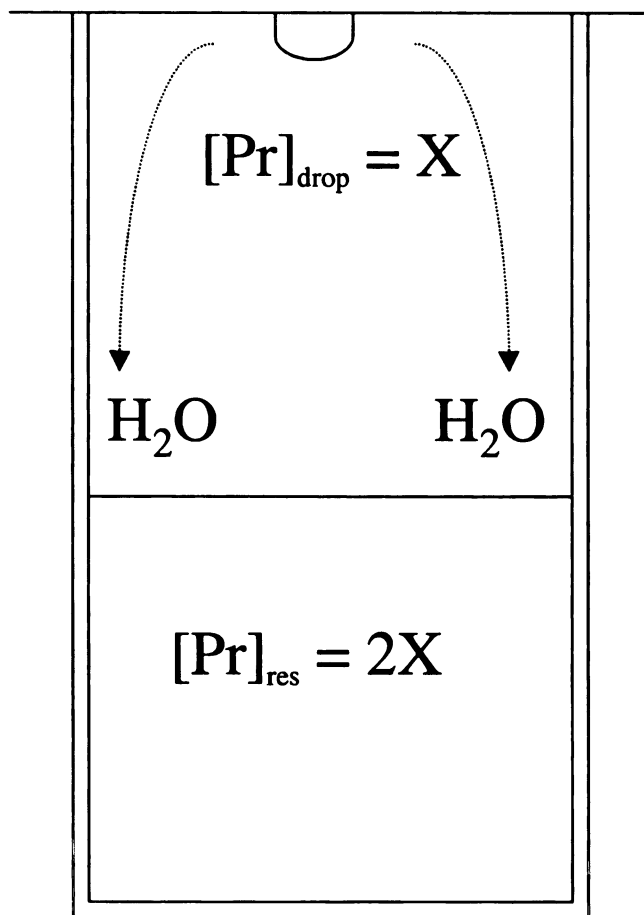


Figure 1.2 This illustration depicts the hanging drop experiment. A protein drop is inverted over a reservoir of higher ionic strength.  $[\text{Pr}]_{\text{res}}$  and  $[\text{Pr}]_{\text{drop}}$  indicate the precipitant ionic strength in the reservoir and the drop, respectively. Typically, the reservoir contains twice the number of ions as the hanging drop. The net result is that water is drawn from the drop to the reservoir.

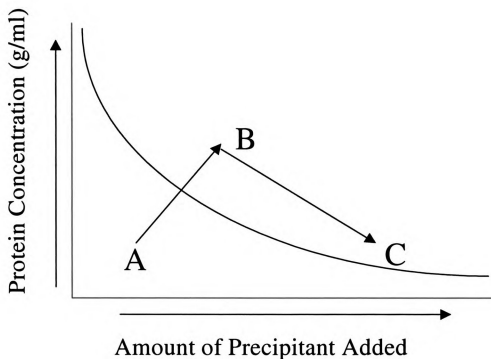


Figure 1.3 A diagram of the hanging drop experiment in terms of protein concentration and solubility. The smooth curve describes the protein solubility with respect to increasing amounts of precipitant. Initially, the hanging drop of protein is below solubility at a low concentration of both protein and precipitant (A). As water is drawn from the hanging drop, the drop concentrates. Eventually, the drop becomes supersaturated and nucleation occurs (B). The protein continues to nucleate and grow crystals, resulting in a decrease in concentration (C).

hanging drop increase. The arrow between points (A) and (B) follows this increase in concentration. Eventually, the increase in protein and precipitant concentrations drives the protein beyond solubility. This increase in concentrations occurs until the protein solution can no longer sustain the level of supersaturation and the protein nucleates (B). The protein solution continues to nucleate and grow crystals, resulting in a decrease in concentration (C). The process will terminate when the protein solution returns to a solubility concentration.

The hanging drop experiment, as all crystallization processes, is a path dependent experiment. The arrows in Figure 1.3 merely serve to illustrate the possible trajectory a protein concentration profile may follow. The difference in ionic strengths between the hanging drop and the reservoir dictates the rate at which the hanging drop will supersaturate. In turn this will determine whether nucleation, growth, or precipitation will be favored. Without *a priori* knowledge of a protein's solubility, the hanging drop method is a trial and error technique. The crystallization conditions for a protein are found by adventitious means via the hanging drop experiment.

In spite of any shortcomings the hanging drop method is the most often implemented experiment to acquire protein crystals [1,4,18]. Plastic trays containing approximately thirty reservoirs are typically employed in matrix screening experiments [1,4]. In global screening experiments protein solutions are exposed to a broad range of reservoir conditions, and the hanging drops are allowed to equilibrate with the reservoirs. After days, weeks, or months a crystal may form. If a protein crystal does form, another screening experiment is performed. The conditions of the reservoir, which produced a protein crystal, are now altered slightly. The second round of screening experiments

attempts to optimize the crystallization conditions of the protein. Though these screening methods are simplistic and labor intensive, a recent issue of the *Journal of Crystal Growth* (196), dedicated solely to the crystallization of biological macromolecules, reported three new protein crystal structures using these screening methods [25,26,27].

Performing crystallization experiments via screening methods in a hanging drop is a daunting task. A change of only a few percent in either ionic strength or pH can completely alter the solubility of the protein and the outcome of the hanging drop experiment. For this reason the number of screening experiments necessary to determine the crystallization conditions of a protein can quickly increase. In an attempt to reduce the number of screening experiments, some research has shifted emphasis from prediction of crystallization conditions to control of the hanging drop experiment.

### **Control of Protein Crystallization Experiments**

Three techniques have been successful in monitoring and controlling crystallization experiments including DLS combined with humidity sensors [14], gravimetric analysis [15], and a thermal gradient approach [16]. The focus of this section is to discuss the experiments, measurements, and shortcomings of each technique related to the crystallization of lysozyme.

The first of these techniques combines the ability of DLS to detect trends in particle size combined with humidity sensors to observe the evaporation rate of water from the drop. This method monitors the increase of aggregate size and presence of small crystals via the DLS response. The humidity sensor measures the relative humidity in the reaction vessel and determines the amount of water leaving the hanging drop as the drop

concentrates. The relative humidity within the reaction vessel is altered by nitrogen flowing across the protein solution. Through regulation of the flowrate of nitrogen the evaporation of water from the protein can be controlled. Therefore, the rate at which the protein becomes supersaturated can be varied.

The DLS measurement allows particle sizes to be monitored; however, this measurement is not specific. Anything in the protein drop, including protein aggregates, denatured protein, protein fragments, buffer molecules, dirt and impurities, or scratches and imperfections on the wall of the glass container, can cause light to scatter. This may give erroneous readings that indicate the formation of protein crystals. Assuming that the experiment is ideal and only protein aggregates scatter, the technique is still flawed. The time autocorrelation function (TCF), which correlates the scattering angle with particle size, is based on spherical particles. Though this may be a good approximation for protein monomers, large protein aggregates and nuclei are definitely not spherical. Additionally, the TCF models usually break down once the particle sizes reach about one micron [14].

The gravimetric technique employs a modified electronic balance. A reservoir surrounds the balance, which is enclosed to keep an airtight seal. Three to five protein drops are placed on the balance and the weight of the drops is monitored. As the drops and reservoir equilibrate, the weight of the drops will decrease. The gravimetric analysis monitors the amount of water leaving the drop but neglects the protein in the drop. This measurement cannot differentiate between the phases of the protein, nor can it detect whether crystals or precipitate are forming. Though the rate at which the protein drop



supersaturates is important in determining the outcome of the experiment, protein in solution should also be monitored.

The technique based on temperature control attempts to control batch protein crystallization experiments [15]. Small volumes of protein solution are subjected to programmed temperature changes. Typically, temperatures varying between 5°C and 30°C are employed in altering the solubility of the protein. This method cannot monitor the protein solution *in situ*, and can be considered another screening technique. Additionally, proteins are highly temperature sensitive and could be subject to thermal denaturation or the creation of different polymorphic crystal structures.

In order to control a protein crystallization experiment the concentration of the protein and the amount of water must be measured simultaneously. The DLS/humidity technique monitors both of these factors; however, two separate measurements are required and the interpretation of the DLS data is suspect. The gravimetric technique shows success in measuring the rate of water evaporation; however, this experimental design neglects the protein in the solution completely. Though the authors claimed success in controlling batch protein crystallization experiments via thermal gradients, the success was limited. A closer investigation of the experiment revealed that the thermal gradient method was merely another screening technique.

### **Vibrational Spectroscopy**

Due to the success of previous crystallizations monitored via vibrational spectroscopy [21,22,23,24], both attenuated total reflectance infrared (ATR-IR) spectroscopy and Raman spectroscopy were examined as possible methods to monitor and control protein

crystallization. Also, since these vibrational spectroscopies directly probe the vibrations due to specific chemical bonds there is no danger of misinterpretation of data as there is with DLS measurements. The hanging drop of protein can be considered a two component mixture, comprised of water and protein. Since the water and protein have distinct vibrational spectra, one measurement is able to differentiate between these species.

Light is an electromagnetic wave composed of an electric vector and a magnetic vector [28]. The vectors are perpendicular to one another. If the electric field of the incident wave interacts with matter, light can be absorbed or scattered. Infrared spectroscopy and Raman spectroscopy are absorbance and scattering techniques, respectively, which probe the vibrational and rotational energy levels of a molecule [28,29,30,31]. Molecules can exhibit either Raman or infrared activity due to different selection rules. Absorbance occurs when the dipole moment changes during a molecular vibration [28,29], and the Raman effect is caused by an oscillating induced dipole moment [28,29]. Therefore, the techniques are said to be complementary.

Vibrational spectra have been used to determine the structure and function of proteins [29,30,32]. The vibrational spectrum of a protein contains many vibrational transitions, which give rise to broad bands due to overlap. The vibrational spectrum of a protein contains contributions from several amino acid side chains and the backbone of the peptide chain. The three most common vibrational bands to protein spectra are the Amide I, II, and III vibrational modes. Miyazawa first studied these vibrational modes using N-methylacetamide, the simplest molecule that contains an amide bond, in 1958 [33]. The frequencies associated with the vibrational modes were first calculated and

later verified by experiment. The Amide I, II, and III vibrational modes are centered at  $1653\text{ cm}^{-1}$ ,  $1567\text{ cm}^{-1}$ , and  $1275\text{ cm}^{-1}$  respectively [33]. It was discovered that the Amide I band was primarily due to the C=O stretch, the Amide II band vibration was due to the N-H in-plane bend and the C-N stretch, and the Amide III band contained nearly equivalent contributions from the C-N stretch and the N-H in-plane bend [33]. Further experiments have determined that the Amide I and III vibrational modes are both infrared and Raman active, while the Amide II mode is Raman inactive [28,29,30,31].

Attenuated total reflection spectroscopy is based on the presence of an evanescent wave in an optically rare medium, a lower index of refraction, in contact with an optically denser medium in which a propagating wave is undergoing total internal reflection [29]. Figure 1.4 is an illustration of this phenomenon. The placement of an optically rarer medium,  $n_2$ , in contact with the denser medium,  $n_1$ , causes the interaction between the evanescent wave and the absorbing medium [29]. The internal reflection element contains the propagating incident wave. The evanescent wave is a component of the propagating wave, which decays exponentially. The field intensity in the rarer medium is nonzero, and there is an instantaneous normal component of energy flow into the rarer medium [29]; however, the time average of this energy is zero. Therefore, there is no loss of energy of the propagating wave and it is internally reflected [29]. Consequently, information specific to the absorbing medium is conveyed by the propagating wave.

Since the evanescent wave decays exponentially, it can only interact with a medium near the surface of the internal reflection element. The penetration of the exponentially decaying wave can be described by a parameter called the depth of penetration [29]. This parameter is related to the angle of incidence of the radiation, the wavelength of the

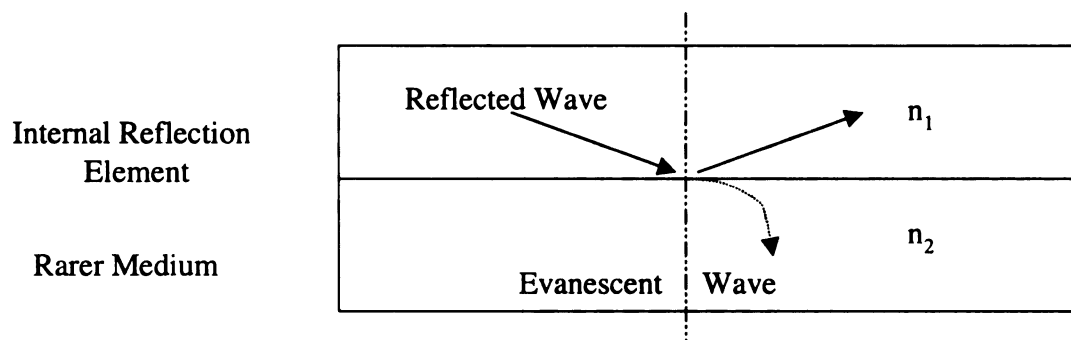


Figure 1.4 A schematic of the operation of attenuated total internal reflection infrared spectroscopy. The optically denser medium,  $n_1$ , is in contact with the optically rarer medium,  $n_2$ . The long vertical line, symbolized by dots and dashes, represents a line normal to the internal reflection element and the rarer medium. The evanescent field is generated by the infrared radiation and penetrates into the rarer medium (sample). The evanescent wave decays exponentially. As a result the sample and internal reflection element must be in intimate contact.

radiation, and the index of refraction of the rarer medium with respect to the index of refraction of the internal reflective element. The use of ATR-IR allows the solution phase of crystallizing systems to be monitored *in situ*, without separation from the solid phase [21,22,23,24].

Raman scattering is caused by the scattering of the incident radiation as it interacts with the electrons in a molecule. Scattering can be elastic resulting in the same frequency of the incident radiation, known as Rayleigh scattering, or it can be inelastic and categorized as Stokes or anti-Stokes Raman scattering [28,30,31]. The Stokes shift is the scattering of light at a longer wavelength (lower energy), while an anti-Stokes shift results in the scattering of light at a shorter wavelength (higher energy) [28,30,31]. The Raman process involves two photons of varying energy. The incident photon and the scattered photon differ in energy due to the inelastic interaction between the incident radiation and the molecule [28,30,31]. Figure 1.5 depicts an energy diagram of a molecule. The incident radiation elevates the molecule to a vibrational excited state. The net effect is an increase or decrease in vibrational energy level of the molecule.

Though protein crystallization has not previously been studied using Raman spectroscopy, there are certain advantages of Raman spectroscopy that make it an ideal for such measurements. Raman vibrational bands are typically sharper than corresponding vibrational bands in infrared spectra [28]. Water absorbs strongly in the infrared spectrum near  $1600\text{ cm}^{-1}$  [29,30,32]. Other than the water peak centered near  $3000\text{ cm}^{-1}$ , water scatters poorly in Raman spectroscopy. Therefore, Raman spectroscopy is ideal for measurements in aqueous media the solvent of choice for protein studies.

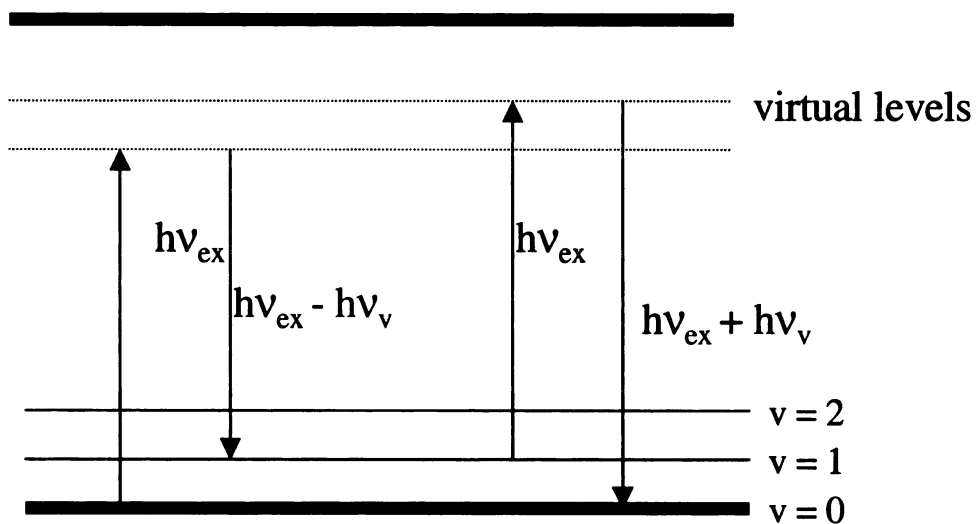


Figure 1.5 Energy-level diagram illustrating Raman scattering: dark solid lines = electronic states, solid lines = vibrationally excited states, dashed lines = virtual states

Finally, unlike ATR-IR that requires intimate contact between the solution and internal reflection element, Raman spectroscopy is noninvasive and does not require contact with the protein solution.

### **Partial Least Squares Regression**

Protein crystallization experiments are conducted at low protein concentrations, leading to low absorbance values in infrared spectroscopy and low intensities in Raman spectroscopy. Water is a major interfering species in the infrared spectrum of a protein. Furthermore, proteins are notoriously poor scattering molecules in Raman spectroscopy. As a result monitoring changing protein concentrations *in situ* relies on distinguishing small changes within the protein spectrum. Therefore, the challenge in monitoring protein crystallization experiments is in accurately predicting the concentration of the protein. Typically univariate calibration and prediction techniques, including peak areas, maximum absorbances or intensities, and peak intensity ratios, are employed in determining concentrations. These univariate approaches can lead to poor experimental precision.

Multivariate data analysis correlates statistically observed spectral variations with known sample properties, making qualitative and quantitative analysis of spectra much easier [34,35,36]. Multivariate calibration and prediction offers a number of advantages over univariate techniques. Multivariate techniques can analyze data for multiple components simultaneously, improve precision of prediction through multiple redundant measurements, and facilitate fault detection through multiple measurements [34].

Therefore, partial least squares regression analysis (PLS) was chosen to correlate and model the protein concentrations with the vibrational spectral features of lysozyme.

PLS is one of the most widely used multivariate calibration techniques in chemometrics [34]. PLS empirically models the variation in the data set and reduces the dimensionality of the data set [34,35]. The mathematics and algorithms governing PLS regression have been described elsewhere [34,35,36,37]. The modeling and regression components of PLS will be described as a “black box” [37]. Figure 1.6 depicts a flow chart of the PLS regression procedure as a “black box” approach.

The method requires three inputs that include the data matrix (spectra), the concentration matrix, and the unknown data matrix (spectrum). The data matrix and the concentration matrix correspond to the protein standards, and should be determined via two independent methods. The data matrix is comprised of vibrational spectra from either infrared or Raman spectroscopy and the concentration matrix is determined from measured weights of protein and volumes of buffer. The PLS algorithm determines an empirical relationship between the protein concentrations and protein spectra [34,35,36]. The PLS algorithm then determines a number of latent variables, which describe the variation in the data set, and builds a regression model. The third input is the spectrum or spectra of unknown concentration. The PLS model is then applied to the unknown data matrix and the output is generated [34,35,36,37]. The generated output is an estimate of the concentration of the unknown data matrix.



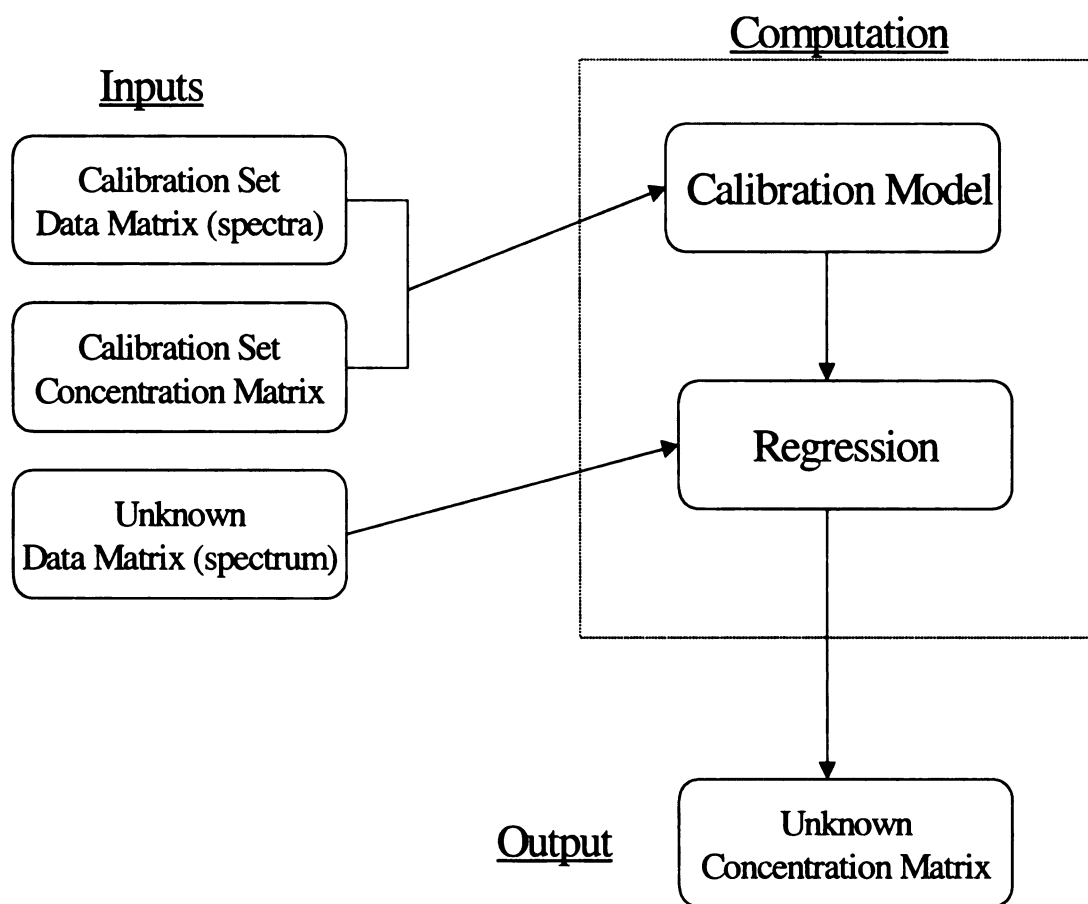


Figure 1.6 A flow chart of the partial least squares regression techniques as a “black box” [37]. The method requires three inputs and produces one output. Two inputs, comprising the calibration set, are needed to build the regression model. The third input is the spectrum of unknown concentration. The PLS algorithm empirically models the variation in the calibration set and builds a regression model. The output is the estimated concentration matrix of the species responsible for the unknown spectrum.

## Literature Cited

- [1] H.W. Wycof, C.H.W. Hirs, and S.N. Timasheff, *Methods in Enzymology* 114 (Academic Press, New York, 1985).
- [2] F. Rosenberger, *J. Crystal Growth* 166 (1996) 40.
- [3] F. Rosenberger, P.G. Velikov, M. Muschol, and B.R. Thomas, *J. Crystal Growth* 168 (1996) 1.
- [4] A. Mcpherson, *The Preparation and Analysis of Protein Crystals* (Krieger Publishing Co., Malabar, FL., 1989).
- [5] C.W. Carter, Jr. and C.W. Carter, *J. Biol. Chem.* 254 (1979) 12219.
- [6] J. Jancarik, and S.-H. Kim, *J. Appl. Cryst.* 24 (1991) 409.
- [7] B.L. Pan and K. A. Berglund, *J. Crystal Growth* 171 (1997) 226.
- [8] M. Muschol and F. Rosenberger, *J. Chem. Phys.* 103 (1995) 10424.
- [9] Y. Georgalis, P. Umbach, A. Zielenkiewicz, E. Utzig, W. Zielenkiewicz, P. Zielenkiewicz, and W. Saenger, *J. Am. Chem. Soc.* 119 (1997) 11959.
- [10] M. Boyer, M.-O. Roy, and M. Jullien, *J. Crystal Growth* 167 (1996) 212.
- [11] Z. Kam, H.B. Shore, and G. Feher, *J. Mol. Biol.* 123 (1978) 539.
- [12] P.A. Darcy and J.M. Weincek, *J. Crystal Growth* 196 (1999) 243.
- [13] N.E. Chayen, *Acta. Cryst.* D54 (1998) 8.
- [14] R.R. Ansari, K.I. Suh, A. Arabshahi, W.W. Wilson, T.L. Bray, and L.J. DeLucas, *J. Crystal Growth* 168 (1996) 216.
- [15] Z.-Y. Shu, H.-Y. Gong, and R.-C. Bi, *J. Crystal Growth* 192 (1998) 282.
- [16] J.R. Luft, D.M. Rak, and G.T. Detitta, *J. Crystal Growth* 196 (1999) 447.
- [17] A.M. Schwartz and K.A. Berglund, *J. Crystal Growth* 203 (1999) 599.
- [18] T. Arakaw and S.N. Timasheff, *Methods in Enzymology* 114 (Academic Press, New York, 1985).
- [19] J.W. Mullin, *Crystallization Third Edition* (Butterworth-Heinamann, Oxford 1993).

- [20] A.S. Meyerson, Handbook of Industrial Crystallization (Butterworth-Heinemann, Boston 1993).
- [21] D.D. Dunuwila and K.A. Berglund, J. Crystal Growth 137 (1994) 561.
- [22] D.D. Dunuwila and K.A. Berglund, J. Crystal Growth 179 (1997) 185.
- [23] D.D. Dunuwila and K.A. Berglund, Org. Process Res. Dev. 1 (1997) 350.
- [24] M. Uusi-Penttilä and K.A. Berglund, J. Crystal Growth 166 (1996) 967.
- [25] T. Soga, H. Sasaki, M. Tanokura, and M. Ataka, J. Crystal Growth 196 (1999) 291.
- [26] I.P. Kuranova, E.V. Blagova, V.M. Levnikov, G.N. Rudenskaya, N.P. Balaban, and E.V. Shakirov, J. Crystal Growth 196 (1999) 313.
- [27] A.M. Stevens, J.L. Pawlitz, R.G. Kurumbail, J.K. Gierse, K.T. Moreland, R.A. Stegeman, J.Y. Loduca, and W.C. Stallings, J. Crystal Growth 196 (1999) 350.
- [28] A.T. Tu, Raman Spectroscopy in Biology Principles and Applications (John Wiley & Sons, New York 1982).
- [29] F.M. Mirabella jr., Internal Reflection Spectroscopy (Marcel Dekker Inc., New York 1993).
- [30] P.R. Carey, Biological Applications of Raman and Resonance Raman Spectroscopies, (Academic Press, New York 1993).
- [31] D.A. Long, Raman Spectroscopy, (McGraw-Hill Co., New York 1977).
- [32] H.H. Mantsch and D. Chapman, Infrared Spectroscopy of Biomolecules, (Wiley Liss Inc., New York 1996).
- [33] T. Miyazawa and T. Shimanouchi, J. Chem. Phys. 29 (1958) 611.
- [34] K.R. Beebe, R.J. Pell, and M.B. Seasholtz, Chemometrics: A Practical Guide, (John Wiley & Sons, Inc., New York 1998).
- [35] K.R. Beebe and B.R. Kowalski, Anal. Chem. 59 (1987) 1007A.
- [36] K. Esbensen, Multivariate Analysis in Practice, (Wennbergs Trykkeri AS, Trondheim Norway 1994).
- [37] T. F. Cullen and S. R. Crouch, *Mikrochem. Acta.*, 126 (1997) 1.

## **Chapter 2: Using ATR-FTIR Spectroscopy to Monitor Lysozyme Crystallization in a Hanging Drop**

### **Introduction**

Infrared spectroscopy can provide information about the chemical nature and the molecular structure of a system. Any change in a system due to reaction or composition should be reflected in the vibrational spectrum. These changes appear in two forms, a change in intensity or a shift in peak position. A change in intensity occurs from a change in the absorbance in infrared spectroscopy. The change in intensity accompanies a change in the composition of the system [1,2]. A change in structure is usually manifested in a shift in peak position [1,2]. The use of infrared spectroscopy will allow the detection of a change in concentration of the protein solution and a change in structure due to the interaction between protein molecules.

Due to the success of previous crystallization experiments monitored via ATR-FTIR spectroscopy [3,4,5,6], ATR-FTIR was employed to monitor lysozyme crystallization. The extension of the ATR-FTIR technology for the measurement of the crystallization process was based upon the assumption that there would be minimal contact between the crystals in slurry and the internal reflection element of the ATR-FTIR probe. As a result of the minimal contact between the crystals and the internal reflection element, there is a decreased probability that the crystals will interact with the evanescent wave. Therefore, measurement of the solution phase without interference from the solid phase is possible. This assertion was proven to be useful in monitoring the decrease in supersaturation in slurries of citric acid [3,4,5] and lysine monohydrochloride [6].

The success of ATR-FTIR in monitoring the solution phase of a crystallizing system is based on the thickness of the wetted surface of the ATR probe. It has been shown empirically that the thickness of the wetted surface is greater than the depth of penetration of the evanescent wave. All previous studies have involved stirred systems, which ensures that the solution in contact with the ATR probe is continuously changing. Therefore, the dynamic concentration of the solution phase could be monitored in real time. Though the hanging drop experiment involves a static system, it was hoped that the diffusion of the lysozyme within the hanging drop would happen quickly enough to allow any changes in solution composition to be monitored. Since protein crystallization experiments tend to take long periods of time, this assumption is justified.

In the hanging drop experiment, water from the exposed surface of the drop diffuses from the drop to the reservoir. The radius of the drop decreases and the concentration of the lysozyme within the drop increases. Though diffusion is expected to return the concentration of the drop to a constant value, initially a lysozyme concentration gradient will form. The outer curved portion of the hanging drop will concentrate more quickly than the remainder of the drop. This will lead the edge of the drop to supersaturate and nucleate. Crystals are expected to form on this boundary away from the glass cover slip. If the hanging drop of protein were placed on the ATR-FTIR probe in a similar fashion, it is expected that the solution phase of the drop and not the solid phase could be monitored.

## Materials and Methods

The applicability of ATR-FTIR spectroscopy for the determination of the lysozyme concentration in a hanging drop was investigated using an ASI Applied Systems, LLC ReactIR series 1000® which employs a DiComp® probe internal reflection element. The ReactIR series 1000® is comprised of an optics module, an electronics module, the K6 conduit, a liquid nitrogen cooled MCT detector, and a DiComp® probe [7]. The optics module contains the infrared source and interferometer. The electronics module allows the optics module, the detector, and the computer to interface. The K6 conduit is an articulated arm that provides a purged path for the infrared source to travel to a remote sampling device and back to the detector [7]. The K6 conduit is comprised of six 45° knuckles (elbows) and two tubes, which allow the probe to be positioned a number of various sampling configurations. The sixth knuckle attaches the probe to the conduit system. The DiComp® probe contains a diamond tip. The diamond tip both rugged and highly sensitive. The tip can be used in solutions ranging in pH from 1 to 14 and temperatures between -80° C and 250° C; it has an optical range of 650 cm<sup>-1</sup> to 4400 cm<sup>-1</sup> [7].

Three times crystallized, dialyzed, and lyophilized chicken egg white lysozyme was purchased from Sigma Chemical Co. and used without further purification. All experiments were performed in a buffer containing 0.1 M sodium acetate at pH 4.2 and ambient temperature. Salt and protein amounts for standards were determined with a Mettler AE50 balance. For all experiments lysozyme was dissolved into the NaCl/buffer system and then filtered through a 45 µm Millipore filter before use. A 5 µl protein drop was deposited on the ATR-FTIR probe. Figure 2.1 contains an illustration

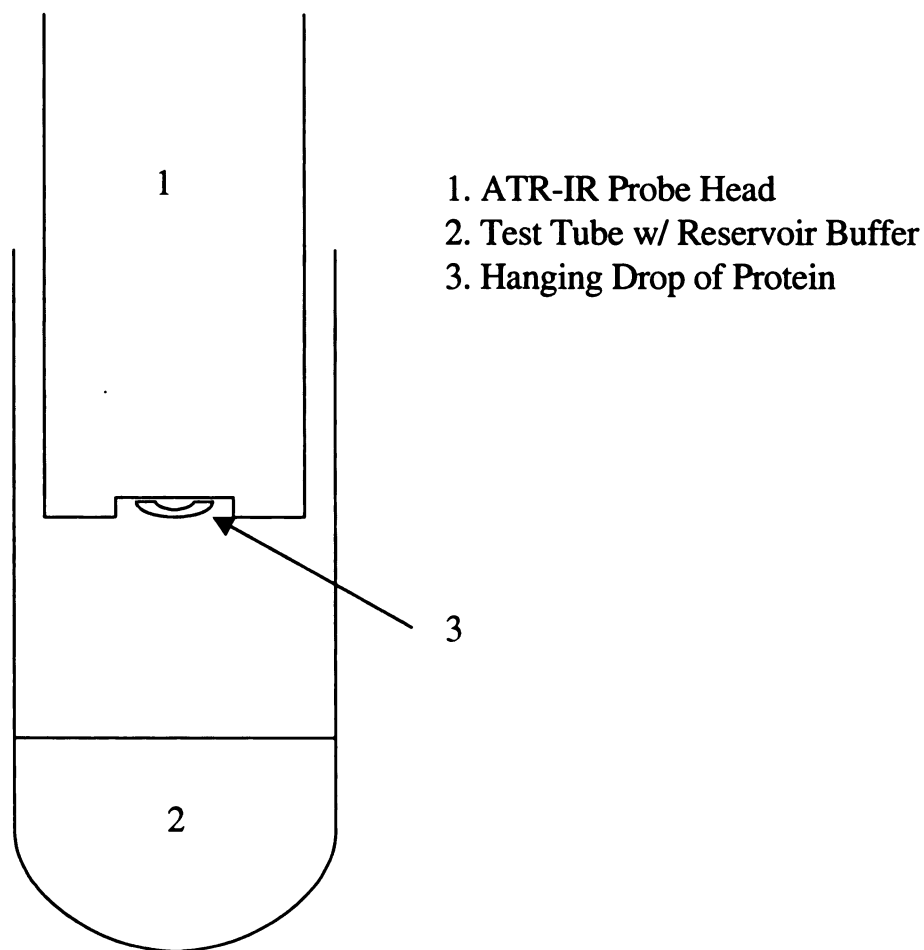


**Figure 2.1** A schematic of the ATR-IR experimental set-up for monitoring protein crystallization in the hanging drop.

of the probe tip. The ATR-FTIR probe was then inverted and placed in a test tube containing 2 ml of a NaCl/buffer reservoir. The gap between the test tube and the probe was wrapped with parafilm® to ensure an airtight seal.

Spectra were acquired for 45 lysozyme standards ranging in concentration from 0 (g/ml) to 0.40 (g/ml). Each spectrum consisted of 250 scans collected over 150 seconds at 8 cm<sup>-1</sup> resolution. The infrared spectra of the standards were used to construct a partial least squares (PLS) regression model using QuantIR®, a PLS regression analysis software package by ASI Applied Systems. The PLS model correlates the spectral region from 1570 cm<sup>-1</sup> to 1720 cm<sup>-1</sup> with the concentration (g/mL) of lysozyme. This spectral region encompasses a broad vibrational band due to the Amide I combination stretch centered at 1650 cm<sup>-1</sup> [1,2]. A leave one out cross validation performed on the standards determined that the model had a root mean square error of calibration (RMSEC) of  $\pm 0.002$  g/ml.

## **Results and Discussion**

The initial ATR-IR experiments were divided into two portions. The first was an investigation of the organization of the lysozyme in solution and the second monitored the lysozyme crystallization experiment in the hanging drop experiment. The study of the organization of the lysozyme molecules in solution investigated the possibility of aggregation prior to nucleation. If the assumption that crystals formed only in the hanging drop were incorrect, ATR-IR experiments could measure the extent of organization as a means of monitoring the hanging drop. If crystals or precipitate were to form at the internal reflection element and hanging drop interface, the recorded ATR-IR



absorbances would be larger than the absorbances produced by the lysozyme standards. Therefore, prediction of a concentration would lead to a nonphysical result. However, if the position of the Amide I band were monitored as a function of concentration, the degree of organization of the lysozyme system could be obtained in real time.

The monomeric unit of lysozyme within the crystal lattice contains 185 molecules of water per molecule [8]. The lysozyme crystal can therefore be thought of as an extremely concentrated protein solution. Solutions ranging in concentration from 0.0 g/ml to 0.5 g/ml of lysozyme, lysozyme precipitate, and crystals of lysozyme were analyzed via ATR-IR. The derivative of each spectrum was taken to determine the position of the Amide I stretch. Figure 2.2 illustrates the results of these experiments. Each point is the average of at least 6 different measurements.

The concentration of the crystal was determined using 185 water molecules per monomer of lysozyme. The concentration of the precipitate was determined by taking the ratio of the spectra of the lysozyme precipitate and the lysozyme crystal. A shift in peak position from a higher to a lower wavenumber ( $\text{cm}^{-1}$ ) is indicative of a change in conformation, typically associated with a change in the degree of organization of the system [2,9]. Figure 2.2 clearly demonstrates this behavior. Though the error in peak position ( $\text{cm}^{-1}$ ) for the crystal and precipitate of lysozyme indicates that there may not be a difference between the solid phases of lysozyme, the graph suggests that there is a conformational change associated with an increase in lysozyme concentration. Whether the conformational change is due to a tightening of the lysozyme structure or the formation of prenucleate aggregates is unknown. However, the curve in Figure 2.2 can

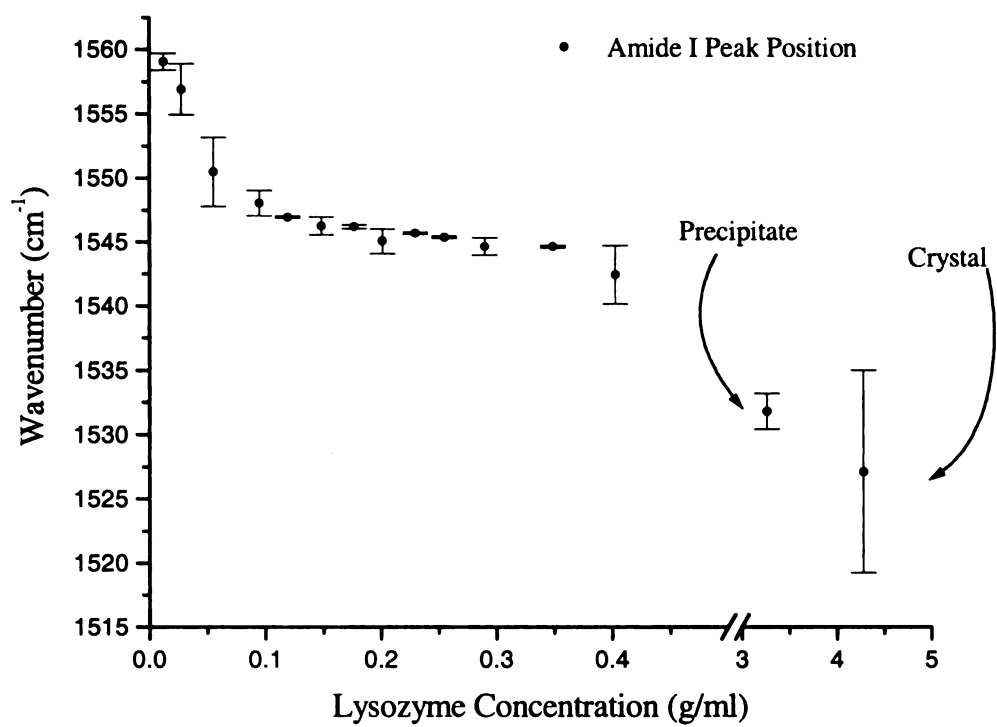


Figure 2.2 A graph representing the relationship between the Amide I peak position in wavenumbers ( $\text{cm}^{-1}$ ) and concentration of lysozyme. As expected the peak shifts toward lower wavenumbers as the concentration of lysozyme approaches that of a crystal.

be employed to monitor hanging drop experiments in the event that crystals form on the internal reflection element.

Two sets of lysozyme hanging drop experiments were attempted. The first consisted of control experiments. The reservoir and hanging drop ionic strength conditions were equal in these experiments. Lysozyme crystals should not form under the control experimental conditions. The second set of experiments employed varying reservoir and hanging drop ionic strengths. The difference between the ionic strengths of the reservoir and the hanging drop will cause water from the hanging drop to evaporate. The level of supersaturation of the hanging drop will increase and should promote the nucleation of lysozyme crystals. Figure 2.3 contains representative concentration profiles from both sets of experiments.

The starting lysozyme concentration for both experiments was approximately 0.26 g/ml and the initial ionic strength of the hanging drop was 0.34 M. The control experiment, represented by the circles, had a reservoir ionic strength of 0.34 M, and the crystallization experiment, represented by the triangles, had a reservoir ionic strength of 2.67 M. Lysozyme, under the conditions of the control experiment, should not form crystals or precipitate. However, lysozyme subjected to the harsh conditions of a 2.67 M ionic strength reservoir should produce crystals within two hours. The experiments were monitored for 4.5 hours. Spectra were taken in intervals of 5 minutes and processed by the PLS model. The graph in Figure 2.3 compares the concentration profiles of these two experiments.

It was expected that for the control experiment the concentration profile would remain constant. However, the concentration profile increases from 0.26 g/ml to a steady

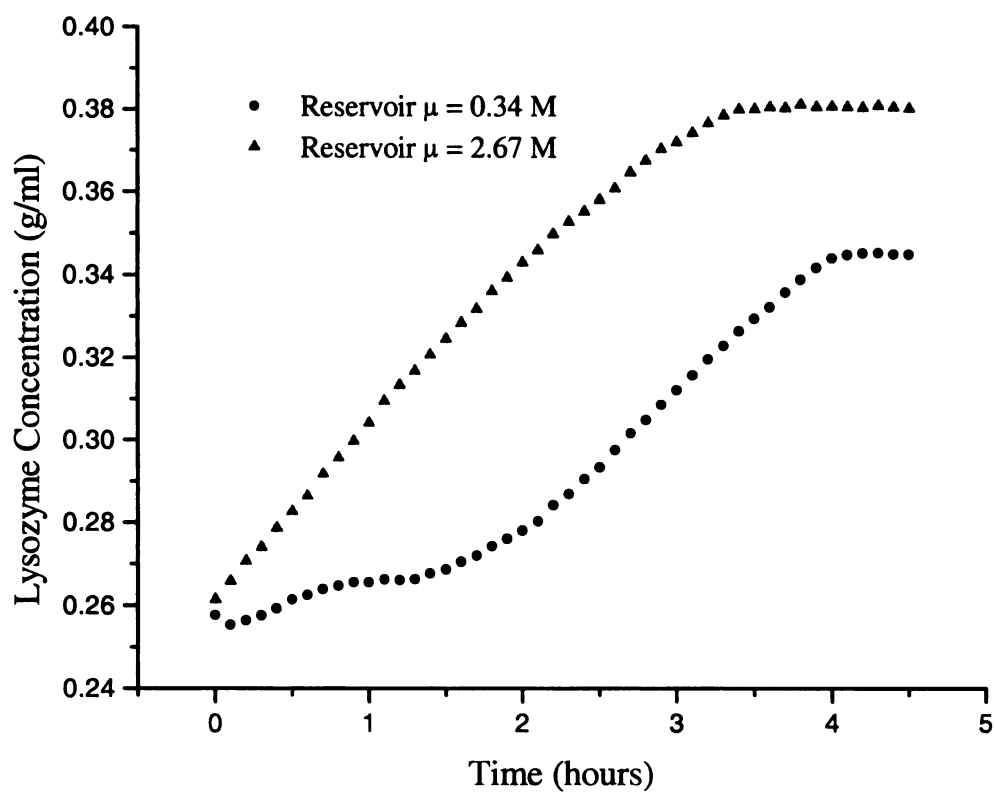


Figure 2.3 A comparison of the concentration profiles of a control experiment (circles) and a crystallization experiment (triangles). Both profiles increase in concentration eventually reaching a steady state value. The process that these profiles describe is the adsorption of lysozyme onto the diamond tip of the ATR-IR probe.

value of 0.34 g/ml. An explanation of this would be that crystals formed at the interface between the hanging drop and the internal reflection element. The Amide I peak position of the lysozyme at the beginning of the control experiment was approximately  $1547\text{ cm}^{-1}$ . The Amide I peak position after 4.5 hours had only changed slightly to  $1545\text{ cm}^{-1}$ . According to the relationship between the Amide I peak position and the concentration of lysozyme depicted in Figure 2.2, the final Amide I peak position of  $1545\text{ cm}^{-1}$  is well out of range of a peak position indicating the presence of crystals. Finally, the hanging drop was removed from the ATR-IR probe and investigated by a microscope. No crystals were present in the hanging drop. However, a film was visible that formed at the interface between the hanging drop and the internal reflection element.

Examination of the hanging drop experiment subjected to the 2.67 M reservoir ionic strength revealed that lysozyme crystals were present in the drop. However, earlier experiments had revealed that lysozyme under these conditions would form crystals within two hours. The concentration profile in Figure 2.3 does not indicate anything unusual near two hours. The profile increases linearly to a steady value of 0.38 g/ml. The Amide I peak position was compared between the initial spectrum and the final spectrum. The Amide I peak position varied from approximately  $1547\text{ cm}^{-1}$  to  $1544\text{ cm}^{-1}$ . Again this did not indicate the formation of crystals at the interface between the drop and the internal reflection element. The drop was removed from the ATR-IR probe revealing the formation of a film at the internal reflection element hanging drop interface.

It has been documented that proteins will adhere to ATR surfaces [1]. The charged surface of the protein binds easily to the inorganic surfaces of the internal reflection elements. The process that the concentration profiles are monitoring in Figure 2.3 is the

adsorption of lysozyme onto the diamond surface of the ATR-IR probe. The ATR-IR method also requires intimate contact between the substance being monitored and the internal reflection element. The ATR-IR probe could therefore serve as a nucleation site for crystals or precipitate. The ATR-IR method is invasive to the hanging drop systems under study. Therefore, ATR-IR was eliminated as a possible method of monitoring protein crystallization in the hanging drop experiment.

## **Literature Cited**

- [1] F.M. Mirabella jr., Internal Reflection Spectroscopy (Marcel Dekker Inc., New York 1993).
- [2] H.H. Mantsch and D. Chapman, Infrared Spectroscopy of Biomolecules, (Wiley Liss Inc., New York 1996).
- [3] D.D. Dunuwila and K.A. Berglund, J. Crystal Growth 137 (1994) 561.
- [4] D.D. Dunuwila and K.A. Berglund, J. Crystal Growth 179 (1997) 185.
- [5] D.D. Dunuwila and K.A. Berglund, Org. Process Res. Dev. 1 (1997) 350.
- [6] M. UusiPenttila and K.A. Berglund, J. Crystal Growth 166 (1996) 967.
- [7] Users Guide Reaction Analysis Systems 3<sup>rd</sup> Edition v2.0 (ASI Applied Systems, LLC 1997).
- [8] K.P. Wilson, B.A. Malcolm, and B.W. Matthews, J. Biol. Chem. (1992) 267.
- [9] A.T. Tu, Raman Spectroscopy in Biology Principles and Applications, (John Wiley & Sons, New York 1982).

### **Chapter 3: The Use of Raman Spectroscopy for *In Situ* Monitoring of Lysozyme Concentration during Crystallization in a Hanging Drop\***

\*Journal of Crystal Growth 203 (1999) 599.

#### **Summary**

Fiber optic Raman spectroscopy combined with a partial least-squares regression model was investigated as a means to monitor lysozyme concentration during crystallization in a hanging drop experiment in real time. Raman spectral features of the buffer and protein were employed to build the regression model. This model was used to calculate the compositional changes within the hanging drop. The use of fiber optic technology coupled with Raman spectroscopy, which is ideal for use with aqueous media, results in a powerful noninvasive probe of the changing environment within the solution. These preliminary findings indicate that solubility as well as supersaturation measurements can be made.

#### **Introduction**

Many studies on the crystallization process of proteins have focused on prediction of whether a particular solution will form crystals. These studies have included fluorescence based anisotropy measurements [1], static light scattering [2,3,4], dynamic light scattering [2,5,6], and microcalorimetric techniques [4]. Each of these studies have cited the bottleneck in determining the three dimensional structure of proteins as the growth of crystals of suitable size and quality. These studies have tried to reduce the number of assays necessary to determine advantageous conditions for protein crystallization. However, each of the preceding experiments employed batch



crystallization techniques, rather than the hanging drop method [7,8], which is preferred by crystallographers. Alternatively, we have chosen an approach for monitoring the hanging drop experiment rather than focusing on the predictive nature of a particular technique. We propose a method of measuring the level of supersaturation of the hanging drop *in situ*.

The ability to measure the real-time concentration of a protein within the hanging drop will allow for eventual control of the experiment. The technique chosen, which allows us to monitor the drop, is Raman spectroscopy. Raman spectroscopy has previously been applied to biological macromolecules in terms of deducing structure and function [9,10]. The normal Raman spectrum of a protein under nonresonance conditions contains contributions from several amino acid side chains and the backbone of the peptide chain [9,11]. Another important consideration is that aside from the OH stretching region between 3000 and 3500  $\text{cm}^{-1}$ , the Raman spectrum of water is weak and only slightly interferes with the solute [9]. Therefore, Raman spectroscopy is ideal for biochemical experiments in aqueous media.

## **Materials and Methods**

The applicability of Raman spectroscopy toward the determination of solubility and supersaturation was investigated using a Kaiser Optical Systems, Inc. HoloLab Series 1000® which employs a 30 mW Helium Neon Laser at 632.8 nm with a Standard Fiber Injector. A CCD camera, spectrograph, and fiber optic probe comprise the HoloLab Series 1000®. The spectrograph section of the HoloLab Series 1000® utilizes holographic optical elements (HOEs) and provides spectral coverage from 400 to 3650

cm<sup>-1</sup> [12]. The HoloLab system makes use of a notch filter to attenuate the laser line while allowing the Raman spectra to be collected [12]. The fiber optic probe consists of six collection fibers bundled around one excitation fiber [12]. Attached to the tip of the probehead is a 10X microscope objective, which focuses the incident beam. It is this configuration of the HoloLab assembly, which makes these measurements possible.

The fiber optic Raman system provides the freedom to position the probehead directly above the hanging drop of protein. Using a translational stage the hanging drop of protein is then brought into the focal point of the laser. The incident laser light is impinged through the cover glass directly into the hanging drop of protein. Since the cover glass does not scatter well at 632.8 nm, the cover glass is optically transparent to the measurement. This permits the measurement of the concentration of the protein drop without contact of the solution. Due to the attenuation of the incident radiation at 632.8 nm on the order of 10<sup>6</sup> [12], a protein spectrum with a signal to noise ratio ranging between 250 and 450 is readily attainable.

Three times crystallized, dialyzed, and lyophilized chicken egg white lysozyme was purchased from Sigma Chemical Co. and used without further purification. All experiments were performed in a buffer containing 0.1 M sodium acetate at pH 4.2 and ambient temperature. Salt and protein amounts for standards were determined with a Mettler AE50 balance. For all experiments lysozyme was dissolved into the NaCl/buffer system and then filtered through a 45 µm Millipore filter before use. A 5 µl protein drop was deposited on a microscope cover glass. The cover glass was then inverted and placed over a 6 ml vessel containing 2 ml of a NaCl/buffer reservoir. The top of each vessel was greased to ensure an airtight seal.

The laser power incident on the cover glass and protein drop ranged from 19 to 22 mW. Each spectrum consisted of 20 scans collected over 129 seconds at  $8\text{ cm}^{-1}$  resolution. The Raman spectra of the standards were used to construct a partial least-squares (PLS) regression model using QuantIR®, a PLS regression analysis software package by Applied Systems. The PLS model correlates the spectral region from 2700 to  $3600\text{ cm}^{-1}$  with the concentration (g/mL) of lysozyme. This spectral region encompasses broad vibrational bands due to the protein CH stretches centered at  $2950\text{ cm}^{-1}$  [9, 11] and the water OH stretches centered at  $3230\text{ cm}^{-1}$  [9, 11].

The PLS model consists of 31 standards, ranging from 0.0 to 0.29 g/ml, and has a standard error of  $\pm 0.01\text{ g/ml}$  determined by a leave one out cross validation. The standard at 0.0 g/ml was necessary because the acetate buffer contributes to the vibrational band near  $2950\text{ cm}^{-1}$ . The NaCl was not included in the standards used to develop the PLS model, since the dissociated  $\text{Na}^+$  and  $\text{Cl}^-$  ions do not exhibit a vibrational mode. It is therefore possible to accurately monitor the change in composition of the lysozyme drop in terms of both water and protein content.

## **Results and Discussion**

The goal of this chapter is to demonstrate that this measurement can be made. The first set of experiments determined a solubility curve for lysozyme. Protein drops ( $5\text{ }\mu\text{l}$ ) containing enough NaCl to give an initial ionic strength of 0.2 M were suspended above reservoirs ranging in ionic strength from 0.3 to 1.5 M. These values of ionic strength reflect the number of ions in solution due to the acetate buffer, NaCl, and pH. The

vessels were then allowed to come to equilibrium at room temperature. After two weeks Raman spectra of the protein drops were taken.

Collected Raman spectra were subjected to the QuantIR® PLS method previously described. Figure 3.1 shows the solubility curve determined via this procedure for lysozyme. Each point on the curve is the average of at least 6 measurements. The error bars represent the reproducibility of the experiment and do not reflect that of the PLS method. Precautions were taken to ensure that the liquid phase and not the crystal phase of the hanging drop were measured. The solubility curve in Figure 3.1 is in good agreement with prior reported values of lysozyme solubility made using an absorbance technique [13]. These authors report solubility values of 0.250, 0.150, and 0.020 g/ml at ionic strength values of 0.2, 0.3, and 0.6 M respectively [13].

The hanging drop was then monitored as it changed composition. Figures 3.2 and 3.3 are representative of the concentration profiles generated using this particular method. These figures show the concentration of lysozyme within the drop changing with time. Both drops were monitored for approximately 18 hours. Figures 3.2 and 3.3 begin with lysozyme concentrations near 0.23 and 0.14 g/ml, respectively, and have ionic strengths of 0.2 M. The ionic strengths of the reservoirs for Figures 3.2 and 3.3 are 0.33 and 0.84 M, respectively. It is expected that the protein drop will first concentrate as water is drawn from the drop to the reservoir. Since the ionic strength of the reservoir in Figure 3.3 is more than double that of Figure 3.2, one would expect the protein concentration in the hanging drop to increase more rapidly in Figure 3.3. By linearly fitting the initial data in these two plots, the slope of the line marked A in Figure 3.3 is about two times as steep as line A in Figure 3.2.

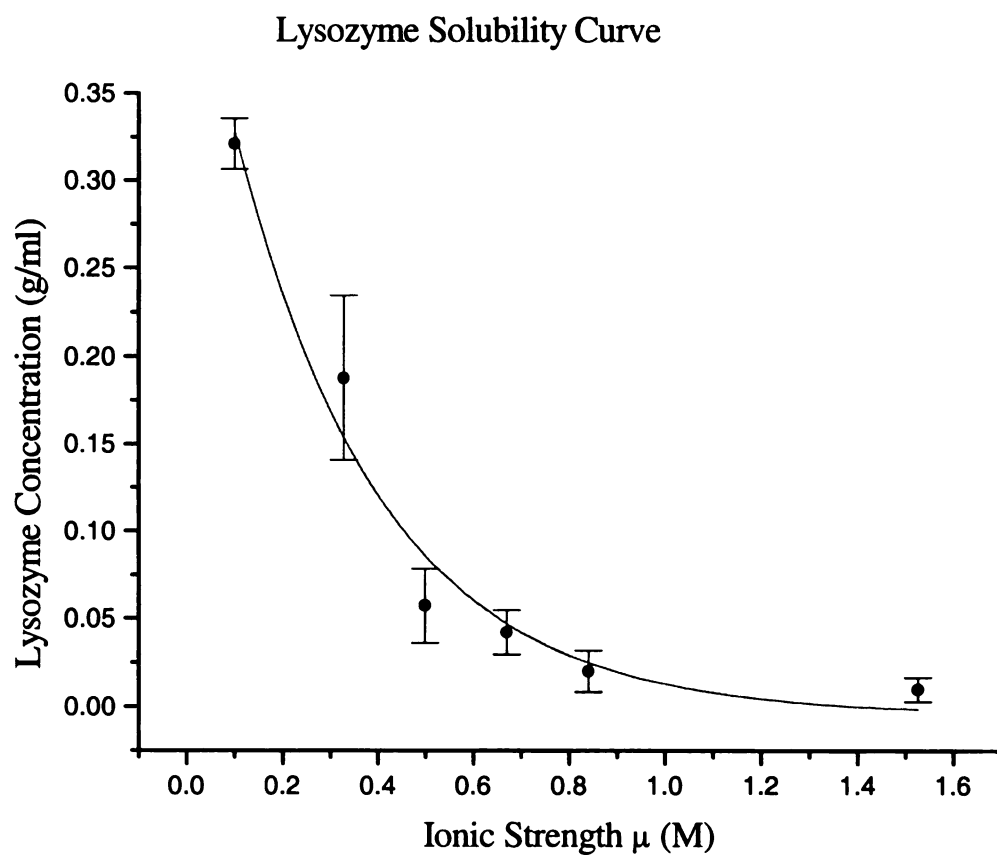


Figure 3.1 Solubilities of lysozyme in buffer solutions of varying ionic strength were determined using Raman spectroscopy. All measurements used 5  $\mu$ l hanging drops of lysozyme solutions.

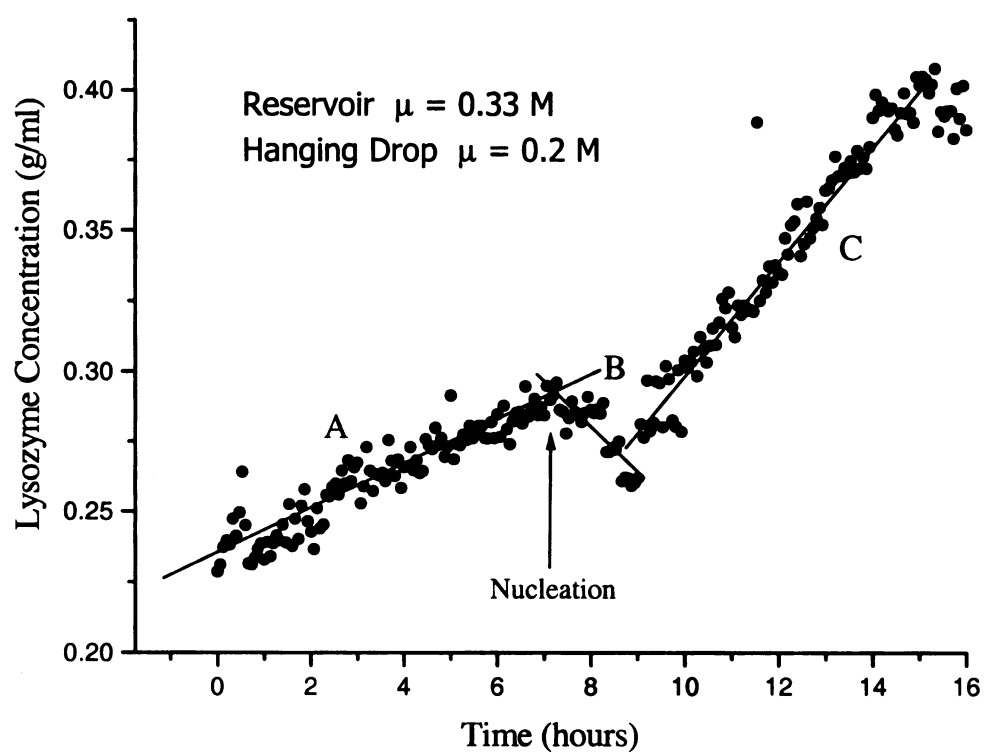


Figure 3.2 Real time concentration change of a hanging drop of lysozyme at 0.2 M ionic strength suspended above a reservoir of 0.33 M ionic strength. The lines represent the following: line A [slope = 0.008 g/(ml·hr)] shows the change in concentration as the hanging drop becomes more concentrated, line B follows the decrease in supersaturation of the drop after nucleation has occurred, and line C follows the growth of lysozyme crystals.

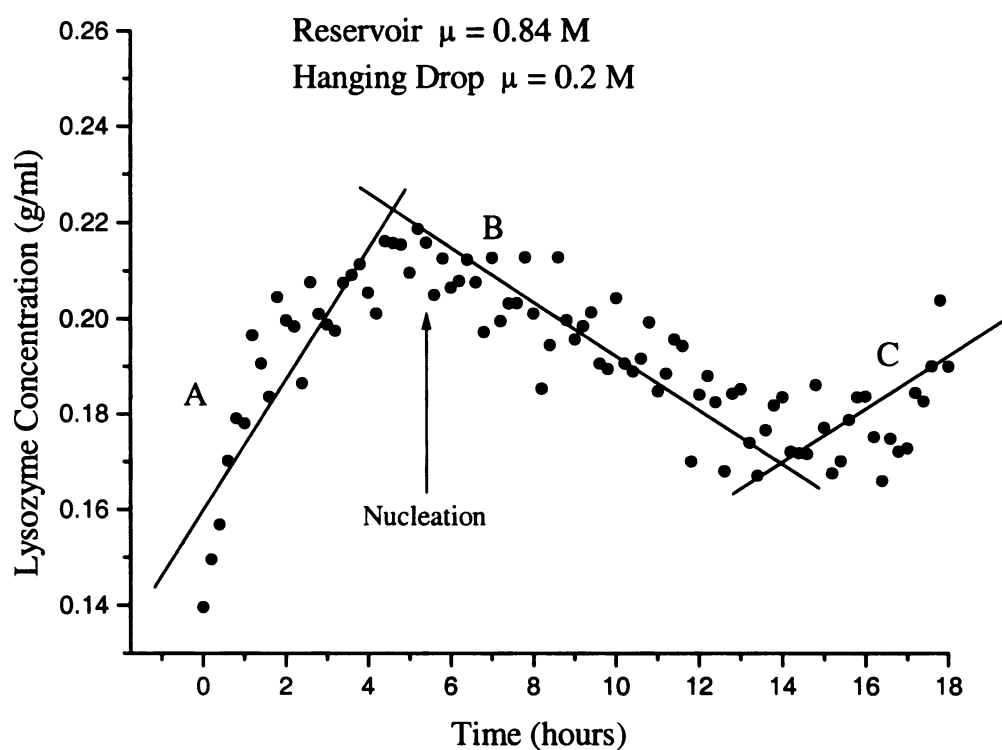


Figure 3.3 Real time concentration change of a hanging drop of lysozyme at 0.2 M ionic strength suspended above a reservoir of 0.84 M ionic strength. The lines represent the following: line A [slope = 0.015 g/(ml·hr)] shows the change in concentration as the hanging drop becomes more concentrated, line B follows the decrease in supersaturation of the drop after nucleation has occurred, and line C follows the growth of lysozyme crystals.

At some later time we expect the drop will reach supersaturation and nucleation will occur. The protein drop should then decrease in concentration as lysozyme nuclei begin to form. In Figures 3.2 and 3.3 the lines marked B reflect the decrease in supersaturation of the lysozyme within the drop. The nucleation event is marked in Figures 3.2 and 3.3 with an arrow. As expected the nucleation of the hanging drop over the higher ionic strength reservoir occurs first. The nucleation event occurs at approximately 7 hours in Figure 3.2 and at approximately 5 hours in Figure 3.3. Finally, the concentration of lysozyme is expected to level off to that of solubility. However in both instances crystals grew directly in the path of the laser. The sudden increase in signal occurs because the concentration of the crystal is much greater than in the bulk solution. The lines marked C in Figures 3.2 and 3.3 indicate these increases.

## Conclusions

This method introduces energy in the form of light into the system, and there may be concern about this effect on the temperature of the system. However, the protein system is a 5  $\mu\text{l}$  drop in a room with a volume on the order of  $10^9$  greater than the protein drop. The laser is small and only produces radiation on the order of 30 mW at the source of the laser and 19 mW at the end of the fiber optic probe. A simple calculation using the heat transfer equation yielded a theoretical temperature increase of  $\pm 0.2^\circ\text{C}$ . Therefore, it is contended that a change in room temperature will have a greater affect on the protein drop than the incident laser radiation. Secondly, agreement in solubility data between the current measurement and previous absorbance measurements made at  $25^\circ\text{C}$  has been shown. Though the solubility data show a large standard error, we would like to



emphasize the fact that this measurement is being made on a 5  $\mu$ l drop of protein *in situ*. Finally, the lysozyme crystals grow indiscriminately within the hanging drop. Crystals form both directly in the path of the laser and in areas of the hanging drop where there is no laser light. This further suggests that the incident laser radiation has a minor effect on the hanging drop. Therefore, the assertion that the method is noninvasive to the lysozyme within the hanging drop appears defensible.

In large part due to the latest technology in the field of Raman spectroscopy, it is possible to measure *in situ* the concentration of a small volume drop of protein. To the authors' knowledge, this work is the first report of a noninvasive real time concentration measurement of the hanging drop experiment based on Raman spectroscopy. The ability to make this type of measurement is the first step in controlling [14] and modeling the hanging drop experiment. This technique will hopefully eliminate the need for guesswork in determining the necessary criteria for protein crystal growth. Additionally, the dynamic control of conditions within the hanging drop is now a possibility.

### **Literature Cited**

- [1] B.L. Pan and K. A. Berglund, J. Crystal Growth 171 (1997) 226.
- [2] F. Rosenberger, P.G. Vekilov, M. Muschol, and B.R. Thomas, J. Crystal Growth 168 (1996) 1.
- [3] M. Muschol and F. Rosenberger, J. Chem. Phys. 103 (1995) 10424.
- [4] Y. Georgalis, P. Umbach, A. Zielenkiewicz, E. Utzig, W. Zielenkiewicz, P. Zielenkiewicz, and W. Saenger, J. Am. Chem. Soc. 119 (1997) 11959.
- [5] M. Boyer, M.-O. Roy, and M. Jullien, J. Crystal Growth 167 (1996) 212.
- [6] Z. Kam, H.B. Shore, and G. Feher, J. Mol. Biol. 123 (1978) 539.
- [7] H.W. Wycof, C.H.W. Hirs, and S.N. Timasheff, Methods in Enzymology 114 (Academic Press, New York, 1985).
- [8] A. Mcpherson, The Preparation and Analysis of Protein Crystals (Krieger Publishig Co., Malabar, FL., 1989).
- [9] P.R. Carey, Biological Applications of Raman and Resonance Raman Spectroscopies (Academic Press, New York, 1982).
- [10] R. Callender, H. Deng, and R. Gilmanishin , J. of Raman Spectroscopy 29 (1998) 15.
- [11] D.A. Long, Raman Spectroscopy (McGraw-Hill, New York, 1977).
- [12] HoloLab 1000 Operations Manual v1.0 (Kaiser Optical Systems Inc., 1997).
- [13] D.F. Rosenbaum and C.F. Zukoski, J. Crystal Growth 169 (1996) 752.
- [14] A.M. Schwartz and K.A. Berglund, accepted J. Crystal Growth.

## **Chapter 4: *In Situ* Monitoring and Control of Lysozyme Concentration during Crystallization in a Hanging Drop\***

\*Journal of Crystal Growth accepted July 1999.

### **Summary**

Fiber optic Raman spectroscopy combined with a partial least-squares regression model was demonstrated as a monitor of lysozyme concentration during crystallization in a hanging drop experiment in real time. Raman spectral features of the buffer and protein were employed to build the regression model. The use of fiber optic technology coupled with Raman spectroscopy, which is ideal for use with aqueous solutions, results in a powerful noninvasive probe of the changing environment within the solution. Lysozyme concentrations were monitored in experiments at a constant reservoir ionic strength. Data from these uncontrolled experiments were used to determine rates of supersaturation, induction times, and the number and size of the resultant lysozyme crystals. Control experiments were performed by introducing step changes in the ionic strength of the reservoir buffer. The step changes were initiated by comparing *in situ* rates of supersaturation with the rates of supersaturation calculated from the uncontrolled data. Monitoring the concentration changes of the lysozyme within the hanging drop permits a measurement of the level of supersaturation of the system and enhances the possibility of dynamic control of the crystallization process.

### **Introduction**

Determination of the conditions for protein crystal growth is most often adventitious. These conditions are found by trial and error screening methods [1,2]. In an attempt to

decrease the amount of time and the number of experiments needed to find the necessary conditions for crystal growth, statistical methods have been employed [3,4]. Striving to better understand the crystal growth process, lead various workers to monitor small batch crystallizers containing protein solutions. These studies have included fluorescence based anisotropy measurements [5], static light scattering [6,7,8], dynamic light scattering (DLS) [6,9,10], and microcalorimetric techniques [8]. Though these findings revealed a wealth of information about protein crystal growth, they were incomplete predictors of whether a solution would nucleate to form crystals.

It is well recognized that the impetus for research in this area is determination of three-dimensional structures of proteins by X-ray crystallography. The experiments previously mentioned have all employed batch or microbatch crystallization techniques. However, the most used crystallization techniques by crystallographers are the vapor-diffusion techniques. Though there are similarities between microbatch and vapor-diffusion techniques [11], their underlying mechanisms are vastly different. Most recently, some workers have shifted their goal from predicting crystal growth in a batch setting to monitoring and controlling crystal growth in a vapor diffusion experiment.

DLS combined with humidity sensors [12], gravimetric techniques [13], and Raman spectroscopy [14] have all been employed in monitoring the hanging drop. The first of these techniques combines the ability of DLS to detect trends in particle size combined with humidity sensors to observe the evaporation rate of water from the drop. The second technique measures the evaporation rate of water from the drop directly. The third technique based on Raman spectroscopy [14], allows simultaneous measurement of the concentration of lysozyme and the amount of water within the drop.

Raman spectroscopy probes the vibrational energy levels of the bonds within the protein and the water. A partial least squares regression model correlates the Raman spectral features with the concentration of lysozyme present in the drop [14]. This data analysis enables us to measure the apparent level of supersaturation of the hanging drop *in situ*. The goal of this study is to demonstrate that quick, real-time measurements of the apparent level of supersaturation can be used to control the rate of supersaturation of the a protein within a hanging drop to affect both the size and quality of the protein crystal produced.

## **Experimental Procedure**

### ***Protein Sample Preparation***

As discussed previously [14], three times crystallized, dialyzed, and lyophilized chicken egg white lysozyme was purchased from Sigma Chemical Co. and used without further purification. All experiments were performed in a buffer containing 0.1 M sodium acetate at pH 4.2. Salt and protein amounts for standards were determined with a Mettler AE50 balance. For all experiments lysozyme was dissolved into the NaCl/buffer system, with an initial ionic strength of about 0.34 M, and then filtered through a 45  $\mu\text{m}$  Millipore filter before use. A 5  $\mu\text{l}$  protein drop was deposited on a microscope cover glass. The cover glass was then inverted and placed over a 6 ml vessel containing 2 ml of a NaCl/buffer reservoir ranging in ionic strength from 0.34 to 2.73 M. The top of each vessel was greased to ensure an airtight seal.

The reaction vessel, shown in Figure 4.1, consists of a 6 ml vial with inlet and outlet channels. Attached to these channels are syringes. The outlet syringe allows the

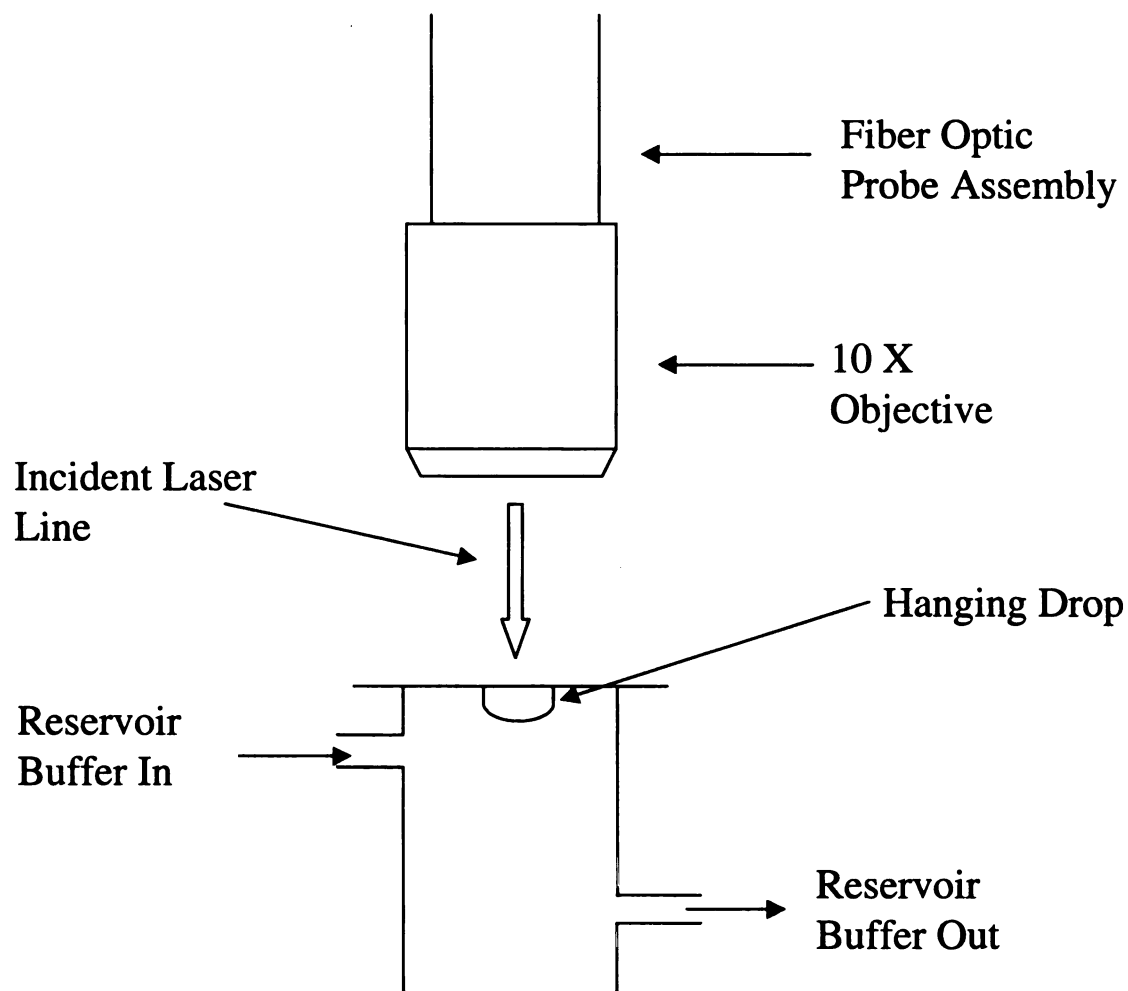


Figure 4.1 A schematic of the experimental set-up used throughout the lysozyme vapor diffusion experiments, consisting of a 6 ml vial with input and output channels. These channels were attached to a set of syringes, which allow the composition of the reservoir to be altered. The fiber optic probe assembly is positioned directly above the hanging drop of lysozyme solution and focused into the drop utilizing a 10X microscope objective.

reservoir to be fully or partially emptied. The inlet syringe allows us to add a new NaCl/buffer solution or to add NaCl/buffer solution to the already existing reservoir. This system permits the ionic strength of the reservoir to be changed completely or incrementally, which in turn will affect the rate of supersaturation of the protein. The reaction vessel sits atop a translational stage that can be adjusted to position the hanging drop of protein within the focal point of the incident laser line.

### *Supersaturation Measurements*

The ideal nature of Raman spectroscopy for biochemical experiments in aqueous media has been recognized [15,16]. The use of Raman spectroscopy to measure the solubility and protein concentration within a hanging drop has been previously demonstrated [14]. The feasibility of Raman spectroscopy toward *in situ* control of the level of supersaturation was investigated using a Kaiser Optical, Inc. HoloLab Series 1000®. A CCD camera, spectrograph, and fiber optic probe comprise the HoloLab Series 1000®. This Raman system employs a 30 mW Helium Neon Laser at 632.8 nm with a Standard Fiber Injector. The spectrograph section of the HoloLab Series 1000® utilizes holographic optical elements and provides spectral coverage from 400 to 3650  $\text{cm}^{-1}$  [17].

The HoloLab system makes use of a notch filter to attenuate the laser line while allowing the Raman spectra to be collected [17]. The fiber optic probe consists of six collection fibers bundled around one excitation fiber [17]. Attached to the tip of the probehead is a 10X microscope objective, which focuses the incident beam. It is this configuration of the HoloLab assembly, which makes these measurements possible. The

incident, laser light travels through the cover glass directly into the hanging drop of protein. Since the cover glass does not scatter well at 632.8 nm, the cover glass is optically transparent to the measurement permitting the measurement of lysozyme concentration without contact with the solution.

### *Data Analysis*

The laser power incident on the cover glass and protein drop ranged from 19 to 22 mW. Each spectrum consisted of 20 scans collected over 129 seconds at 8 cm<sup>-1</sup> resolution. Raman spectra have previously been subjected to quantitative infrared partial least squares (PLS) models with remarkable success [18]. The Raman spectra of 31 lysozyme standards were used to construct a PLS regression model utilizing QuantIR®, a PLS regression analysis software package by Applied Systems. The PLS model generated correlates the spectral region from 2700 to 3600 cm<sup>-1</sup> with the concentration (g/ml) of lysozyme. This spectral region encompasses vibrations due to the protein CH stretches centered at 2950 cm<sup>-1</sup> [15,16] and the water OH stretches centered at 3230 cm<sup>-1</sup> [15,16].

A leave one out cross validation performed on the standards determined that the model had a root mean square error of calibration (RMSEC) of  $\pm 0.01$  g/ml. In addition to the leave one out cross validation process, the regression model was also used to determine the concentration of a test set of standards. The test set consisted of eleven standard solutions of known lysozyme concentration, which were not a part of the calibration standards of the PLS regression model. Evaluation of the PLS regression model using the test set yielded a root mean square error of prediction (RMSEP) of  $\pm 0.01$  g/ml. This method has been shown to be effective in measuring both the solubility



of lysozyme at varying ionic strengths and monitoring the change in composition of the hanging drop *in situ* [14]. The Raman method has been employed to measure lysozyme concentrations ranging from 0.32 g/ml to 0.02 g/ml [14]. Lysozyme concentrations of 0.16 g/ml and 0.23 g/ml and reservoir ionic strengths ranging from 0.67 M to 2.73 M were selected for this study by virtue of the relatively short nucleation times produced under these conditions. Therefore, it is the goal of the present work to utilize this method for the dynamic control of the crystallization of lysozyme within a hanging drop.

## **Results and Discussion**

Initially, the goal was to obtain the relative kinetics of the lysozyme crystallization process with respect to varying reservoir ionic strength. Figure 4.2 shows a concentration profile with respect to time and is representative of the data which is attainable from the method we have developed. The change in lysozyme concentration is due to three factors: the mass transfer between the water in the drop and reservoir, the nucleation process of the lysozyme in solution, and the growth of lysozyme crystals. The initial rise in concentration is due to the loss of water from the hanging drop of lysozyme solution. The loss of water is driven by the difference in ionic strength between the hanging drop and the NaCl/buffer reservoir.

This initial amount of water exiting the drop has been pursued as a possible avenue of control in vapor diffusion experiments [12,13]. It is expected that the rate at which the water evaporates or the rate at which the hanging drop supersaturates affects the number and quality of protein crystals produced. Previous attempts at measuring the evaporation rate have resulted in mass profiles of water, which eventually come to a steady state

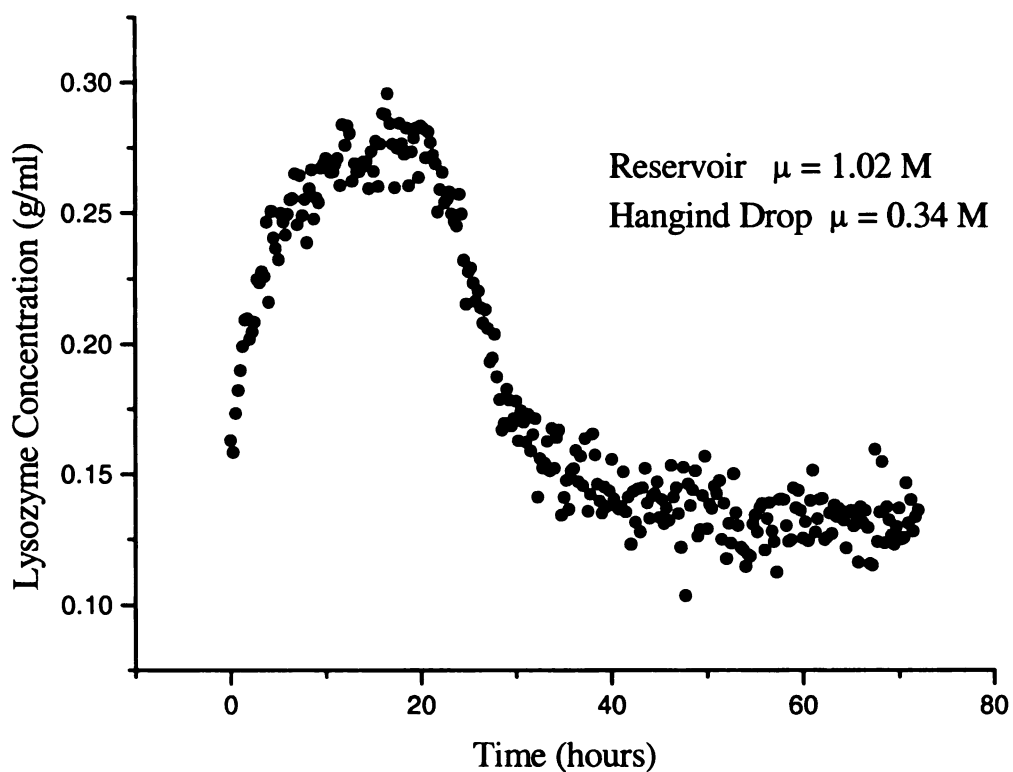


Figure 4.2 A real time concentration change of a hanging drop of lysozyme obtained with the fiber optic Raman method. The ionic strengths of the reservoir and the drop are 1.02 M and 0.34 M, respectively. The rate of supersaturation, the time of nucleation, and the eventual decrease in supersaturation of the protein within the solution of the hanging drop can be measured in real time.

value [13]. At this point no water is leaving the drop, and the ionic strength of the drop is now in equilibrium with that of the reservoir. The formerly mentioned methods, including gravimetric measurements and humidity sensors, of monitoring the drop can only give estimates as to where the effect of vapor diffusion becomes negligible and where the effects of nucleation and growth become dominant.

However, our method allows both the measurement of the amount of water and the amount of lysozyme in solution in the hanging drop. At approximately 20 hours, Figure 4.2, the concentration of protein ceases to increase, and begins to decrease. The system is now supersaturated and is driven by the difference between the supersaturated concentration and that of solubility. It is at this point that the influences of nucleation and growth become dominant within the system. Our method permits the determination of an induction time for lysozyme, because we can accurately measure the concentration of lysozyme.

The measurement of this concentration is what we define as the apparent level of supersaturation. Since the ionic strength of the hanging drop is varying with time and the dissociated sodium and chloride ions do not have a vibrational Raman spectrum, we can not measure the exact ionic strength of the hanging drop. In turn, the exact value of supersaturation can not be calculated. However, it is our intent to show that the ability to make these concentration measurements ensures the possibility of controlling the vapor diffusion experiment by monitoring the apparent level of supersaturation.

Figures 4.3 and 4.4 depict the concentration trajectories of lysozyme at varying reservoir ionic strengths. The trajectories shown in Figures 4.3 and 4.4 have an average starting concentration of 0.16 g/ml and 0.23 g/ml, respectively. The starting ionic

strength of the hanging drops in Figures 4.3 and 4.4 is 0.34 M. This ionic strength includes the sodium acetate buffer, the level of pH, and the amount of NaCl added. In Figures 4.3 and 4.4 the circles represent the lowest ionic strength reservoir, the squares represent the mid-level ionic strength, and the triangles represent the highest ionic strength reservoir. The arrows in Figures 4.3 and 4.4 trace the trajectories of the lysozyme concentration through time as the hanging drops supersaturate, nucleate, and finally decrease in supersaturation.

In Figure 4.3 the induction times vary from 20 hours to 6 hours as the reservoir ionic strength is increased from 1.02 M to 2.73 M. Figure 4.4 exhibits the same behavior. As the reservoir ionic strength is increased from 0.67 M to 1.54 M, the induction times decrease from 20 hours to 0.8 hours. These figures indicate that as the ionic strength of the reservoir increases the measured induction time of lysozyme decreases. By considering the trajectories in Figures 4.3 and 4.4 with an equal reservoir ionic strength of 1.02 M, an increase in initial concentration of lysozyme within the hanging drop corresponds to a decrease in the measured induction time. These trends agree with theory that as the rate of supersaturation increases the time of nucleation, or induction time, decreases [19].

Figures 4.3 and 4.4 represent the kinetics of the lysozyme crystallization process when no intervention, or control, is applied to the system. These hanging drop experiments can be described as miniature uncontrolled reactors. The reaction, in this case the crystallization of lysozyme, is allowed to go to completion at a rate dictated by the difference in ionic strengths of the reservoir and the drop. Table 4.1 summarizes the data acquired from typical crystallization experiments similar to those described in

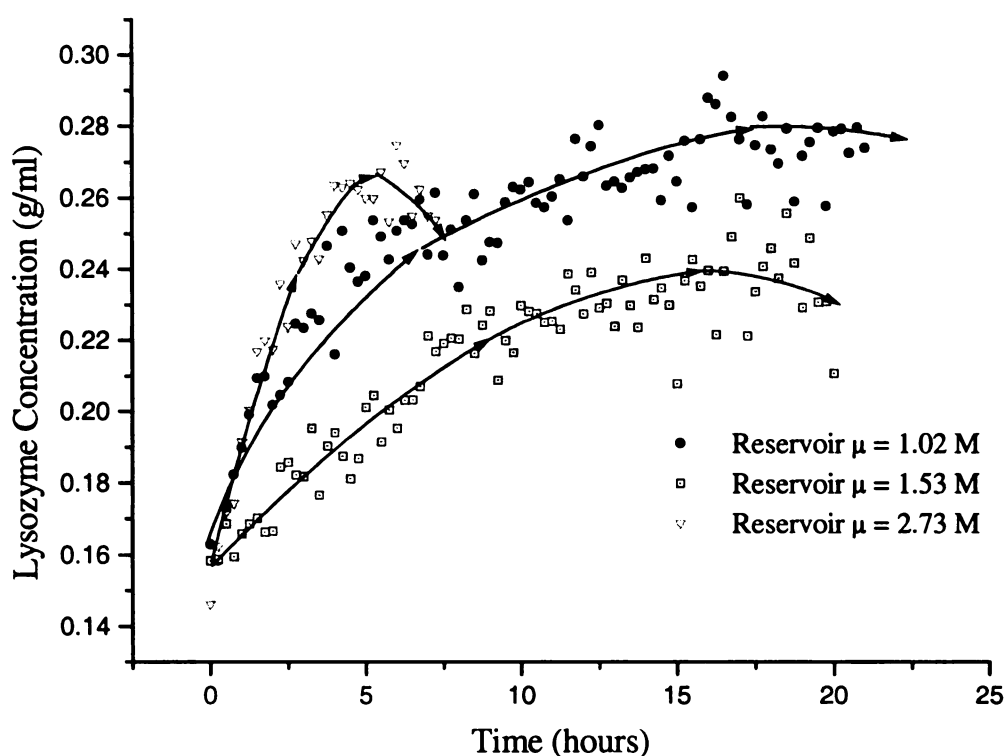


Figure 4.3 A comparison of the relative crystallization kinetics between hanging drop experiments with an initial lysozyme concentration of about 0.16 g/ml and varying reservoir ionic strengths. As the reservoir ionic strength decreases the concentration trajectories of the lysozyme begin to flatten out.

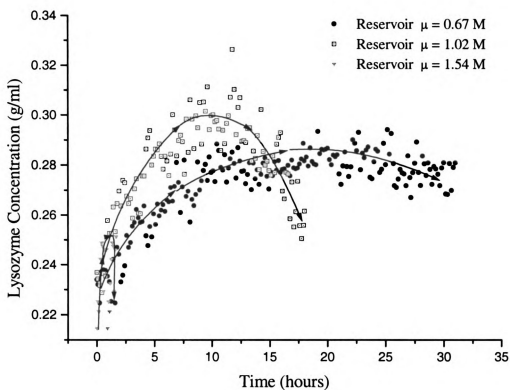


Figure 4.4 A comparison of the relative crystallization kinetics between hanging drop experiments with an initial lysozyme concentration of about 0.23 g/ml and varying reservoir ionic strengths. As the reservoir ionic strength decreases the concentration trajectories of the lysozyme begin to flatten out.

Figures 4.3 and 4.4. Table 4.1 relates the initial lysozyme concentration and difference in ionic strength between the hanging drop and reservoir to both the rate of supersaturation and the eventual outcome of the experiments.

By examining the data in Table 4.1 some generalizations can be made. The difference in ionic strength can be correlated with the rate of supersaturation of the lysozyme in the hanging drop. Generally, as the rate of supersaturation increases the time of nucleation decreases. Accordingly, higher rates of supersaturation exhibit larger numbers of small crystals or the formation of precipitate. The supersaturation rates were determined by an initial rate method. The lysozyme concentration data were fit to a first order equation over the linear range of the concentration profiles. The linear regressions were performed by Microcal Origin® software and were determined to be highly significant. The slope of the linear model was then taken as the rate of supersaturation. The rates of supersaturation are reported in Table 4.1 with the associated standard deviations of the regression. The concentration profiles from Figures 4.3 and 4.4 combined with the experimental data summarized in Table 4.1 indicate that the initial supersaturation rate is integral in determining both the time of induction and the number of crystals produced.

A high initial rate of supersaturation will produce large numbers of protein crystals or lead to amorphous precipitate. Conversely, a small initial supersaturation rate will lead to long induction times or no crystal growth. The goal of the hanging drop experiment is to grow protein crystals of suitable size and quality. Low numbers of crystals are desired, because these will be larger and not be as likely to be twinned. However, the production

## Summary of Uncontrolled Hanging Drop Experiments

[lysozyme] (g/ml)	Reservoir $\mu$ (M)	Drop $\mu$ (M)	$\Delta \mu$ (M)	Supersaturation Rate (g/ml*hr)	Approximate # of Crystals
0.16	1.02	0.34	0.68	$0.014 \pm 0.001$	42
0.16	1.53	0.34	1.19	$0.0076 \pm 0.0004$	63
0.15	2.73	0.34	2.39	$0.026 \pm 0.002$	ppt
0.23	0.67	0.34	0.33	$0.005 \pm 0.0003$	15
0.24	1.02	0.34	0.68	$0.007 \pm 0.0006$	44
0.21	1.54	0.34	1.20	$0.072 \pm 0.01$	$\approx 150$

$\mu$  = Ionic Strength

**Table 4.1** A summary of the results of uncontrolled crystallization experiments in terms of rates of supersaturation and numbers of crystals produced. The abbreviation ppt indicates that the outcome of the experiment was the formation of amorphous precipitate. As the rate of supersaturation increased the number of crystals produced also increased.



of low numbers of protein crystals is dependent on a low rate of supersaturation. This dilemma epitomizes the problems facing those who rely on vapor diffusion experiments.

The inability to measure the transient composition of the hanging drop meant either forcing crystallization with a large rate of supersaturation or applying a small driving force, rate of supersaturation, to the hanging drop. The former will lead to small crystals or precipitate and the latter may never lead to protein crystal growth. The need for control has been recognized [12,13], but merely implemented in terms of the amount of water leaving the drop. Previous methods have had to estimate induction times by the amount of water diffusing out of the hanging drop. These estimates have completely neglected the protein within the drop. Our method allows us to differentiate between the water exiting the drop, the protein in solution, and the protein crystal.

Figure 4.5 represents two concentration profiles, the first follows the concentration profile of an uncontrolled experiment (circles) and the second follows the concentration profile of a controlled experiment (diamonds). The first consists of a hanging drop of lysozyme with an initial protein concentration of 0.21 g/ml, a drop ionic strength of 0.34 M, and an initial reservoir concentration of 1.54 M. This uncontrolled hanging drop experiment results in the formation of approximately 150 crystals. See Table 4.1. The uncontrolled experiment results in an induction time on the order of 0.8 hours. The second profile in Figure 4.5 represents a controlled vapor diffusion experiment. The second experiment contains a hanging drop containing a lysozyme concentration is 0.21 g/ml, a drop ionic strength of 0.34 M, and an initial reservoir ionic strength of 1.54 M. The ionic strength of the reservoir in the controlled experiment was then changed at 20

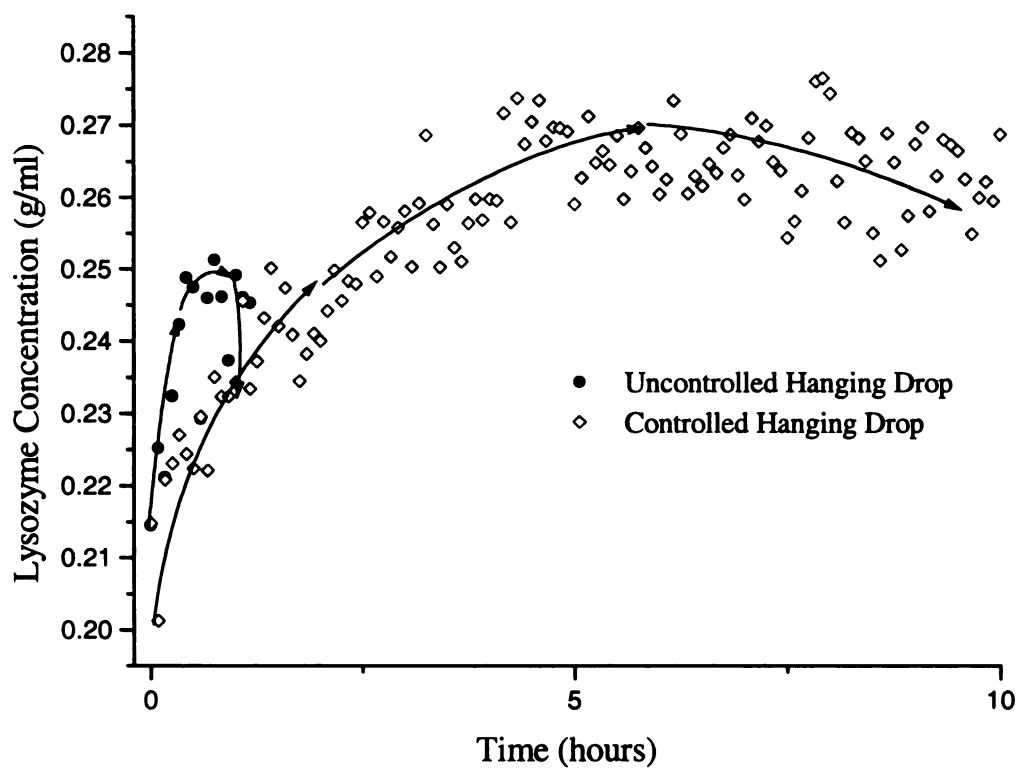


Figure 4.5 A direct comparison of the lysozyme concentration trajectories for hanging drop crystallization experiments which were controlled and uncontrolled. By applying control of the ionic strength of the reservoir, the induction time in the controlled experiment is increased by a factor of 4.

minutes to a value of 0.67 M. Just after 5 hours the reservoir was again changed to a value of 0.5 M.

The initial rate of supersaturation in the uncontrolled experiment at a reservoir ionic strength of 1.54 M was approximately 0.07 (g/ml\*hr). The initial supersaturation rate of the controlled experiment over the first twenty minutes was approximately 0.06 (g/ml\*hr). Since we had previously run an experiment near these conditions we knew that if we continued to allow the supersaturation to occur at this pace the crystals might be too small or contain too many defects. After the change in reservoir concentration, the rate of supersaturation decreased to approximately 0.01(g/ml\*hr) within three hours. Once the concentration profile began to level off, or approach nucleation, the ionic strength of the reservoir was reduced to promote the growth of crystals. The induction time was therefore increased from 0.8 hours to about 6 hours.

Through a reduction in the rate of supersaturation, the experiment promoted growth rather than nucleation of lysozyme crystals. By controlling the hanging drop experiment, the average number of crystals produced has also dropped to 48. The controlled experiment has produced fewer crystals than the uncontrolled experiment at a reservoir ionic strength of 1.54 M (150 crystals) and has produced more crystals than the uncontrolled experiment at a reservoir ionic strength of 0.67 M (15 crystals).

The photographs in Figure 4.6 are at the same degree of magnification and illustrate the difference between an uncontrolled versus a controlled crystallization. The viewing area has a diameter of approximately 1mm, and encompasses about half of the surface area of the hanging drop, which is in contact with the glass slide. The top picture, labeled A, is of the lysozyme crystals produced during the uncontrolled experiment at a reservoir

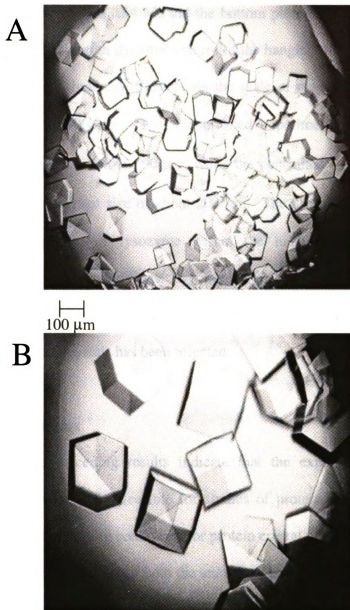


**Figure 4.6** These lysozyme crystals correspond to the trajectories of the controlled and uncontrolled experiments in Figure 5. These photographs are at the same magnification, and encompass identical viewing areas. The top picture represents the uncontrolled experiment, and the bottom picture represents the controlled experiment. Through the application of control of the crystallization process the size of the resultant crystals is increased and the number of crystals is decreased.

ionic strength of 1.54 M, and the bottom picture, labeled B, is of the lysozyme crystals produced through dynamic control of the hanging drop experiment. Between the pictures is a length indicator to illustrate the scale of magnification. The indicator represents a length of 100  $\mu\text{m}$ . The uncontrolled experiment yielded lysozyme crystals with an average size of about 90  $\mu\text{m}$ , while the controlled experiment lead to lysozyme crystals with an average size of about 200  $\mu\text{m}$ . The use of Raman spectroscopy to measure the concentration of lysozyme within the hanging drop has allowed control of the crystallization conditions. By monitoring the rate of supersaturation and initiating step changes in the ionic strength of the reservoir, both the number and size of the resultant lysozyme crystals has been affected.

## Conclusions

The preceding results indicate that the experimental design and *in situ* Raman measurements are feasible for studies of protein crystallization. The method may be applied to finding conditions for protein crystal growth and crystallization kinetic studies. The ability to monitor both the amount of water diffusing out of the hanging drop and the amount of protein within the drop allows for dynamic control of the crystallization process. Both components of the drop can be measured simultaneously with Raman spectroscopy.

Previously the components of the hanging drop have been monitored with multiple techniques [12,13]. Relative humidity measurements were made while monitoring the drop microscopically or using DLS measurements. However, both the microscopic and DLS measurements require the presence of small crystals or nuclei. Ideally the level of

supersaturation should be reduced at the point of nucleation to promote crystal growth [19]. However, if the crystals are visible or are scattering, as in these previous methods, the point of nucleation has already passed. Once nuclei or small crystals have appeared, any change to the system may be too late to implement control.

Before lysozyme crystals appear the concentration profile begins to reach a steady value. When the concentration profile begins to level off, the rate of supersaturation becomes nonlinear. At this point measurement of the rate of water evaporation rate is not enough to describe the events occurring within the hanging drop. The method we present allows the concentration of the lysozyme to be monitored in real time, since the amount of water and concentration lysozyme can be calculated independently. Though the exact time of nucleation can not be determined to the absolute second, our method allows for a better estimate as to when nucleation occurs. In turn this should permit better dynamic control of the experiment.

In addition, our method produces fast and reliable concentration measurements due to the use of PLS regression. The PLS model utilizes the OH and CH stretches of the vibrational spectrum to assign a concentration value. By using these generic frequencies it is our hope that the PLS model derived for lysozyme can be used as a standard in monitoring the crystallization of proteins without an *a priori* knowledge of solubility [20]. We have shown that measured apparent supersaturation values in conjunction with calculated rates of supersaturation can be used to control the crystallization process within the hanging drop.

### **Literature Cited**

- [1] H.W. Wycof, C.H.W. Hirs, and S.N. Timasheff, *Methods in Enzymology* 114 (Academic Press, New York, 1985).
- [2] A. Mcpherson, *The Preparation and Analysis of Protein Crystals* (Krieger Publishig Co., Malabar, FL., 1989).
- [3] C.W. Carter, Jr. and C.W. Carter, *J. Biol. Chem.* 254 (1979) 12219.
- [4] J. Jancarik, and S.-H. Kim, *J. Appl. Cryst.* 24 (1991) 409.
- [5] B.L. Pan and K. A. Berglund, *J. Crystal Growth* 171 (1997) 226.
- [6] F. Rosenberger, P.G. Velikov, M. Muschol, and B.R. Thomas, *J. Crystal Growth* 168 (1996) 1.
- [7] M. Muschol and F. Rosenberger, *J. Chem. Phys.* 103 (1995) 10424.
- [8] Y. Georgalis, P. Umbach, A. Zielenkiewicz, E. Utzig, W. Zielenkiewicz, P. Zielenkiewicz, and W. Saenger, *J. Am. Chem. Soc.* 119 (1997) 11959.
- [9] M. Boyer, M.-O. Roy, and M. Jullien, *J. Crystal Growth* 167 (1996) 212.
- [10] Z. Kam, H.B. Shore, and G. Feher, *J. Mol. Biol.* 123 (1978) 539.
- [11] N.E. Chayen, *Acta. Cryst.* D54 (1998) 8.
- [12] R.R. Ansari, K.I. Suh, A. Arabshahi, W.W. Wilson, T.L. Bray, and L.J. DeLucas, *J. Crystal Growth* 168 (1996) 216.
- [13] Z.-Y. Shu, H.-Y. Gong, and R.-C. Bi, *J. Crystal Growth* 192 (1998) 282.
- [14] A.M. Schwartz and K.A. Berglund, *J. Crystal Growth* 203 (1999) 599.
- [15] D.A. Long, *Raman Spectroscopy* (McGraw-Hill, New York, 1977).
- [16] P.R. Carey, *Biological Applications of Raman and Resonance Raman Spectroscopies* (Academic Press, New York, 1982).
- [17] *HoloLab 1000 Operations Manual v1.0* (Kaiser Optical Systems Inc., 1997).
- [18] J.B. Cooper, K.L. Wise, J. Groves, and W.T. Welch, *Anal. Chem.* 67 (1995) 4096.

[19] J.W. Mullin, Crystallization 3<sup>rd</sup> Edition (Butterworth Heinemann Ltd., Oxford, 1993).

[20] A.M. Schwartz and K.A. Berglund, submitted J. Crystal Growth.



## **Chapter 5: Extension of the Raman Control Scheme for the Hanging Drop Experiment to Proteins other than Lysozyme\***

\* Submitted to the Journal of Crystal Growth

### **Summary**

Fiber optic Raman spectroscopy combined with a partial least-squares regression model was demonstrated as a real time monitor of lysozyme concentration during crystallization in a hanging drop experiment in real time. Raman spectral features of the buffer and protein were employed to build a regression model. The use of fiber optic technology coupled with Raman spectroscopy, which is ideal for use with aqueous solutions, results in a powerful noninvasive probe of the changing environment within the solution.

Monitoring the concentration changes of the lysozyme within the hanging drop permits a measurement of the level of supersaturation of the system. The resulting concentration profiles allowed both the calculation of the rate of supersaturation and the identification of the nucleation time of the lysozyme. In turn these measurements were used to enhance control of the crystallizing lysozyme by affecting the size and number of growing crystals.

Since the Raman spectra of many proteins are similar over the wavenumber range of the lysozyme regression model, the model was extended to other proteins. The numbers generated by the lysozyme PLS regression model were used as a ratio of CH to OH vibrations. These ratios were used to control the crystallization of barley malt  $\alpha$ -amylase and Carlsberg subtilisin in the hanging drop vapor-diffusion experiment.

## **Introduction**

The growth of protein crystals has been cited as the hindrance in determining the three dimensional structures of biologically important proteins. Research in the area of protein crystallization has been directed at understanding the underlying mechanisms by which proteins crystallize. The objective of these studies was to reduce the number of screening experiments necessary to determine the appropriate conditions for protein crystallization. These studies have included statistical methods [1,2,3], fluorescence based anisotropy measurements [4], static and dynamic light scattering techniques [5,6,7,8,9], and calorimetric techniques [7,10]. Though these experiments revealed a wealth of information about protein crystal growth, they were mainly confined to studies on lysozyme and were incomplete predictors of whether a solution would nucleate to form crystals.

To this day many of the proteins which are newly crystallized rely on matrix screening techniques [11,12,13]. The matrix screening experiments can be divided into two categories, the broad based and the fine screen. The broad-based matrix screen includes changing the solubility of a protein with inorganic salts, organic solvents, polyethylene glycol of varying molecular weights, or combinations of these precipitants. The fine screen is employed when one of the precipitants from the broad-based screen results in protein crystals. The fine screen varies the reservoir parameters of the hanging drop slightly to determine the optimum conditions for crystallization of a particular protein. This type of experiment offers no control of the level of supersaturation within the hanging drop. The expectation is that the reservoir conditions will not be too severe,

and will not supersaturate the hanging drop to a point where precipitation occurs. Essentially, these screening experiments reduce to a trial and error approach, which may or may not lead to the correct conditions necessary for crystallization.

Recently, some investigators have shifted focus from prediction of crystallization conditions to the control of the vapor-diffusion experiment. Dynamic light scattering (DLS) combined with humidity sensors [14], a gravimetric technique [15], and a Raman spectroscopic technique [16,17] have been employed to control the vapor-diffusion experiment. The first of these methods monitors the increase of aggregate size and presence of small crystals via the DLS response. The humidity sensor measures the relative humidity in the reaction vessel and gives insight into the amount of water leaving the hanging drop as the drop concentrates. The authors showed success with the method in monitoring the crystallization of lysozyme and thaumatin [14]. The second technique merely measures the amount of water, which is leaving the hanging drop. This method employs the rate of water evaporation to control the crystallization of both lysozyme and trichosanthin [15].

The Raman technique, which has been previously described [16,17] can simultaneously measure the amount of water and protein within the hanging drop. A partial least squares regression model correlates the Raman spectral features with the amounts of protein and water present in the drop. This data analysis enables the authors to measure the apparent level of supersaturation of the hanging drop *in situ*. The Raman method is an improvement upon earlier techniques since one measurement can describe the change in composition of the hanging drop either due to a change in the amount of water leaving the hanging drop or the amount of protein leaving solution. Also, since the

method is directly probing vibrations due to specific chemical bonds there is no danger of misinterpretation of data as there is with DLS measurements.

The premise behind the Raman control scheme combines a measurement of the time of nucleation with a measurement of the rate of supersaturation to affect the size and quality of the resultant protein crystals. Since both nucleation and growth are dependent upon the level of supersaturation [18], measurement of the level of supersaturation of the protein in the hanging drop increases the possibility of control of the crystallization. Higher levels of supersaturation promote nucleation whereas lower levels of supersaturation promote growth [18]. The goal of the hanging drop experiment is to produce single protein crystals of X-ray diffraction quality. This creates a dilemma because high levels of supersaturation typically lead to small crystals, twinned crystals, poor quality crystals, or precipitate. However, low levels of supersaturation may lead to extremely long induction times or no protein crystal formation.

Therefore, the Raman method of control utilizes the measured concentration of the protein to approximate the level of supersaturation within the hanging drop. To either promote the nucleation or growth of the protein crystals, step changes in the reservoir ionic strength can be made accordingly. Initially, the reservoir ionic strength is set at a high level. When the concentration of the protein within the hanging drop increases to the concentration known to promote the nucleation, the high ionic strength reservoir is removed and a lower ionic strength reservoir injected. Previously, the Raman method was demonstrated to work on the lysozyme/NaCl system [16,17]. The goal of this study is to demonstrate that the lysozyme calibration model can be applied to other protein

systems to control the rate of supersaturation of the protein within a hanging drop to affect both the size and quality of the protein crystal produced.

## **Experimental Procedure**

### *Protein Sample Preparation*

Chicken egg white lysozyme [19],  $\alpha$ -chymotrypsin [20], Carlsberg subtilisin [21],  $\alpha$ -amylase from barley malt [22],  $\alpha$ -amylase *bacillus* [23], ovalbumin [24], human serum albumin [25], alkaline phosphatase [26], and bovine liver catalase [19] were purchased from Sigma Chemical Co. and used without further purification. All experiments were performed in a buffers specified for each protein in the referred literature citations. Salt and protein concentrations were prepared gravimetrically with a Mettler AE50 balance. For all experiments each protein was dissolved into the pertinent precipitant/buffer solution and then filtered through a 45  $\mu$ m Millipore filter before use. A 5  $\mu$ l protein drop was deposited on a microscope cover glass. The cover glass was then inverted and placed over a 6 ml vessel containing 2 ml of a higher ionic strength precipitant/buffer reservoir. The top of each vessel was greased with silicone to ensure an airtight seal. Precautions were taken to ensure that the grease did not come into contact with the hanging drop of protein.

The reaction vessel, previously described [17], consists of a 6 ml vial with an inlet and an outlet channel. Syringes are attached to these channels. The outlet syringe allows the reservoir to be fully or partially emptied. The inlet syringe allows a new precipitant/buffer solution to be added to the reservoir. This system permits the ionic strength of the reservoir to be changed in steps, which in turn will affect the rate of

supersaturation of the protein. The reaction vessel sits atop a translational stage that can be adjusted to position the hanging drop of protein within the focal point of the incident laser line [16,17].

### *Raman Spectra of the Proteins*

The utility of Raman spectroscopy for biochemical experiments in aqueous media has been discussed [27,28]. The interference of water in the vibrational spectrum of the solute in Raman spectroscopy is reduced compared to infrared spectroscopy [27,28]. Therefore, the region of the Raman spectrum between 1550 and 1650  $\text{cm}^{-1}$  should contain more information than comparable absorbance techniques. However, there are two problems with Raman spectroscopy competing fluorescence and scattering intensity.

The scattering intensity of a given chemical species decreases as the reciprocal of wavelength to the fourth power [27,28]. As the wavelength of the incident laser line increases, the intensity of the vibrational spectrum will decrease. Conversely, a decrease in incident wavelength constitutes an increase in intensity of the resultant Raman spectrum. However, the probability of competing fluorescence increases with the use of a lower wavelength laser beam. This situation creates a problem for collecting Raman spectra of biological macromolecules. Since the Raman cross section of most proteins is small, the Raman effect is weak [28,29]. The natural conclusion is to apply lower wavelength laser lines to generate higher intensity Raman spectra. This creates a problem, because the aqueous protein solutions are comprised of amino acid side chains, active sites with metal centers, buffer molecules, and precipitants that may fluoresce.

Additionally, due to the nature of the experiment a low power laser is required. This is to ensure that the hanging drop of protein is not being extensively heated. A laser with an incident line of 632.8 nm was chosen for the following experiments. Since this is a red laser the background fluorescence should be reduced. To compensate for the low intensities typically associated with a high wavelength source; a high throughput transmission instrument was employed. The Kaiser Optical, Inc. Hololab Series 1000®, which has previously been described [16,17], was used throughout this study.

### *Data Analysis*

Protein solutions of 5  $\mu\text{l}$  were deposited onto a microscope cover slip. The glass cover slip was then inverted above the reaction vessel, which contained a reservoir of higher ionic strength than the hanging drop of protein solution. The hanging drop of protein was then brought into the focal point of the laser. The laser power incident on the cover glass and protein drop was approximately 18 mW. Each spectrum consisted of 20 scans collected over 129 seconds at 8  $\text{cm}^{-1}$  resolution. The Raman spectra of 31 lysozyme standards were used to construct a PLS regression model utilizing QuantIR®, a PLS regression analysis software package by Applied Systems. The PLS model generated correlates the spectral region from 2700  $\text{cm}^{-1}$  to 3600  $\text{cm}^{-1}$  with the concentration (g/ml) of lysozyme. This spectral region encompasses vibrations due to the protein CH stretches centered at 2950  $\text{cm}^{-1}$  and the water OH stretches centered at 3230  $\text{cm}^{-1}$ . A validation of both the calibration of the PLS model and predictive capabilities of the PLS model led to a root mean square error (RMSE) of  $\pm 0.01$  g/ml for lysozyme [17].

Initially, the Raman control scheme was shown to work for lysozyme [17]. In order to exhibit the utility of this method the experiment would have to be extended to other protein systems. This could be accomplished in two ways. A new protein system could be chosen, standards could be made, and a new regression model could be validated, or the previously developed lysozyme calibration model could be extended to other protein systems. The first of these two choices represents an unrealistic manner of performing the experiment. Typically, purified proteins are not available on the scale necessary to construct a PLS model. These proteins are either too expensive to buy or it would take too long a time to generate the amount of purified protein necessary.

In order for the second of these methods to work, the Raman spectrum of the protein of interest would have to be similar to that of lysozyme. Since the PLS model correlates spectral features of the CH and OH stretching region to changes in concentration of lysozyme [16], the CH and OH stretching region of the protein of interest needs to be comparable to that of lysozyme. Knowing that the scattering efficiency of proteins varies, the scattering intensity of equivalent amounts of proteins will also vary. Therefore, the numbers generated by the lysozyme PLS model for proteins other than lysozyme will not be concentration values. Rather they can be considered concentration ratios. The PLS model takes into account any change in either the CH or OH stretch, and then reports a concentration value. If the lysozyme model is extended to other proteins, the PLS model will account for changes in either the CH or OH stretch and report a value. Though this value is based on the changes in spectral features of lysozyme, we will show that this value can be used to observe the relative supersaturation of proteins other than lysozyme in the hanging drop.



## Results and Discussion

Initially, the following proteins, chicken egg white lysozyme,  $\alpha$ -chymotrypsin, Carlsberg subtilisin,  $\alpha$ -amylase from barley malt,  $\alpha$ -amylase *bacillus*, ovalbumin, human serum albumin, alkaline phosphatase, and bovine liver catalase, were screened to determine if their Raman spectra could be obtained. Figure 5.1 depicts a typical Raman spectrum of lysozyme. This is a spectrum of a 0.22 g/ml solution of lysozyme in 0.1 M sodium acetate buffer at a pH of 4.2. Though the amide I, amide III, CH, and OH stretches are readily distinguished in the Raman spectrum, a relatively large fluorescence background is present. Attempts were made to decrease the amount of competing fluorescence in the spectra by reducing the exposure times of the spectra, increasing the number of spectra averaged, and decreasing the incident laser power. Though these attempts were made to minimize the effect of competing fluorescence while obtaining the highest level of Raman scattering possible, a fluorescence background remained. The line shape of the background is representative of the fluorescence the authors have seen while studying the Raman spectra of proteins. However, each of the proteins studied varies in the intensity of the fluorescent background.

Each of the nine proteins, examined in this study, were treated in a similar manner as lysozyme. Each protein was dissolved in an appropriate buffer/precipitant system. A 5  $\mu$ l drop of the protein solution was placed on a microscope cover slip and inverted above a reservoir that was equal in ionic strength to the hanging drop. The hanging drop was then positioned within the focal point of the laser, and a Raman spectrum was obtained. Table 5.1 contains a summary of these initial results.

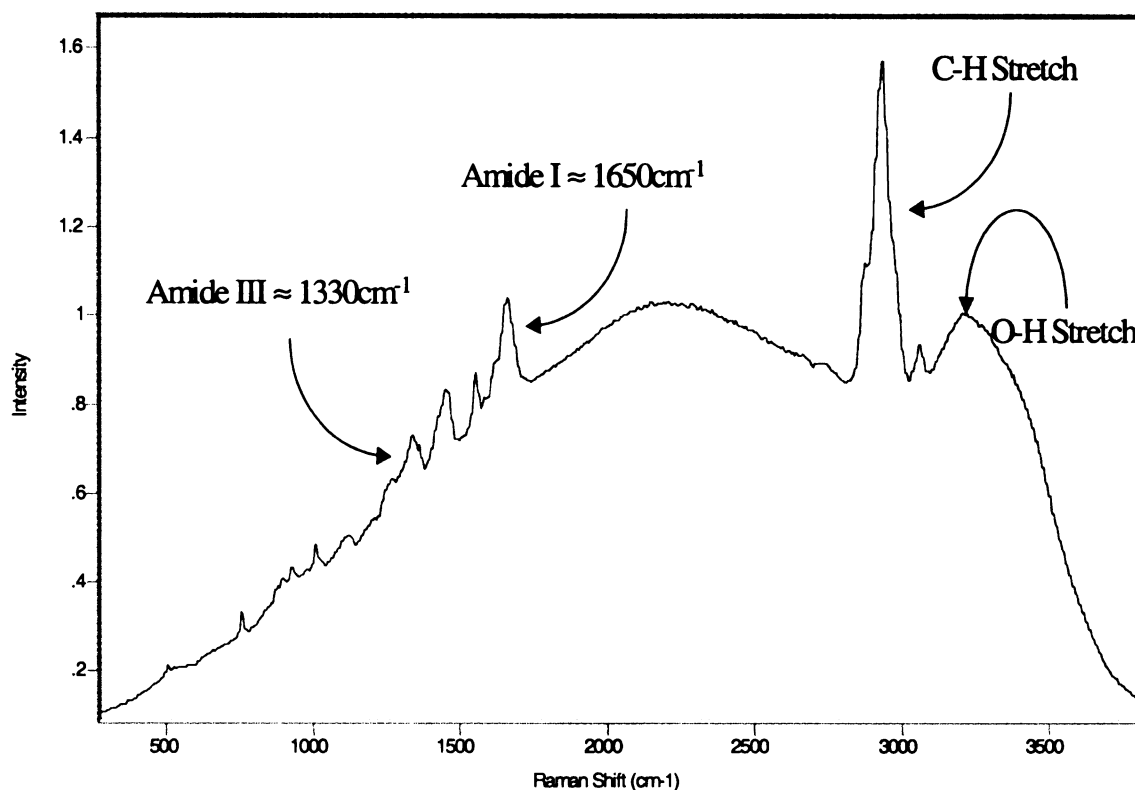


Figure 5.1 A typical Raman spectrum of a 5  $\mu$ l hanging drop of lysozyme obtained with the Kaiser Optical, Inc. Hololab Series 1000® instrument. The Raman spectrum depicts a 0.22 g/ml sample of lysozyme over the Raman shift range of 200  $\text{cm}^{-1}$  to 3900  $\text{cm}^{-1}$ . The vibrational regions corresponding to the Amide I stretch, the Amide III stretch, the CH stretches, and the OH stretches are labeled. The fluorescence background is also clearly visible. The fluorescence distorts the baseline yielding a Raman baseline with convex curvature.

The nine proteins used in this experiment ranged in molecular weight from 14 to 250 kDa. Each of the nine proteins utilized a slightly different buffer system yet none of these buffers yielded any detectable fluorescence with the 632.8 nm incident radiation. However, each of the protein solutions fluoresced to some degree. This list of proteins is not meant to be all inclusive and only generalizations about trends can be made. Therefore, as the molecular weight of the protein increases the background fluorescence also tends to increase. A qualitative rating scheme was designed to differentiate between the varying degrees of fluorescence background, which were encountered. The rating system is as follows: excellent, good, poor, and none.

To receive an "excellent" rating the fluorescent background needed to be relatively weak in intensity. An example of this is the Raman spectrum of lysozyme in Figure 5.1. A "good" rating meant that the fluorescent background intensity increased to the highest intensity level within the Raman spectrum. However, the Amide I & III, CH, and OH stretches remained discernible within the Raman spectrum. The "poor" rating indicated that the background fluorescence interfered with the recognition of the Amide I & III stretches. The rating "none" describes the situation where the fluorescence masks any vibrational stretches in the Raman spectrum. A rating of "excellent", "good", or "poor" meant that the spectra were adequate enough to calculate concentration ratios. A rating of "none" implied that the CH and OH stretches could not be used to follow the crystallization of the protein within the hanging drop. For this reason alkaline phosphatase and bovine liver catalase were removed from the study.

Since the impetus behind this study was to show that the calibration model developed for lysozyme could be extended to other proteins, proteins that had previously been

Protein	Molecular Weight (kDa)	Raman Spectrum Rating
Lysozyme	14.4	"Excellent"
$\alpha$ -chymotrypsin	25.3	"Excellent"
Carlsberg subtilisin	27.3	"Good"
Ovalbumin	45	"Good"
$\alpha$ -amylase from barley malt	45	"Poor"
$\alpha$ -amylase bacillus	45	"Poor"
human serum albumin	65	"Good"
alkaline phosphatase	94	"None"
bovine liver catalase	250	"None"

**Table 5.1** A comparison of the quality of Raman spectrum acquired with respect to the molecular weight of the protein. As the molecular weight of the protein increases the Raman spectrum is more susceptible to interference due to background fluorescence.

crystallized were selected. In an attempt to duplicate the crystallization conditions, the reported literature conditions were utilized [19, 20, 21, 22, 23, 24, 25]. The experiment was to be run in triplicate at each reservoir condition for each protein studied. Therefore, ovalbumin and  $\alpha$ -chymotrypsin were eliminated from the study because their reported induction times were too large for the repetitive nature of this experiment. The authors were unable to grow crystals of  $\alpha$ -amylase *bacillus*; therefore it was also removed from the study.

Of the remaining four proteins, three were chosen to prove that the ratio of the relative intensities of the CH and OH stretches is sufficient to monitor and control protein crystallization within the hanging drop. The three proteins were lysozyme with an "excellent" rating, Carlsberg subtilisin with a "good" rating, and  $\alpha$ -amylase from barley malt with a "poor" rating. The monitoring and control experiments performed on lysozyme have previously been discussed [17]. The remainder of this study was concentrated on monitoring and controlling the hanging drop crystallization of  $\alpha$ -amylase from barley malt and Carlsberg subtilisin.

In order for the PLS model to calculate the concentration ratios necessary to control the hanging drop experiment, the Raman spectra of  $\alpha$ -amylase from barley malt and Carlsberg subtilisin needed to be similar to the Raman spectrum of lysozyme. Figure 5.2 contains the Raman spectra of lysozyme,  $\alpha$ -amylase from barley malt, and Carlsberg subtilisin over the Raman shift range of 2200  $\text{cm}^{-1}$  to 3900  $\text{cm}^{-1}$ . These spectra have been corrected for any background fluorescence and scaled to more easily exhibit the similarities between the spectra. Though the spectra vary in intensity of the CH stretching region, the line shapes of the CH and OH stretches between the three spectra

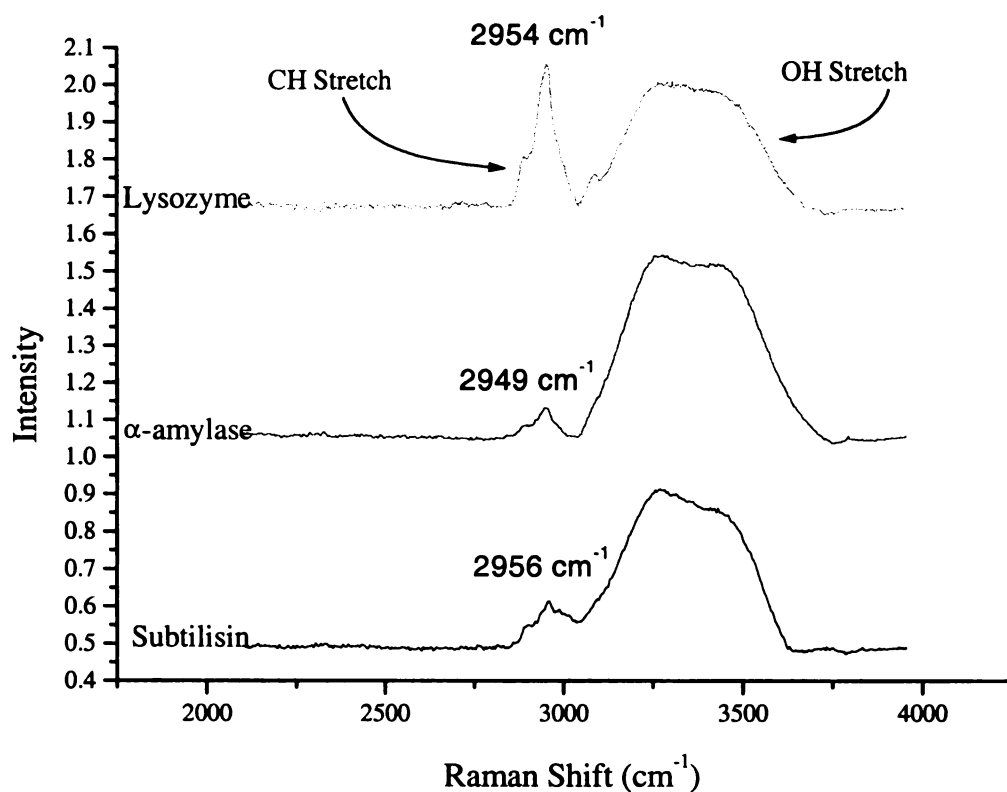


Figure 5.2 A comparison of the fluorescence corrected Raman spectra of lysozyme,  $\alpha$ -amylase from barley malt, and Carlsberg subtilisin. The CH stretches in all three spectra contain shoulders near  $2900 \text{ cm}^{-1}$  and peak maxima near  $2950 \text{ cm}^{-1}$ . The OH stretching region in all the spectra is comprised of a single broad peak ranging from  $3100 \text{ cm}^{-1}$  to  $3700 \text{ cm}^{-1}$ .

are comparable. Each of the broad CH stretches contains a faint shoulder near  $2900\text{ cm}^{-1}$  with the apex of the peak centered near  $2950\text{ cm}^{-1}$ , and each of the OH stretching regions is comprised of a single broad peak ranging from  $3100\text{ cm}^{-1}$  to  $3700\text{ cm}^{-1}$ .

The experiments were performed in the same manner as the previous lysozyme experiments. First, the protein is placed above a reservoir of a given ionic strength and Raman spectra are taken of the hanging drop every five minutes. The process within the hanging drop is allowed to go to completion. The protein within the hanging drop will remain in solution, crystallize, or precipitate. The Raman data is then processed and a supersaturation profile is generated from the concentration ratios. This supersaturation profile is then used to determine the time of nucleation of the protein and the rate of generation of supersaturation of the drop when the ionic strength of the reservoir is held constant.

The experiments were completed in triplicate and then averaged. The rate of generation of supersaturation is defined here as the slope of the supersaturation profile from the time the experiment was initiated until the time nucleation occurred. The concentration ratio data was fit to a first-order equation over the linear range of the supersaturation profile. The slope was then taken as the rate of generation of supersaturation. The linear regressions were performed by Microcal Origin® software and were determined to be significant. The rate of generation of supersaturation term gives insight into the amount of water that is being drawn out of the hanging drop due to the reservoir with higher ionic strength.

The experimental conditions for  $\alpha$ -amylase from barley malt and Carlsberg subtilisin were obtained from literature [22, 21]. The  $\alpha$ -amylase was dissolved in a buffer

comprised of 1 mM calcium chloride and 10 mM MES at a pH of 6.7. The suggested precipitant was ammonium sulfate. Ammonium sulfate was added to the buffer to create an  $\alpha$ -amylase solution with an initial ionic strength of 0.45 M. Ammonium sulfate was added to in greater amounts to the  $\text{CaCl}_2$ /MES buffer to produce reservoir solutions ranging in ionic strength from 1.30 to 1.90 M. The subtilisin was dissolved in a solution comprised of 560 mM sodium sulfate at neutral pH, resulting in a subtilisin solution with an initial ionic strength of 1.4 M. Reservoir solutions of sodium sulfate were made ranging in ionic strength from 2.50 to 3.20 M.

Employing these conditions the uncontrolled supersaturation profiles were obtained for both  $\alpha$ -amylase and subtilisin. Figure 5.3 represents the supersaturation profiles for  $\alpha$ -amylase when the reservoir ionic strengths were constant. The triangles denote the supersaturation profile of the reservoir with an ionic strength of 1.90 M, and the circles denote the supersaturation profile of the reservoir with an ionic strength of 1.30 M. Figure 5.4 represents the supersaturation profiles for subtilisin at reservoir ionic strengths of 3.20 M (triangles) and 2.50 M (circles). In Figure 5.3 and Figure 5.4 the concentration ratios increase with time. Eventually the supersaturation profile begins to change direction and the concentration ratio begins to decrease.

The initial increase in concentration ratios is due to the amount of water evaporating from the hanging drop. As the water leaves the hanging drop, the OH stretch in the Raman spectrum decreases in intensity. The denominator of the concentration ratio becomes smaller and therefore the concentration ratio increases. As water leaves the hanging drop, the protein drop concentrates and will eventually become supersaturated. The reversal of the supersaturation profile is due to nucleation within the hanging drop.



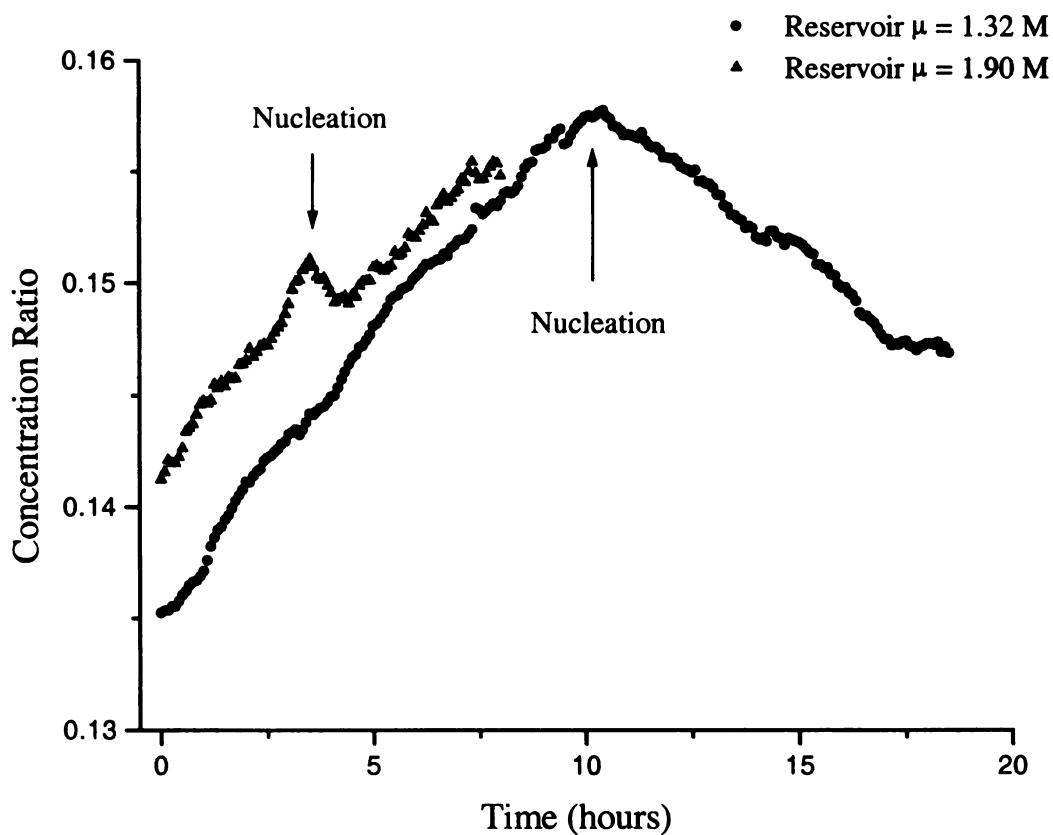


Figure 5.3 A comparison of the relative crystallization kinetics between hanging drop experiments with an initial  $\alpha$ -amylase concentration of about 0.11 g/ml and varying reservoir ionic strengths. The profile plotted as triangles corresponds to a reservoir ionic strength of 1.90 M and the profile plotted as circles corresponds to a reservoir ionic strength of 1.32 M.

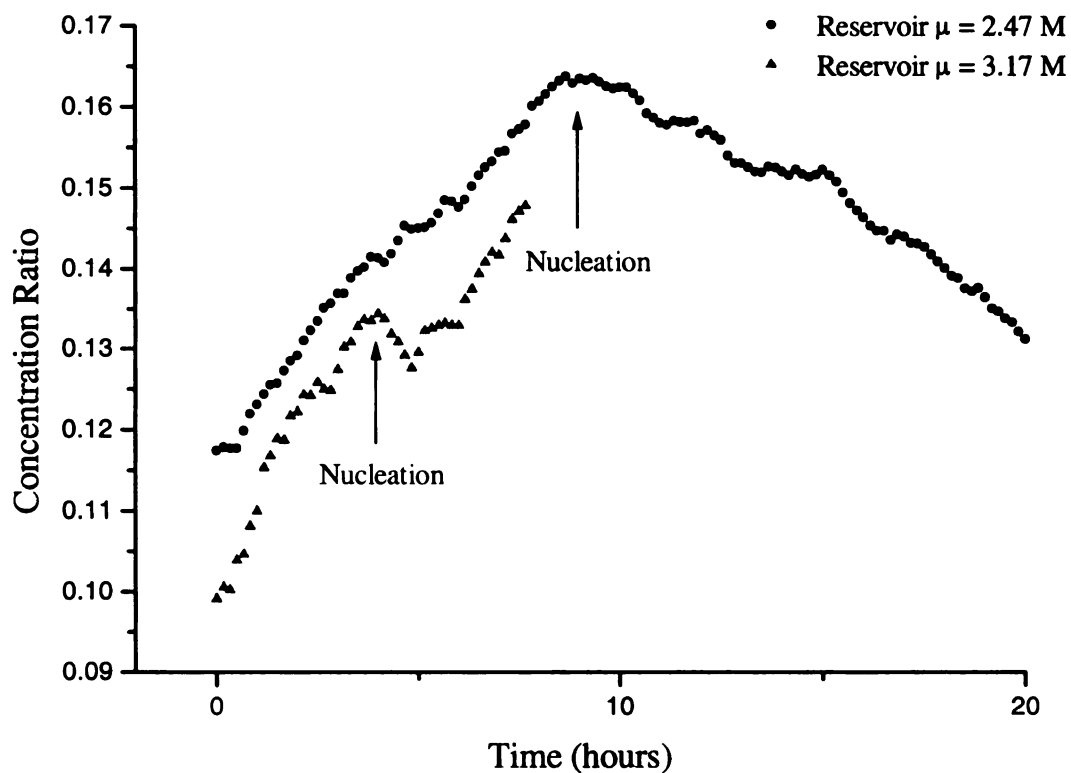


Figure 5.4 A comparison of the relative crystallization kinetics between hanging drop experiments with an initial subtilisin concentration of about 0.05 g/ml and varying reservoir ionic strengths. The profile plotted as triangles corresponds to a reservoir ionic strength of 3.17 M and the profile plotted as circles corresponds to a reservoir ionic strength of 2.47 M.

After nucleation, protein begins to leave the solution phase and enter the solid phase. Accordingly, the concentration of the hanging drop decreases. The decrease in concentration is accompanied by a decrease in the CH stretch of the Raman spectrum. In turn the numerator of the concentration ratio decreases, this leads to a decrease in the supersaturation profile.

The reversal of direction of the supersaturation profile reveals the time of nucleation for the protein in the hanging drop. In Figure 5.3 and Figure 5.4 the reversal of the supersaturation profile for the experiment with the lower ionic strength reservoir (circles) occurs at a longer time. The opposite is true for the experiments with the higher ionic strength reservoirs (triangles). Rates of supersaturation generation were then extracted from the supersaturation profile data. For both the  $\alpha$ -amylase and subtilisin experiments with the higher ionic strengths (triangles) the profile changes direction a second time and begins to increase. This can be explained by the fact that in both of these experiments protein crystallization was immediately followed by the onset of precipitation. The increase in concentration ratio is a result of the greater scattering intensity of the precipitate over the solution.

Summaries of these findings are listed in Table 5.2 and Table 5.3. These results demonstrate that as the difference between the initial ionic strength of the hanging drop and the reservoir ionic strength increased the rate of generation of supersaturation also increased. As expected a larger rate of supersaturation generation leads to a shorter time of nucleation. The final column in Table 5.2 and Table 5.3 describes the results of the experiments. The abbreviations "xtal" and "ppt" indicate the formation of protein crystals

### Uncontrolled $\alpha$ -amylase Hanging Drop

Initial $\alpha$ -amylase Concentration	Initial Drop Ionic Strength	Reservoir Ionic Strength	Rate of Generation of Supersaturation (ratio/hr)	Time of Nucleation (hours)	Result
0.11 g/ml	0.45 M	1.30 M	$0.0022 \pm 0.0001$	10	1 xtal
0.11 g/ml	0.45 M	1.90 M	$0.0031 \pm 0.0001$	3.5	xtal/ppt

### Controlled $\alpha$ -amylase Hanging Drop

Initial $\alpha$ -amylase Concentration	Initial Drop Ionic Strength	Reservoir Ionic Strength	Rate of Generation of Supersaturation (ratio/hr)	Time of Nucleation (hours)	Result
0.11 g/ml	0.45 M	1.90 M (initial)	$0.007 \pm 0.0002$	4.1	1 xtal
		1.30 M (1.5 hours)	$0.005 \pm 0.0005$		

Table 5.2 A summary of the results of uncontrolled and controlled crystallization experiments for  $\alpha$ -amylase in terms of rates of supersaturation, times of nucleation, and numbers of crystals produced. The abbreviation “ppt” indicates that the outcome of the experiment was the formation of amorphous precipitate and the abbreviation “xtal” indicates the formation of crystal. As the rate of supersaturation increased the time of nucleation decreased and the onset of precipitate formation increased.

### Uncontrolled subtilisin Hanging Drop

Initial subtilisin Concentration	Initial Drop Ionic Strength	Reservoir Ionic Strength	Rate of Generation of Supersaturation (ratio/hr)	Time of Nucleation (hours)	Result
0.05 g/ml	1.40 M	2.50 M	$0.0052 \pm 0.0001$	9	10 xtals
0.05 g/ml	1.40 M	3.20 M	$0.014 \pm 0.001$	4	xtals/ppt

### Controlled subtilisin Hanging Drop

Initial subtilisin Concentration	Initial Drop Ionic Strength	Reservoir Ionic Strength	Rate of Generation of Supersaturation (ratio/hr)	Time of Nucleation (hours)	Result
0.05 g/ml	1.40 M	3.20 M (initial)	$0.012 \pm 0.001$		
		2.50 M (1.5 hours)	$0.003 \pm 0.0005$	5.0	30 xtal

Table 5.3 A summary of the results of uncontrolled and controlled crystallization experiments for subtilisin in terms of rates of supersaturation, times of nucleation, and numbers of crystals produced. The abbreviation “ppt” indicates that the outcome of the experiment was the formation of amorphous precipitate and the abbreviation “xtal” indicates the formation of crystal. As the rate of supersaturation increased the time of nucleation decreased and the onset of precipitate formation increased.

or precipitate, respectively. The combination of these terms, "xtal/ppt", indicates the formation of both crystals and precipitate.

The ability to monitor these ratios and calculate a rate of generation of supersaturation in real time, enables the comparison of the real time data with that of the uncontrolled experiments. To display the utility of the Raman control scheme, concentration ratios were monitored in real time and affected by making step changes in the reservoir ionic strength. Following the same procedure performed on lysozyme [17], the hanging drop first encountered a reservoir with high ionic strength followed by a reservoir of lower ionic strength. The step change in reservoir ionic strength was implemented as a result of the *in situ* calculation of the slope of the supersaturation profile.

Figure 5.5 depicts a comparison of the  $\alpha$ -amylase concentration ratio profiles for both the controlled (triangles) and uncontrolled (circles) experiments. The nucleation event is marked with an arrow. By adjusting the ionic strength of the reservoir in the controlled experiment the time of nucleation was increased over that of the uncontrolled experiment. The bottom portion of Table 5.2 describes the conditions of the experiment. The starting ionic strength of the hanging drop, the initial concentration of  $\alpha$ -amylase, and the initial ionic strength of the reservoir were the same as the uncontrolled experiment. By monitoring the initial slope of the supersaturation profile of the controlled experiment it was evident that the concentration was increasing at a faster rate than that in the uncontrolled experiment (Table 5.2).

The slope of the supersaturation profile was determined to be 0.003 (ratio/hour) in the uncontrolled experiment. The *in situ* calculation of the slope of the supersaturation

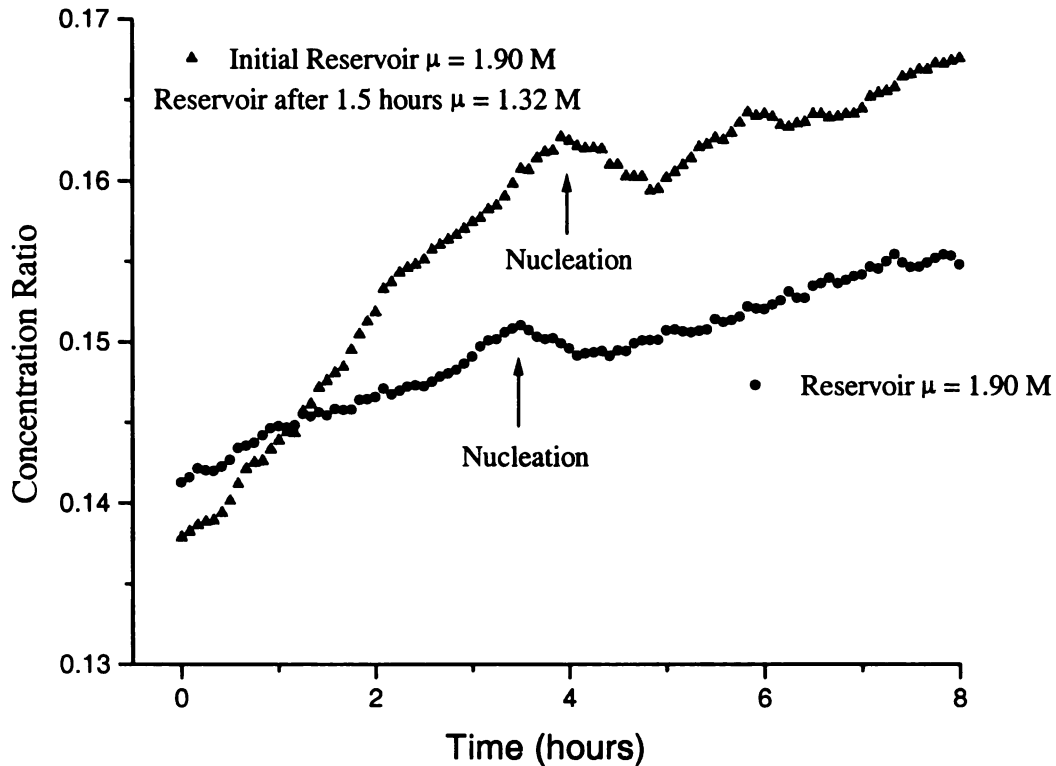


Figure 5.5 A direct comparison of the  $\alpha$ -amylase concentration ratio profiles for hanging drop crystallization experiments which were controlled and uncontrolled. By applying control of the ionic strength of the reservoir, the induction time in the controlled experiment is increased by approximately 1 hour.

profile in the control experiment was determined to be 0.007 (ratio/hour) at 1.5 hours. Knowing that the rate of supersaturation generation in the uncontrolled experiment lead to both crystal and precipitate formation, a change in reservoir was initiated. At 1.5 hours the reservoir in the controlled experiment was changed from an ionic strength of 1.90 M to an ionic strength of 1.30 M. This decreased the rate of supersaturation generation in the controlled experiment from 0.007 (ratio/hour) to 0.005 (ratio/hour). As a result the time of nucleation was increased and only crystal formation occurred.

Figure 5.6 displays photographs of the results of the uncontrolled (A) and controlled (B) experiments, which correspond to the supersaturation profiles in Figure 5.5. The viewing area of the photographs has a diameter of approximately 1mm, and encompasses about  $\frac{1}{2}$  of the surface area of the hanging drop, which is in contact with the glass slide. The top picture, labeled A, is of the  $\alpha$ -amylase crystal produced during the uncontrolled experiment, and the bottom picture, labeled B, is of the  $\alpha$ -amylase crystal produced through dynamic control of the hanging drop experiment. Between the pictures is a length indicator to illustrate the scale of magnification. The indicator represents a length of 100  $\mu\text{m}$ . The uncontrolled experiment yielded  $\alpha$ -amylase crystals with an average size of about 190  $\mu\text{m}$ , while the controlled experiment lead to  $\alpha$ -amylase crystals with an average size of about 240  $\mu\text{m}$ . Though the control only achieved an increase in size of about 50  $\mu\text{m}$ , the  $\alpha$ -amylase crystal in photograph B is of better quality. The  $\alpha$ -amylase crystal in photograph A does not have sharp edges and it contains a large defect in the center of the crystal. In addition the area surrounding the crystal contains small dark images, which are regions of precipitate formation.



A

  
100  $\mu\text{m}$ 

B

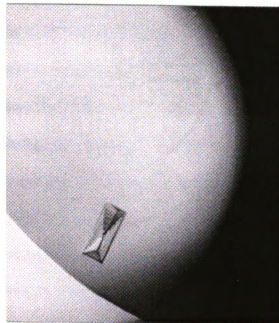


Figure 5.6 These  $\alpha$ -amylase crystals correspond to the concentration ratio profiles of the controlled and uncontrolled experiments in Figure 5. These photographs are at the same magnification, and encompass identical viewing areas. The top picture represents the uncontrolled experiment, and the bottom picture represents the controlled experiment. Through the application of control of the crystallization process both the size of the resultant crystal and the quality of the crystal was increased.

Figure 5.7 depicts a comparison of the subtilisin supersaturation profiles for both the controlled (triangles) and uncontrolled (circles) experiments. Again, an arrow marks the nucleation event. The bottom portion of Table 5.3 describes the conditions of the experiment. The starting ionic strength of the hanging drop, the initial concentration of  $\alpha$ -amylase, and the initial ionic strength of the reservoir were the same as the uncontrolled experiment. In the uncontrolled experiment the slope of the supersaturation profile was determined to be 0.014 (ratio/hour) and in the control experiment the *in situ* calculation of the slope of the supersaturation profile was determined to be 0.012 (ratio/hour) at 1.5 hours. This rate of generation of supersaturation produced both crystal and precipitate in the uncontrolled experiment. At 1.5 hours the reservoir in the controlled experiment was replaced with a lower ionic strength reservoir. Consequently, the supersaturation profile levels and the rate of generation of supersaturation decreased in the controlled experiment from 0.012 (ratio/hour) to 0.003 (ratio/hour). As a result the induction time was increased and only crystal formation dominated.

Figure 5.8 displays photographs of the results of the uncontrolled (A) and controlled (B) experiments, which correspond to the supersaturation profiles in Figure 5.7. There are three photographs in Figure 5.8. The pictures labeled A<sub>1</sub> and A<sub>2</sub> correspond to the uncontrolled experiment at times 6 hours and 10 hours respectively. The picture labeled B corresponds to the controlled subtilisin hanging drop experiment taken at 10 hours. Though the size of crystal has not dramatically been affected by changing the reservoir ionic strength, the step change favored the formation of crystals and inhibited precipitate formation.

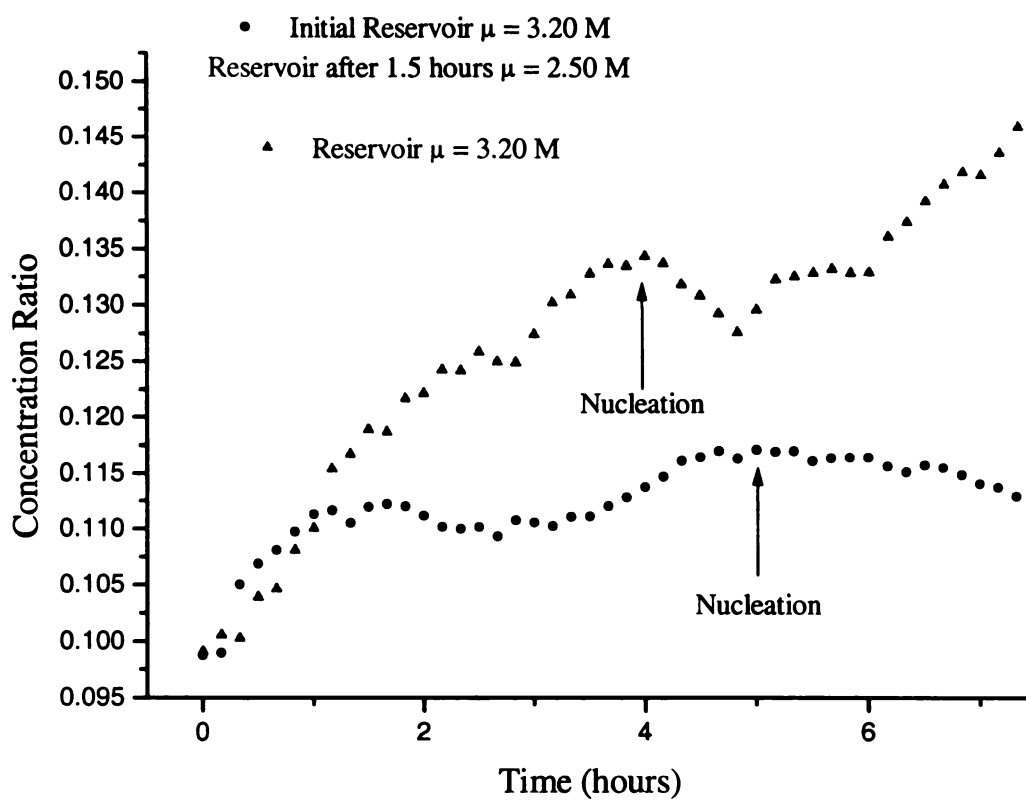
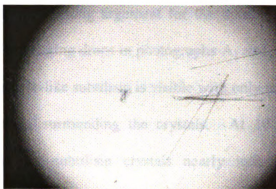


Figure 5.7 A direct comparison of the subtilisin concentration ratio profiles for hanging drop crystallization experiments which were controlled and uncontrolled. By applying control of the ionic strength of the reservoir, the induction time in the controlled experiment is increased by approximately 1 hour.

A<sub>1</sub>  
Uncontrolled  
Time = 6 hours



A<sub>2</sub>  
Uncontrolled  
Time = 10 hours



B  
Controlled  
Time = 10 hours



Figure 5.8 These subtilisin crystals correspond to the concentration ratio profiles of the controlled and uncontrolled experiments in Figure 7. These photographs are at the same magnification, and encompass identical viewing areas. The top pictures represent labeled A<sub>1</sub> and A<sub>2</sub> represent the uncontrolled experiment, and the bottom picture represents the controlled experiment. Through the application of control of the crystallization process the onset of precipitate formation was avoided and the nucleation and growth of subtilisin crystals was favored, picture B.

These pictures also constitute a strong argument for the continuous monitoring of hanging drop experiments. The hanging drops in photographs A<sub>1</sub> and A<sub>2</sub> are of the same drop. At 6 hours crystalline needle-like subtilisin is visible with only minor dark regions, suggesting precipitate formation, surrounding the crystals. At 10 hours precipitate formation dominates making the subtilisin crystals nearly indistinguishable. By monitoring the subtilisin concentration ratio over time, a supersaturation profile was generated. The appearance of an inflection in the supersaturation profile for the 3.20 M reservoir suggested a nucleation event occurred at approximately 4 hours. This finding warranted further scrutiny. In subsequent trials photographs of the hanging drop were taken at 4, 5, and 6 hours. These photographs revealed the existence of subtilisin crystals. If the drop was not continuously monitored, the subtilisin crystals may have gone undetected.

## **Discussion and Conclusions**

Following the method previously employed on lysozyme [17], we have demonstrated that the Raman method of monitoring the hanging drop experiment can be extended to the  $\alpha$ -amylase from barley malt and the subtilisin protein systems. These experiments have demonstrate the utility of the PLS method devised for lysozyme. The PLS method, which can be considered a ratio calculation of CH to OH stretches in the vibrational spectrum, can be utilized on protein spectra that are similar to lysozyme. Though these experiments were limited to proteins that produced a Raman spectrum from incident radiation at 632.8 nm, the method could be extended to other proteins systems with the choice of a different laser source. Higher wavelength lasers are available, which would

further reduce the background fluorescence encountered with certain proteins in this study.

These experiments have extended the model derived for lysozyme to other protein systems, but more importantly this method has been extended to protein systems other than the ideal case of lysozyme. As with lysozyme [17], supersaturation profiles were generated. The supersaturation profiles of  $\alpha$ -amylase from barley malt and subtilisin reveal similarities to prior experiments performed on lysozyme. The profiles share an inversion point and subsequent reversal of direction at the point of nucleation. Additionally, in the event crystalline solid or amorphous precipitate formed directly in the path of the incident laser the supersaturation reversed direction and increased in value dramatically. The PLS method has proven to be an effective means of monitoring the amount of water being drawn out of the hanging drop. In turn the generated rates of supersaturation can be calculated and correlated with the outcome of the experiment either crystal or precipitate formation. The ability to compute these values *in situ* has proven to be invaluable in affecting an online change and controlling crystallization in the hanging drop experiment.

Finally, these results indicate that the hanging drop experiment should be monitored continuously. Simply suspending a protein drop above a reservoir and checking the drop every day, week, or month is an ineffective method of conducting the hanging drop experiment. Findings also verify that merely allowing the hanging drop to equilibrate with a reservoir of higher ionic strength will not always produce quality crystals. If hanging drop experiments are run in this manner, there is no control. Chance dictates whether a crystal that forms can be used for three-dimensional structure elucidation.

Hanging drop experiments performed in this fashion are assumed to path independent. However, the authors have clearly demonstrated, with lysozyme [17],  $\alpha$ -amylase from barley malt, and Carlsberg subtilisin, that crystallization in the hanging drop is definitely path dependent. It is the authors' hope that focus will further shift to development of strategies to both better monitor and control the hanging drop experiment.

## Literature Cited

- [1] C.W. Carter, Jr. and C.W. Carter, J. Biol. Chem. 254 (1979) 12219.
- [2] J. Jancarik, and S.-H. Kim, J. Appl. Cryst. 24 (1991) 409.
- [3] B.D. Prater, S.C. Tuller, and L.J. Wilson, J. Crystal Growth 196 (1999) 674.
- [4] B.L. Pan and K. A. Berglund, J. Crystal Growth 171 (1997) 226.
- [5] F. Rosenberger, P.G. Velikov, M. Muschol, and B.R. Thomas, J. Crystal Growth 168 (1996) 1.
- [6] M. Muschol and F. Rosenberger, J. Chem. Phys. 103 (1995) 10424.
- [7] Y. Georgalis, P. Umbach, A. Zielenkiewicz, E. Utzig, W. Zielenkiewicz, P. Zielenkiewicz, and W. Saenger, J. Am. Chem. Soc. 119 (1997) 11959.
- [8] M. Boyer, M.-O. Roy, and M. Jullien, J. Crystal Growth 167 (1996) 212.
- [9] Z. Kam, H.B. Shore, and G. Feher, J. Mol. Biol. 123 (1978) 539.
- [10] P.A. Darcy and J.M. Wiencek, J. Crystal Growth 196 (1999) 243.
- [11] T. Soga, H. Sasaki, M. Tanokura, and M. Ataka, J. Crystal Growth 196 (1999) 291.
- [12] F. Sica, S. Adinolfi, R. Berisio, C. De Lorenzo, L. Mazzarella, R. Piccoli, L. Vitagliano, and A. Zagari, J. Crystal Growth 196 (1999) 305.
- [13] I.P. Kuranova, E.V. Blagova, V.M. Levnikov, G.N. Rudenskaya, N.P. Balaban, and E.V. Shakirov, J. Crystal Growth 196 (1999) 313.
- [14] R.R. Ansari, K.I. Suh, A. Arabshahi, W.W. Wilson, T.L. Bray, and L.J. DeLucas, J. Crystal Growth 168 (1996) 216.
- [15] Z.-Y. Shu, H.-Y. Gong, and R.-C. Bi, J. Crystal Growth 192 (1998) 282.
- [16] A.M. Schwartz and K.A. Berglund, J. Crystal Growth 203 (1999) 599.
- [17] A.M. Schwartz and K.A. Berglund, J. Crystal Growth accepted July 1999.
- [18] J.W. Mullin, Crystallization 3<sup>rd</sup> Edition (Butterworth Heinemann Ltd., Oxford, 1993).
- [19] A. McPherson, The Preparation and Analysis of Protein Crystals (Krieger Publishing Co., Malabar, FL., 1989).



- [20] P.B. Sigler, D.M. Blow, B.W. Matthews, and R. Henderson, *J. Mol. Biol.* 35 (1968) 143.
- [21] Petsko et. al., *J. Mol. Biol.* 106 (1976) 453.
- [22] B. Svensson, R.M. Gibson, R. Haser, and J.P. Astier, *J. Biol. Chem.* 262 (1987) 13682.
- [23] C. Chang et. al., *J. Mol. Biol.* 229 (1993) 235.
- [24] M. Miller, J.N. Weinstein, and A. Wlodawer, *J. Biol. Chem.* 258 (1983) 5864.
- [25] X.M. He and D.C. Carter, *Nature* 358 (1992) 209.
- [26] S. Olafsdottir, C. Wright, H.T. Wright, and J.F. Chlebowski, *J. Biol. Chem.* 263 (1988) 10002.
- [27] D.A. Long, *Raman Spectroscopy* (McGraw-Hill, New York, 1977).
- [28] P.R. Carey, *Biological Applications of Raman and Resonance Raman Spectroscopies* (Academic Press, New York, 1982).
- [29] P. R. Carey, *J. Raman Spectrosc.* 29 (1998) 7.

## **Chapter 6: A Comparison of Control Mechanisms Employed on Lysozyme Crystallization Experiments in a Hanging Drop\***

\*Submitted to the Journal of Crystal Growth

### **Summary**

Fiber optic Raman spectroscopy combined with a partial least-squares regression model was demonstrated for real time monitoring of lysozyme concentration during crystallization in a hanging drop experiment in real time. Raman spectral features of the buffer and protein were employed to build the regression model. The use of fiber optic technology coupled with Raman spectroscopy, which is ideal for use with aqueous solutions, results in a powerful noninvasive probe of the changing environment within the solution. Monitoring the concentration changes of the lysozyme within the hanging drop permits a measurement of the level of supersaturation of the system and enhances dynamic control of the crystallization process. Previously, hanging drop experiments have been monitored in real time. These experiments have given insight into the changing environment of the hanging drop as the lysozyme within the hanging drop concentrates, nucleates, and as crystal growth continues. By altering the ionic strength of the reservoir the number, size, and quality of the resultant crystals has been affected. This investigation will compare three methods of controlling the lysozyme crystallization within the hanging drop by employing various reservoir conditions. These conditions include a constant ionic strength reservoir, a step change in reservoir ionic strength, and a differential change in reservoir ionic strength.

## Introduction

The impetus in studying protein crystallization has been the desire to understand the mechanisms that drive protein crystallization. If the underlying crystallization mechanisms could be measured and fully understood, then crystallization conditions could be predicted by these measurements. Initially, methods employing dynamic and static light scattering [1,2,3,4,5], fluorescence anisotropy [6], calorimetric techniques [7,3] were examined. The light scattering based techniques were by far the dominant techniques applied in studying protein crystallization. Unfortunately these techniques were incomplete predictors of crystallization conditions. Recently, in a brief literature survey of newly crystallized proteins, the authors found that most of the crystallization conditions were still found by trial and error matrix screening methods [8,9,10].

Performing crystallization experiments via screening methods in a hanging drop is time consuming and labor intensive. A change of only a few percent in either ionic strength or pH can completely change the solubility of the protein and alter the outcome of the hanging drop experiment. For this reason the number of screening experiments necessary to determine the crystallization conditions of a protein can quickly increase. In an attempt reduce the number of screening experiments, some research has shifted emphasis from prediction to control. These studies have included dynamic light scattering combined with humidity sensors [11], a gravimetric technique [12], and fiber optic Raman spectroscopy [13,14]. The third technique based on Raman spectroscopy allows simultaneous measurement of the concentration of lysozyme and the amount of water within the drop [13]. Raman spectroscopy probes the vibrational energy levels of the bonds within the protein and the water. A partial least squares regression model

correlates the Raman spectral features with the concentration of lysozyme present in the drop [13]. The control method, based on Raman spectroscopy, has proven to be a noninvasive probe capable of measuring the level of supersaturation of the lysozyme within the hanging drop *in situ* [14].

These experiments have given the authors an understanding into the changing environment of the hanging drop as the lysozyme concentrates, nucleates, and as the lysozyme crystals grow. By altering the ionic strength of the reservoir the number, size, and quality of the resultant crystals has been affected [14]. This investigation compares three methods of controlling the lysozyme crystallization within the hanging drop by applying various reservoir conditions. These conditions include a constant ionic strength reservoir, a step change in reservoir ionic strength, and a differential change in reservoir ionic strength.

## **Experimental Procedure**

### ***Protein Sample Preparation***

Three times crystallized, dialyzed, and lyophilized chicken egg white lysozyme was purchased from Sigma Chemical Co. and used without further purification. All experiments were performed in a buffer containing 0.1 M sodium acetate at pH 4.2. Salt and protein solutions for standards were prepared gravimetrically with a Mettler AE50 balance. For all experiments lysozyme was dissolved into the NaCl/buffer system, with an initial ionic strength of about 0.34 M, and then filtered through a 45  $\mu$ m Millipore filter before use. A 5  $\mu$ l protein drop was deposited on a microscope cover glass. The cover glass was then inverted and placed over a 6 ml vessel containing 2 ml of a

NaCl/buffer reservoir. The top of each vessel was greased with silicone to ensure an airtight seal. Precautions were taken to ensure that the grease did not come into contact with the hanging drop of protein.

### *Experimental Design*

The reaction vessel, shown in Figure 6.1, consists of a 6 ml vial with inlet and outlet ports. Depending upon the desired control scheme a syringe or peristaltic pump can be attached to these channels. If step changes in reservoir ionic strength are desired, an outlet syringe allows the reservoir to be withdrawn and the inlet syringe allows the addition of a new NaCl/buffer solution. If a differential change in reservoir ionic strength is desired, a peristaltic pump can be attached to the inlet as seen in Figure 6.1. To facilitate a differential change in reservoir ionic strength two peristaltic pumps, located between the high and low ionic strength containers and the reaction vessel, are required. By adjusting pumps (7) and (8) to have identical flowrates, the ionic strength profile can be altered by changing the ionic strength of vessel (5). These experimental designs permit the ionic strength of the reservoir to be changed completely or incrementally, which in turn will affect the rate of supersaturation of the protein. The reaction vessel sits atop a translational stage, which allows the hanging drop of protein to be positioned within the focal point of the incident laser line.

### *Data Analysis*

The laser power incident on the cover glass and protein drop ranged from 19 to 22 mW. Each spectrum consisted of 20 scans collected over 129 seconds at  $8\text{ cm}^{-1}$

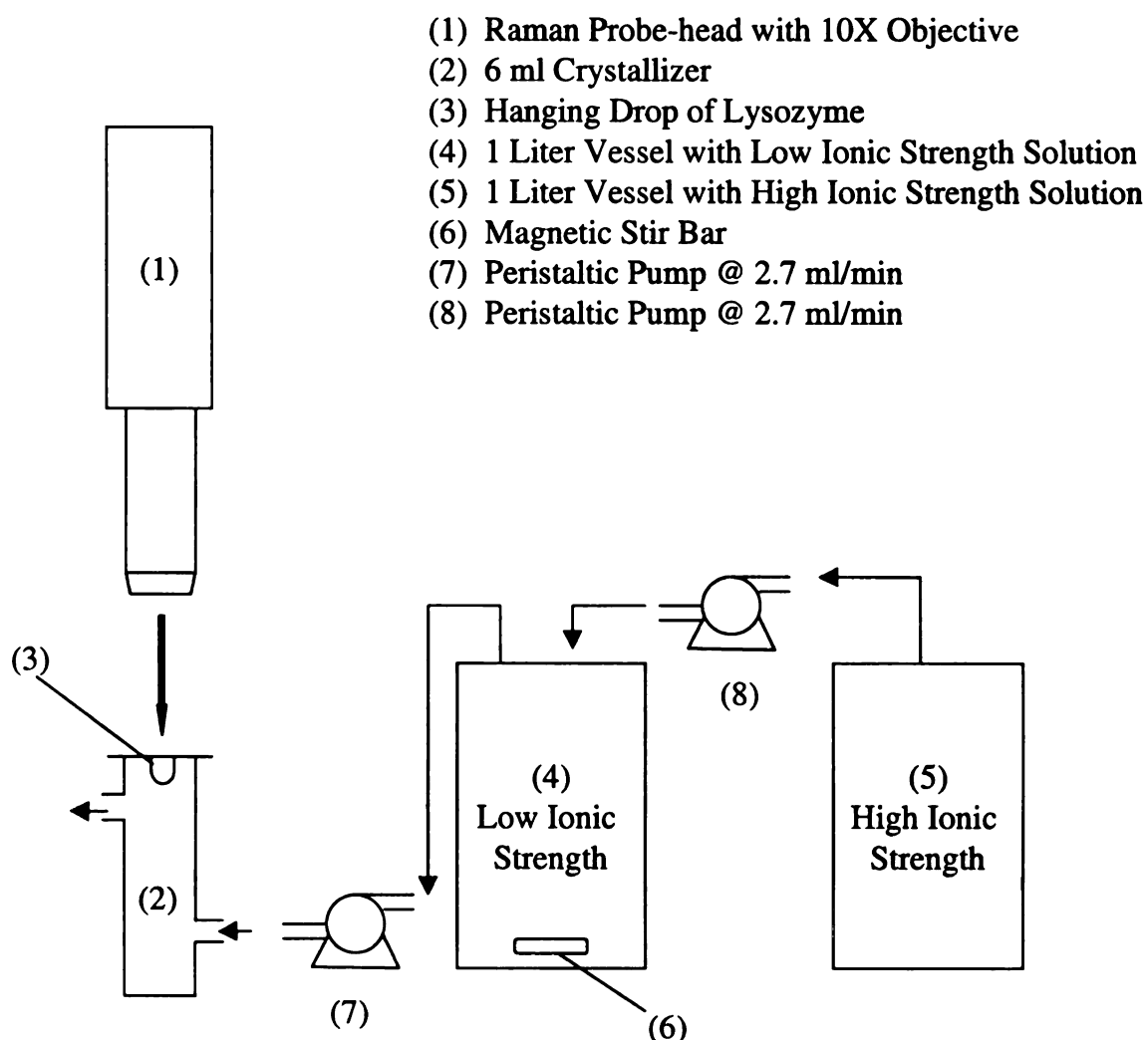


Figure 6.1 A schematic of the experimental set-up used throughout the lysozyme vapor diffusion experiments, consisting of a 6 ml vial with input and output channels. These channels were attached to syringes or peristaltic pumps, which allow the composition of the reservoir to be altered. The fiber optic probe assembly is positioned directly above the hanging drop of lysozyme solution and focused into the drop utilizing a 10X microscope objective.

resolution. The Raman spectra of 31 lysozyme standards were used to construct a PLS regression model utilizing QuantIR®, a PLS regression analysis software package by Applied Systems. The PLS model generated correlates the spectral region from 2700  $\text{cm}^{-1}$  to 3600  $\text{cm}^{-1}$  with the concentration (g/ml) of lysozyme. This spectral region encompasses vibrations due to the protein CH stretches centered at 2950  $\text{cm}^{-1}$  and the water OH stretches centered at 3230  $\text{cm}^{-1}$  [15,16].

A leave one out cross validation performed on the standards determined that the model had a root mean square error of calibration (RMSEC) of  $\pm 0.01$  g/ml. In addition to the leave one out cross validation process, the regression model was also used to determine the concentration of a test set of standards. The test set consisted of eleven standard solutions of known lysozyme concentration, which were not a part of the calibration standards of the PLS regression model. Evaluation of the PLS regression model using the test set yielded a root mean square error of prediction (RMSEP) of  $\pm 0.01$  g/ml.

This method has been shown to be effective in measuring both the solubility of lysozyme at varying ionic strengths and monitoring the change in composition of the hanging drop *in situ* [13,14]. The Raman method has been employed to measure lysozyme concentrations ranging from 0.32 g/ml to 0.02 g/ml [13]. A lysozyme concentration of approximately 0.23 g/ml and reservoir ionic strengths ranging from 0.34 M to 1.54 M were selected for this study by virtue of the relatively short nucleation times produced under these conditions. Additionally, by performing the experiments at higher protein concentrations the error in prediction of the PLS model becomes negligible. Therefore, it is the goal of the present work to utilize the Raman spectroscopic method in

monitoring the crystallization of lysozyme within a hanging drop under various control schemes.

## **Results and Discussion**

As protein crystallization occurs in the hanging drop experiment, the difference between the ionic strengths of the reservoir and the drop is integral in realizing the success of the experiment [14]. As the difference between the ionic strengths of the reservoir and the drop increase, the rate at which water is drawn from the hanging drop also increases. The protein within the hanging drop will concentrate and eventually nucleate. If the rate of water evaporation is too great, the protein within the hanging drop will supersaturate too quickly. Consequently, numerous tiny crystals or precipitate will be produced. Since large single protein crystals are preferred, small crystals or precipitate are undesirable experimental outcomes. Therefore, the level of supersaturation of the protein within the hanging drop must be controlled.

Figure 6.2 illustrates the three types of reservoir profiles employed to achieve control of lysozyme crystallization in a hanging drop. The types of control implemented on the system were a constant reservoir ionic strength, a step change in ionic strength, and a differential change in ionic strength. These various ionic strength profiles relate to uncontrolled protein crystallization, manual feedback control of the protein crystallization, and programmed control of the protein crystallization, respectively.

The uncontrolled crystallization occurs via a constant ionic strength reservoir, represented by the diamonds in Figure 6.2A. This experiment configuration is the typical hanging drop experiment. The driving force of the crystallization process is the



difference between the ionic strength of the protein drop and the reservoir. Eventually, enough water is withdrawn from the hanging drop to balance the ionic strengths of the drop and reservoir. If the hanging drop is concentrated to a level of supersaturation that facilitates crystal growth then the experiment is a success. However, it is more common for an experiment of this type to produce an amorphous precipitate.

Figure 6.2B is a representation of feedback control for a hanging drop experiment. This feedback system has previously been presented and shown to be an effective control scheme [14]. The *in situ* monitoring of the protein concentration via Raman spectroscopy allows a rate of generation of supersaturation to be calculated. This rate is compared with the generated rates of supersaturation from uncontrolled experiments. Accordingly, a step change in reservoir ionic strength is made. This type of experiment allows the concentration of the protein within the hanging drop to be monitored. When the concentration of the protein reaches a level of supersaturation that promotes nucleation, the reservoir ionic strength is reduced. Manual control of the experiment is achieved by the observation of the Raman measurement. The ability to measure the concentration *in situ* dictates the action that should be pursued.

Figure 6.2C depicts a differential change in the ionic strength of the reservoir. The rate of increase in the ionic strength is programmed into the experiment. By changing the ionic strength of the high ionic strength vessel (5) in Figure 1, the programmed ionic strength of the reservoir can be altered. In these experiments the peristaltic pumps were set to a constant flowrate of 2.7 ml/min, and the high ionic strength vessel initially contained a NaCl/buffer solution with an ionic strength of 2.4 M. The low ionic strength vessel contained a NaCl/buffer solution with an ionic strength of 0.33 M.

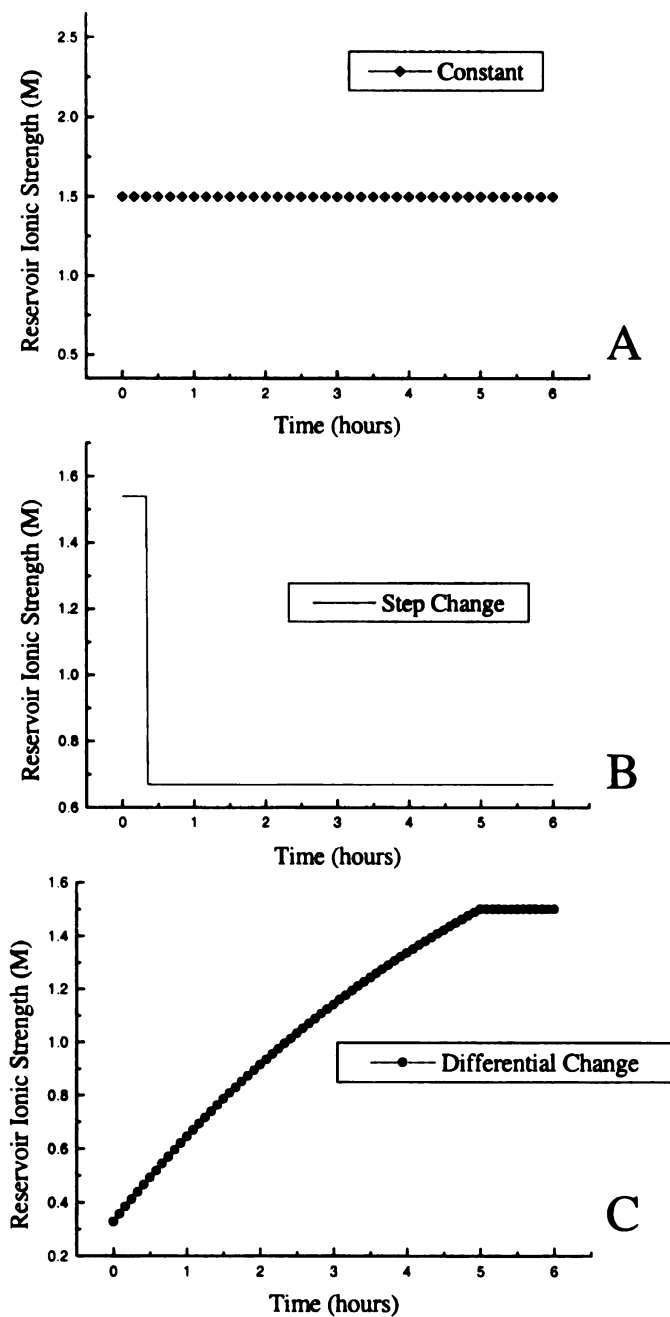
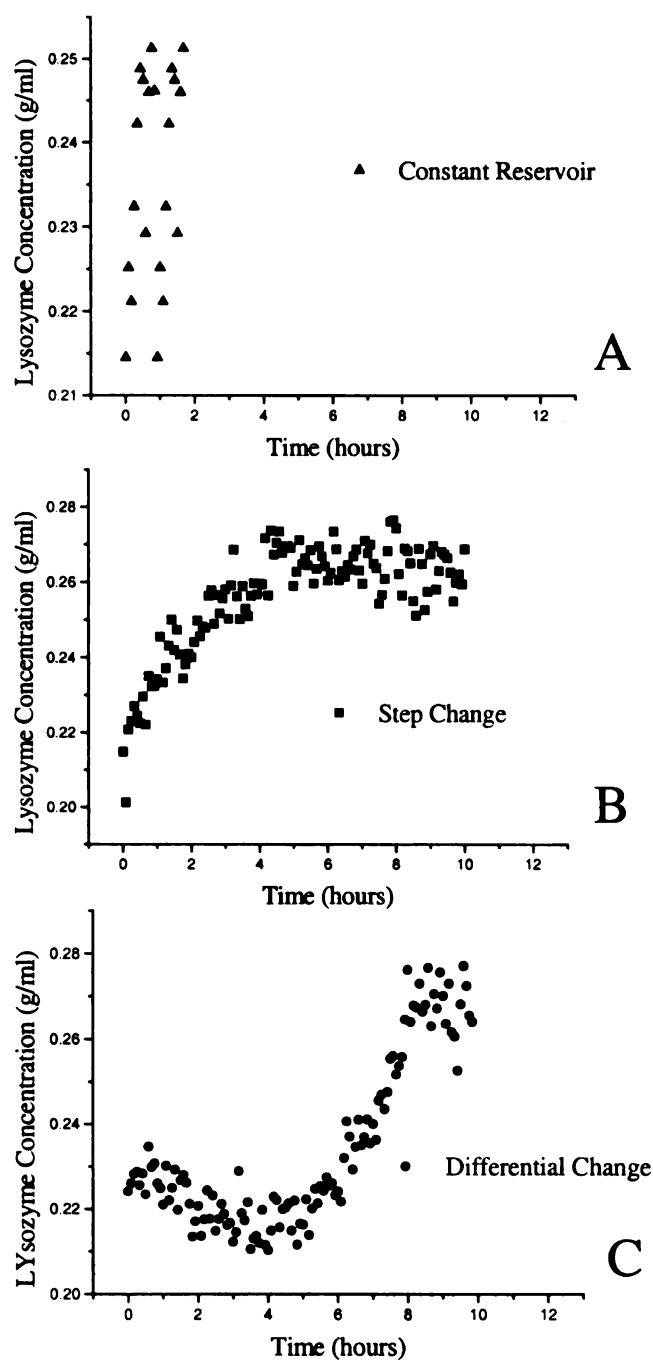


Figure 6.2 A real time ionic strength profile of the reservoir conditions. The three profiles depict a constant reservoir ionic strength (diamonds), a step change in reservoir ionic strength (line), and a differential change in ionic strength (circles). These profiles are associated with the three control schemes applied to the lysozyme hanging drop. The three control mechanisms are uncontrolled, feedback control, and programmed control of the ionic strength of the reservoir.

At the beginning of the protein crystallization experiment the pumps were started simultaneously. By keeping the pumps at equal volumetric flowrates the volume of the low ionic strength vessel, labeled (6) in Figure 6.1, remains constant. The contents of the low ionic strength vessel are constantly stirred and pumped to the crystallizer. This experimental design ensures that the mixing can be describe by a first order differential equation. The graph in Figure 6.3C symbolized by the circles describes the linear increase in ionic strength from 0.33 M to 1.5 M. After 5 hours the pump between the high and low ionic strength vessels was stopped. This ensured that the NaCl/buffer solution in the low ionic strength vessel would have a constant ionic strength of 1.5 M for the duration of the experiment. Fifteen minutes later pump (7) was turned off, ensuring that the ionic strength of the reservoir retained a constant value of 1.5 M.

Figure 6.3 depicts the measured lysozyme concentration profiles associated with the three control schemes. All of the lysozyme concentration profiles are plotted against the same time scale to better illustrate the effect of the reservoir ionic strength on the lysozyme concentration. Respectively, Figure 6.3A, Figure 6.3B, and Figure 6.3C represent lysozyme concentration profiles associated with a constant reservoir, a reservoir step change, and a differential change in reservoir ionic strength. The concentration profiles related to the constant reservoir and step change in reservoir have previously been reported [14]. These concentration profiles share similar shapes. Initially, the concentration of the lysozyme increases as water is drawn from the drop to the higher ionic strength reservoir. The profile then changes direction and begins to decrease. The change in direction of the concentration profile signals the nucleation of lysozyme. The



**Figure 6.3** A comparison of the relative crystallization kinetics between hanging drop experiments with an initial lysozyme concentration of about 0.23 g/ml. The lysozyme concentration profiles correspond to the control schemes depicted in Figure2. The difference in trajectory of the lysozyme concentration indicates that the path taken by the lysozyme concentration is dependent on the control scheme implemented.

continuing decrease in lysozyme concentration is associated with the decrease in supersaturation due to growth of the lysozyme crystals.

The profile associated with the differential change in reservoir ionic strength follows a much different trajectory than the other lysozyme concentration profiles. Initially, the ionic strengths of the drop and the reservoir were approximately equal to 0.33 M. However, the concentration profile decreases. Lysozyme can have a net positive surface charge due to the level of pH. At pH of 4.2 lysozyme has between 10 to 12 positive surface charges [17]. This number was not taken into account in determining the ionic strength of the hanging drop. Under these conditions lysozyme is a positive ion, which gives the hanging drop a larger ionic strength than the reservoir. This results in the hanging drop obtaining water from the reservoir. The hanging drop decreases in concentration until the ionic strength of the reservoir becomes greater than that of the drop. At approximately 3.5 hours when the reservoir ionic strength reaches a value of 1.1 M, the concentration profile begins to increase. Finally, at about 8 hours the profile reverses direction indicating the nucleation of lysozyme.

Figure 6.4 contains photographs of the hanging drop experiments related to the three control schemes. Photographs A, B, and C relate to the constant reservoir ionic strength, the step change in reservoir ionic strength, and the differential change in reservoir ionic strength. The photographs were taken of the actual experiments, which produced the lysozyme concentration profiles in Figure 6.3. The photographs are all at the same level of magnification. Table 6.1 summarizes the nucleation times, the number of crystals produced, and the resultant crystal sizes from these experiments. The addition of control to the hanging drop experiments decreased the number of lysozyme crystals produced

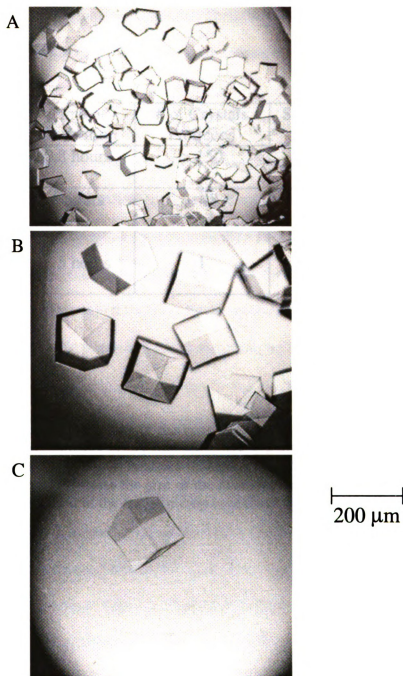


Figure 6.4 These lysozyme crystals correspond to the trajectories of the experiments in Figure 3. These photographs are at the same magnification, and encompass identical viewing areas. The pictures represent the uncontrolled experiment at a constant reservoir ionic strength (A), the feedback control experiment obtained through a step change in reservoir ionic strength (B), and the programmed control obtained through a differential change in reservoir ionic strength (C). The application of control to the crystallization process of lysozyme increases the size of the resultant crystals and decreases the number of crystals produced.

Experiment	Time of Nucleation	# of Crystals Produced	Size of Crystals Produced
Constant Reservoir	0.8 hours	> 150	$\approx 90 \mu\text{m}$
Reservoir Step Change	6 hours	$\approx 48$	$\approx 200 \mu\text{m}$
Reservoir Differential Change	8.5 hours	1	$\approx 200 \mu\text{m}$

**Table 6.1** A summary of the results of the controlled crystallization experiments in terms of nucleation times, numbers of crystals produced, and size of crystals produced. The application of control by either feedback control (step change) or programmed control (differential change) increases the size of the resultant crystal. The data indicate that the method most often used in the hanging drop experiment (constant reservoir) does not give the best results.

while increasing the size of the resultant crystals. These trends indicate that continuous monitoring to enable control of the crystallizing system is essential.

## Conclusions

From these results it is obvious that control of the hanging drop experiment results in fewer numbers of larger crystals. All of the lysozyme solutions in this study achieved nearly the same level of supersaturation. Yet the outcomes of the experiments were quite different. The lysozyme concentration profiles reveal that the lysozyme crystallization follows different paths under the different control mechanisms. Crystallization is dominated by kinetics and not thermodynamics; therefore, path dependent behavior is observed.

Crystals grown under constant reservoir conditions are subjected to high rates of supersaturation and short nucleation times resulting in many tiny crystals. The constant reservoir experiment, which contains no elements of control, mimics the design of the matrix screening methods. Comparing the various control mechanisms indicates that protein crystallization experiments performed over constant reservoirs will ensure that a number of trials fail. Therefore, typical screening experiments are not being run at optimal levels for large single crystal formation. As a result tiny crystals or precipitate will dominate experiments run at a constant reservoir ionic strength.

The need for control was the impetus behind the development of the Raman spectroscopic monitoring technique [13,14]. The ability to make *in situ* lysozyme concentration measurements allowed the rate of generation of supersaturation and induction time to be determined. Accordingly, step changes in reservoir ionic strength



could be made to either increase or decrease the rate of water leaving the drop. Though the feed back control is manual, the diffusion of the water between the drop and reservoir occurs faster than the crystallization kinetics. Therefore, we are able to affect a change in the crystallizing lysozyme system. The step change in ionic strength changes the rate of supersaturation and alters the trajectory of the lysozyme concentration. The net effect is an increase in nucleation time, which results in crystals that are 200  $\mu\text{m}$  length.

Though the differential ionic strength experiments employed high lysozyme concentrations at elevated ionic strengths, large single crystals were produced. The same level of ionic strength that was used in the constant reservoir experiment was attained in these experiments. However, due to the programmed increase in ionic strength the protein concentration traveled an alternate trajectory. The difference in supersaturation resulted in crystals that were 200  $\mu\text{m}$  in length. In order to obtain a similar crystal size via a constant reservoir technique, an ionic strength below 0.67 M would be necessary, and the resultant time of nucleation would be on the order of 20 hours. Therefore, control of the crystallization process has produced larger crystals in less time.

It is evident from these experiments that control of the hanging drop facilitates the formation of large single crystals. The ability to measure the concentration of lysozyme *in situ* allows the level of supersaturation to be monitored. Therefore, path of the lysozyme crystallization can be affected. These results confirm that the crystallization process is path dependent as is seen in more conventional batch crystallization. Although the lysozyme reached nearly the same level of supersaturation in each of the three experiments, the outcomes of these experiments varied markedly. Finally, these findings indicate that the current method of conducting the hanging drop experiment can see

significant improvement. It is the authors' hope that focus will further shift to development of strategies to both better monitor and control the hanging drop experiment.

## Literature Cited

- [1] F. Rosenberger, P.G. Velikov, M. Muschol, and B.R. Thomas, *J. Crystal Growth* 168 (1996) 1.
- [2] M. Muschol and F. Rosenberger, *J. Chem. Phys.* 103 (1995) 10424.
- [3] Y. Georgalis, P. Umbach, A. Zielenkiewicz, E. Utzig, W. Zielenkiewicz, P. Zielenkiewicz, and W. Saenger, *J. Am. Chem. Soc.* 119 (1997) 11959.
- [4] M. Boyer, M.-O. Roy, and M. Jullien, *J. Crystal Growth* 167 (1996) 212.
- [5] Z. Kam, H.B. Shore, and G. Feher, *J. Mol. Biol.* 123 (1978) 539.
- [6] B.L. Pan and K. A. Berglund, *J. Crystal Growth* 171 (1997) 226.
- [7] P.A. Darcy and J.M. Weincek, *J. Crystal Growth* 196 (1999) 243.
- [8] T. Soga, H. Sasaki, M. Tanokura, and M. Ataka, *J. Crystal Growth* 196 (1999) 291.
- [9] I.P. Kuranova, E.V. Blagova, V.M. Levnikov, G.N. Rudenskaya, N.P. Balaban, and E.V. Shakirov, *J. Crystal Growth* 196 (1999) 313.
- [10] A.M. Stevens, J.L. Pawlitz, R.G. Kurumbail, J.K. Gierse, K.T. Moreland, R.A. Stegeman, J.Y. Loduca, and W.C. Stallings, *J. Crystal Growth* 196 (1999) 350.
- [11] R.R. Ansari, K.I. Suh, A. Arabshahi, W.W. Wilson, T.L. Bray, and L.J. DeLucas, *J. Crystal Growth* 168 (1996) 216.
- [12] Z.-Y. Shu, H.-Y. Gong, and R.-C. Bi, *J. Crystal Growth* 192 (1998) 282.
- [13] A.M. Schwartz and K.A. Berglund, *J. Crystal Growth* 203 (1999) 599.
- [14] A.M. Schwartz and K.A. Berglund, *J. Crystal Growth* accepted July 1999.
- [15] D.A. Long, *Raman Spectroscopy* (McGraw-Hill, New York, 1977).
- [16] P.R. Carey, *Biological Applications of Raman and Resonance Raman Spectroscopies* (Academic Press, New York, 1982).
- [17] F. Rosenberger, *J. Crystal Growth* 166 (1996) 40.

## **Chapter 7: Conclusions**

### **Methods Used to Monitor Protein Crystallization**

Though there are some similarities between the hanging drop and batch methods, most protein crystal screening experiments are accomplished via the hanging drop experiment. However, the techniques initially applied to monitor protein crystallization experiments required large volumes of protein solution and were more suited to the batch experiment. In an attempt to replicate the exact experimental conditions of protein crystallographers, the hanging drop method was employed in this study. In order to accomplish this, a noninvasive probe of the hanging drop was necessary. The two possible candidates for spectroscopically monitoring protein crystallization in the hanging drop were ATR-IR and fiber optic Raman spectroscopy.

The flexibility in sampling configurations of the ReactIR 1000® ATR-IR allowed the probe tip to be inverted. With the internal reflection element of the probe tip facing down, the surface of the internal reflection element could be used in place of the glass coverslip for the hanging drop experiment. A drop of protein solution was deposited on the internal reflection element. As described in chapter 2, the probe tip was then placed into a test tube containing a reservoir. Though the versatile sampling configuration of the ATR-IR introduced a novel approach in monitoring the hanging drop, the experiment contained three major flaws. The first drawback was that the experiment only allowed one protein drop to be monitored at a time. Crystallographers have hundreds of hanging drop experiments occurring simultaneously. By using the internal reflection element of the probe as a surrogate for the glass cover slip only one of the hundreds of experiments

could be monitored. Secondly, the surface of the internal reflection element could serve as a nucleation site to protein crystals, which could artificially increase the nucleation rate of the protein. Finally, as described in chapter 2, the charged surface of the protein molecules can bond to the inorganic surface of the internal reflection element. This resulted in fouling of the probe tip by adsorption of the lysozyme molecules onto the diamond surface. For these reasons monitoring the hanging drop experiment by ATR-IR was abandoned.

The use of Raman spectroscopy to monitor the hanging drop experiment provides similar information as the ATR-IR method, but accomplishes this in a more practical manner. The fiber optic probe head of the HoloLab 1000® Raman spectrometer allows the hanging drop of protein solution to be brought into the focal point of the laser without intimate contact. This configuration allows the fiber optic probe to be positioned above any hanging drop experiment; therefore, more than one experiment can be monitored simultaneously. The Raman spectroscopic method of monitoring the hanging drop experiment has been shown to be noninvasive, Chapter 3. Through calculations the increase in the temperature of the hanging drop due to constant exposure to the laser has been estimated at  $\pm 0.2^{\circ}\text{C}$ . This is far beneath the  $\pm 1.0^{\circ}\text{C}$  temperature fluctuations in the laboratory. Next, solubility measurements were made by the Raman method and were found to be comparable with literature values acquired by absorbance techniques. Furthermore, experiments have shown that crystals form indiscriminately in and out of the path of the laser.

The success of Raman spectroscopy in measuring the solubility and transient concentration of a lysozyme hanging drop experiment, led to the continued development

of the Raman method. In Chapters 3 & 4, the CH and OH vibrations were employed to build a PLS regression model to describe the relationship between the vibrational spectral features and the lysozyme concentration. The PLS method was used to predict lysozyme concentration values *in situ*. The predicted concentration values were then used to construct concentration profiles. Rates of generation of supersaturation and induction times were obtained from these concentration profiles.

Through the use of the information collected in uncontrolled experiments an empirical relationship between the slope of the concentration profile and the outcome of the experiment was formed. The hanging drop experiment was ultimately controlled by monitoring the slope of the concentration profile of lysozyme *in situ*, then generating a step change in the ionic strength of the reservoir, Chapter 4. Through the addition of control to the hanging drop experiment, the quality and size of the resultant lysozyme crystals were affected. This method was then extended to protein systems other than the ideal lysozyme system with similar results, Chapter 5.

The intent of the initial work on protein crystallization was to promote the ability to monitor and control the hanging drop experiment. Protein crystallization done in the hanging drop mode to date is nothing more than trial and error. Though statistical methods have been employed to design the screening experiments, the odds of acquiring a protein crystal are quite low. The ability to control to the hanging drop experiment should alleviate some of the guesswork in protein crystallization. The Raman method has been proven to be an effective tool for monitoring protein concentrations *in situ*.

The ability to continuously monitor the hanging drop protein concentration will allow the scientist to ascertain where the system is headed. Experiments with subtilisin have

shown that protein crystals can form prior to the formation of amorphous precipitate, Chapter 5. If the system were not continuously monitored, there would be no evidence of crystals having formed. By continuously monitoring the hanging drop of subtilisin, indications that a nucleation event happened prior to the precipitation of the subtilisin were present in the concentration profile. These examples epitomize the need for introducing the capacity to monitor and control the hanging drop experiment.

### **The Hanging Drop Experiment**

In the process of developing the Raman method to monitor the protein concentration in a hanging drop, the hanging drop experiment was also examined. Though the need for control was stressed throughout Chapters 3, 4, & 5, the need to develop the hanging drop experiment was also recognized. The goal of the matrix screening hanging drop experiments is to generate large single crystals. However, experiments have revealed that the hanging drop method typically produces many tiny crystals or an amorphous precipitate. The main drawback of the hanging drop experiment is the nature of its design. The hanging drop experiment is designed as a thermodynamic experiment. Although thermodynamics does play a role in determining the solubility of the protein, the kinetic aspect of the experiment cannot be ignored.

In Chapter 1, crystallization was introduced as kinetic process governed by two rates, the rate of nucleation and the rate of growth. Yet the hanging drop experiment does not take these factors into account. The experiment is not concerned by how nucleation or growth is obtained, but rather if nucleation or growth is obtained. The hanging drop experiment has been historically considered path independent. However, results from

Chapters 4 & 5 indicate that the rate at which the drop supersaturates is directly related to the success of the experiment. Uncontrolled hanging drop experiments with constant ionic strength reservoirs can subject the protein within the hanging drop to extremely harsh conditions. By controlling the rate of supersaturation, Chapters 4 & 5, the quality and size of the resultant crystals were affected.

Chapter 6 compared three possible methods to control the hanging drop experiment. The initial protein concentrations and ionic strengths were approximately equal in order to draw comparisons between the experiments. The three methods studied were an uncontrolled experiment (constant reservoir ionic strength), a feedback control experiment (step change in ionic strength), and a programmed control experiment (linear increase in ionic strength). These methods relied heavily on the ability to monitor the system *in situ* to determine the apparent level of supersaturation of the protein in the hanging drop before altering the system conditions. The results indicate that control of the experiment either through manual feedback or a programmed ionic strength profile increased the success of the experiment over the uncontrolled lysozyme hanging drop experiments.

The control offered via a programmed ionic strength profile generated the fewest number of protein crystals while retaining a crystal size of greater than 200  $\mu\text{m}$ . Each of the control strategies resulted in varying protein concentration profiles. These concentration profiles revealed the extent that the kinetic pathway plays in the hanging drop experiment. Therefore, these experiments have shown the importance of monitoring the hanging drop for control purposes and the importance of experimental design on the outcome of the hanging drop crystallization experiment.



## Chapter 8: Future Directions

### The Raman Method

Although a method to monitor and control the hanging drop experiment has been introduced, there is still much to be done. The Raman method that has been developed has added control to an area of science, which has historically been classified as an art form. Though the Raman method has been lauded for its capability in monitoring the hanging drop *in situ*, the method does have some drawbacks. These obstacles relate to interferences in the spectra of the proteins monitored.

This study deliberately employed proteins, which could be crystallized by using salts as precipitants. The dissociation of the salts upon dilution ensured that the salts would not interfere with the vibrational spectra of the proteins. However, many proteins are crystallized by the addition of polymers or organic solvents. Typically, the scattering efficiency of the polymers and organic solvents is greater than that of the protein being monitored, which results in a Raman spectrum of the precipitant and not the protein. To combat this problem low concentrations of the polymers or organic solvents should be used. A second problem in using polymers or organic solvents as precipitants is overlapping vibrational bands. The Raman method employs the CH vibrational stretch of the Raman spectrum. However, the Raman spectra of most polymers and organic solvents will also contribute to the CH vibrational stretch. Therefore, PLS models that employ the Amide I and Amide III vibrational modes should be investigated.

Competing fluorescence has been a problem in acquiring the Raman spectra of proteins, Chapter 5. Alkaline phosphatase and bovine liver catalase were eliminated from this study due to the saturation of the detector from the fluorescent background.

Changing the laser source to a higher incident wavelength may alleviate this problem and allow for the extension of the Raman method to more protein systems. Fluorescence backgrounds were treated by normalizing the Raman spectra throughout this study. However, the subtraction or baseline correction of the fluorescence background should be investigated in future experiments and PLS models.

### **The Hanging Drop Experiment**

A possible criticism of this work is the empirical nature of the feedback control mechanism. Uncontrolled hanging drop experiments were used to determine rates of supersaturation and the nucleation times of proteins. These values became indicators, and were used to determine when a change in reservoir ionic strength should be made. Future development should focus on modeling the resultant concentration profiles. This model could be incorporated into a fully automated control scheme for the hanging drop experiment. A completely automated hanging drop experiment may only require one drop of protein to generate protein crystals. This would ensure a reduction in time and money in determining the necessary conditions for protein crystallization. Finally, the Raman method of monitoring and controlling protein crystallization in the hanging drop should be implemented on a protein that has not yet been crystallized. This should prove the effectiveness of the Raman method to its detractors.